

THE CANADIAN MALARTIC DEPOSIT: AN EXAMPLE OF OXIDIZED,
INTRUSION-RELATED GOLD MINERALIZATION IN THE ABITIBI
GREENSTONE BELT, QUÉBEC, CANADA

By

Kayla M. Helt

Earth and Planetary Sciences, McGill University
3450 University Street, Montreal, QC
Canada H3A 0E8

April, 2012

A thesis submitted to McGill University in partial fulfillment of the requirements of the degree
of Master of Science

©Kayla Helt, 2012

ABSTRACT

The Canadian Malartic deposit is Canada's largest producing gold mine, with a resource of 17.6 million ounces gold, and is an example of oxidized intrusion-related gold mineralization in the Archean Abitibi greenstone belt of Québec. The deposit hosts fine-grained, disseminated native gold and subordinate gold telluride minerals, which are accompanied by pyrite and minor fine-grained chalcopyrite, galena, sphalerite, hematite, molybdenite and a suite of Ag-Pb-Bi-bearing telluride minerals. Ore minerals occur in altered wall rock and early quartz-carbonate \pm albite \pm biotite veins, which are commonly surrounded by alteration haloes of K-feldspar-biotite \pm calcite, and later veins of quartz-pyrite-calcite \pm chlorite \pm muscovite \pm biotite. The gold mineralization is intimately associated with potassic alteration and associated carbonitization, and involved replacement of iron-bearing minerals in wall rock by pyrite. Mass changes reflect this alteration with nearly all altered rocks gaining K, Ca and S (almost entirely as pyrite). Barium, Cd, W, Pb, As, Sb, Bi and Mo underwent large mass gains, and Ag, Te and Au underwent extremely large mass gains. There was a mass loss of copper from nearly all the altered rocks. Isotopic ratios ($\delta^{18}\text{O}_{\text{fluid}}$ of +5.15 to +9.77‰, $\delta\text{D}_{\text{fluid}}$ of -52.00 to -45.00‰, $\delta^{34}\text{S}_{\text{fluid}}$ of -4.45 to +3.30‰ and small, positive $\Delta^{33}\text{S}$ values) suggest a dominantly magmatic origin for the fluid and sulfur and a small contribution of sulfur from a sedimentary source. A dominantly magmatic source for the fluid is also suggested by the compositions of fluid inclusion leachates. Stable isotope and trace element geothermometers yield a temperature of $\sim 475^\circ\text{C}$ for the gold mineralization.

A model is presented in which relatively oxidized ($\log f_{\text{O}_2} \sim 19$), CO_2 - and sulfur-rich ($\sum a_{\text{S}} \geq 0.1$), auriferous fluids were exsolved from felsic to intermediate, alkaline to sub-alkaline magmas emplaced at mid-crustal levels. These fluids rose to higher levels where they interacted with more shallowly emplaced monzodiorite intrusions and clastic Pontiac Group metasedimentary rocks, and locally with mafic to ultramafic rocks of the Piché Group. Interaction with the porphyries and Pontiac Group metasediments buffered the fluids to near neutral pH, and interaction with the Piché Group rocks to higher pH and lower f_{O_2} conditions. Ore deposition resulted from pyritization of the host rocks and oxidation of the ore fluid (due to

mixing with meteoric waters), which reduced $a_{\text{H}_2\text{S}}$ and caused destabilization of aqueous gold bisulphide species, leading to the precipitation of native gold and telluride minerals at $\sim 475^\circ\text{C}$.

This thesis provides a detailed description of the first clearly demonstrable example of a large oxidized intrusion-related gold system in the Archean Abitibi greenstone belt of Québec, and has considerably enhanced our understanding of the genesis of deposits of the type represented by Canadian Malartic. The study will aid in the exploration for similar deposits elsewhere, which could lead to the discovery and exploitation of other world class Archean oxidized intrusion-related gold deposits.

SOMMAIRE

Le gisement Canadian Malartic alimente la plus grande mine d'or en production au Canada avec une ressource de 17,6 millions d'onces d'or et est un exemple de minéralisation aurifère oxydée associée à des intrusions dans la ceinture archéenne de roches vertes d'Abitibi au Québec. Le dépôt accueille l'or natif à grains fins disséminés et subordonnés de minéraux de tellurure d'or, qui sont accompagnés de pyrite, d'un peu de chalcoppyrite à grains fins, de galène, de sphalérite, d'hématite, de molybdénite et de minéraux de tellurure ayant une suite d'Ag-Pb-Bi. Le minerai est présent dans les roches hôtes altérées, dans les premières veines de quartz-carbonate \pm albite \pm biotite formées ces dernières étant couramment entourées de halos d'altération de K-feldspath-biotite \pm calcite ainsi que dans les veines de quartz-pyrite-calcite \pm chlorite \pm muscovite \pm biotite plus récentes. La minéralisation de l'or est étroitement liée à une altération potassique ainsi qu'à une carbonatation et implique un remplacement des minéraux ferreux présent dans les roches hôtes par de la pyrite. Les changements de masse observés reflètent cette altération puisque la majorité des roches altérées gagnent en K, Ca et S (presque entièrement tous sous forme de pyrite). Le Baryum, Cd, W, Pb, As, Sb, Bi et le Mo ont subi des gains de masse importants tandis que l'Ag, le Te et l'Au ont subi des gains de masse extrêmement importants. Il y a également une perte de masse en cuivre de la quasi-totalité des roches altérées qui ont été analysées. Les rapports isotopiques ($\delta^{18}\text{O}_{\text{fluid}}$ de +5.15 à +9.77 ‰, de $\delta\text{D}_{\text{fluid}}$ -52.00 à -45.00 ‰, de $\delta^{34}\text{S}_{\text{fluid}}$ -4.45 à +3.30 ‰ et de petites valeurs positives de $\Delta^{33}\text{S}$) indiquent une origine magmatique dominante pour le fluide et le soufre accompagné d'une petite contribution de soufre d'une source sédimentaire. La source majoritairement magmatique pour le fluide est également suggérée par la composition des inclusions de fluides. La géothermométrie des isotopes stables et celle des traces d'éléments obtiennent une température de ~ 475 °C pour la minéralisation de l'or.

Un modèle est présenté dans lequel les fluides relativement oxydés ($\log f_{\text{O}_2} \sim 19$), étant riche en soufre ($\sum a_{\text{S}} \geq 0,1$), ainsi qu'en CO_2 , furent exsolvés d'un magma felsique à intermédiaire et d'alcalins à sous alcalins et mis en place à des niveaux de mi-croûte. Ces fluides ont été élevés à des niveaux supérieurs où ils ont interagi avec les intrusions monzodiorite peu profondes des roches métasédimentaires clastiques du Groupe Pontiac ainsi que localement avec les roches mafiques à ultramafiques du Groupe Piché. L'interaction entre les porphyres et les

métasédiments du Groupe Piché ont tamponné les fluides à un pH presque neutre tandis que l'interaction avec les roches du Groupe Piché donna un pH plus élevé avec un niveau de f_{O_2} moindre. Le dépôt du minerai est le résultat de la pyritisation des roches hôtes ainsi que de l'oxydation du fluide du minerai (en raison du mélange avec les eaux souterraine), ce qui a réduit a_{H_2S} et causé la déstabilisation des espèces bisulfites d'or aqueux, résultant la précipitation de l'or natif et des minéraux tellurures à ~ 475 °C.

Cette thèse donne une description détaillée du premier exemple clairement démontrable d'un grand système d'or oxydé associé à des intrusions dans la ceinture archéenne de roches vertes d'Abitibi au Québec en plus de considérablement améliorer notre compréhension de la genèse des dépôts de type représenté par le Canadian Malartic. L'étude contribuera à l'exploration des gisements similaires ailleurs, et pourrait éventuellement conduire à la découverte et l'exploitation de d'autres gisements archéens ayant une minéralisation aurifère oxydée associée à des intrusions.

CONTRIBUTION OF AUTHORS

This thesis has been written in manuscript format and in accordance with the regulations set forth by the Faculty of Graduate Studies, McGill University. The manuscript entitled “Constraints on the genesis of oxidized intrusion-related gold mineralization in the Archean, Canadian Malartic Deposit, Québec, Canada” has been co-authored by Kayla M. Helt, Anthony E. Williams-Jones, James R. Clark and Boswell A. Wing. Research was carried out by Kayla M. Helt in collaboration with Anthony E. Williams-Jones, James R. Clark and Boswell A. Wing. Samples were collected by Helt in summer 2009 with the guidance of Williams-Jones and Clark. Sample preparation, analyses and interpretation of results were primarily conducted by Helt with petrological interpretations guided by Clark, collection of isotope data guided by Wing and interpretations of ore deposit genesis guided by Williams-Jones.

ACKNOWLEDGEMENTS

Although the undertaking of a thesis is largely an independent endeavor, several contributors lent their hands, each of whom I have much appreciation for, and who deserve particular recognition. Firstly, I'd like to thank my supervisor "Willy" Williams-Jones for presenting the opportunity to work on the Canadian Malartic project.

Throughout this project Willy has piqued my curiosity and shared his enthusiasm for science and for this I am grateful. I am also grateful for the insights of Jim Clark concerning various aspects of this project. I very much appreciate the time taken by Jim to move my research along, from suggesting analytical techniques to editing my writing. I also thank Boz Wing for being there to share his expertise of isotopic systems. The stable isotope component of this study greatly improved this thesis and I learned a great deal from him directly and from working in his lab. The guidance, knowledge and experience Willy, Jim and Boz shared with me provided encouragement and gave confidence in constructing a comprehensive thesis.

I am also appreciative of a number of technicians, laboratory staff and fellow graduate students for sharing their expertise by training me to use equipment and/or for directly analyzing samples. Thanks to Lang Shi of the Electron Microprobe Micro-analytical Facility at McGill for aiding in probe analyses, Thi Hao Bui and André Pellerin of Boswell Wing's research group for providing instruction on operating the sulfur extraction line and the mass spectrometer, Kerry Klassen of Queen's Facility for Isotope Research (QFIR) for oxygen and hydrogen isotopic analyses, and to Colin Bray and Neil Bennett of the Inductively Coupled Plasma-Mass Spectrometry Lab at the University of Toronto for organizing the analysis of a suite of samples for minor elemental concentrations.

I'd like to give special thanks to David Albert of Cygnus Consulting Inc., and to Robert Wares and François Bouchard of Osisko Mining Corp. which generously funded this project, for being interested and involved in the research throughout. I also gratefully acknowledge NSERC for providing Anthony E. Williams-Jones with research grants which contributed to the success of this thesis.

Lastly, thanks to my family, friends, EPS, et mon chum for constant encouragement and assurance that there is light at the end of the tunnel.

TABLE OF CONTENTS

ABSTRACT	I
SOMMAIRE	III
CONTRIBUTION OF AUTHORS	V
ACKNOWLEDGEMENTS	VI
TABLE OF CONTENTS.....	VII
LIST OF FIGURES.....	IX
LIST OF TABLES	XI
LIST OF APPENDICES.....	XII
CHAPTER I: INTRODUCTION	1
MOTIVATION	2
BACKGROUND	4
OBJECTIVES	7
METHODOLOGY	7
THESIS ORGANIZATION	8
CHAPTER II: JOURNAL MANUSCRIPT	9
<i>CONSTRAINTS ON THE GENESIS OF OXIDIZED INTRUSION-RELATED GOLD MINERALIZATION IN THE ARCHEAN, CANADIAN MALARTIC DEPOSIT, QUÉBEC, CANADA</i>	<i>10</i>
ABSTRACT	11
INTRODUCTION	13
GEOLOGIC SETTING	14
REGIONAL GEOLOGY	14
LOCAL GEOLOGY	16
METAMORPHISM	17
VEINS	24
NATURE OF GOLD MINERALIZATION	24
STABLE ISOTOPES	33
TITANIUM CONCENTRATIONS IN VEIN QUARTZ	34
FLUID INCLUSION LEACHATES.....	38
DISCUSSION	41
TEMPERATURE-PRESSURE CONDITIONS	41
<i>f</i> O ₂ , pH AND $\sum aS$	45
FLUID EVOLUTION	52
GENETIC MODEL	54
CLASSIFICATION OF THE CANADIAN MALARTIC DEPOSIT	56

ACKNOWLEDGEMENTS	58
REFERENCES	59
CHAPTER III: CONCLUSIONS AND CONTRIBUTIONS TO KNOWLEDGE	67
CONCLUSIONS	68
CONTRIBUTIONS TO KNOWLEDGE	69
REFERENCES	70
APPENDICES	80

LIST OF FIGURES

FIGURE 1:	Regional and local geological maps	15
FIGURE 2:	Geochemical plots for porphyritic monzodiorite	18
FIGURE 3:	Geological map of the Canadian Malartic deposit showing the location of orebodies and near-surface mineralized zones	20
FIGURE 4:	Paragenetic sequence for monzodiorite porphyry, greywacke and Piché Group rocks	22
FIGURE 5:	Photomicrographs showing alteration minerals and their mode of occurrence.	23
FIGURE 6:	Photomicrographs showing gold-bearing minerals and their mode of occurrence.	26
FIGURE 7:	Plot of alumina against titania concentrations in greywacke for the Canadian Malartic deposit.....	29
FIGURE 8:	Bar charts showing relative mass changes for other selected trace elements within greywacke from the Canadian Malartic deposit	30
FIGURE 9:	Binary plots of bulk-rock gold versus concentrations of other selected elements in greywacke from the Canadian Malartic deposit	32
FIGURE 10:	Diagram of $\delta^{34}\text{S}$ against $\Delta^{33}\text{S}$ for pyrite in all lithotypes	36
FIGURE 11:	Photomicrographs of fluid inclusions in hydrothermal quartz	40
FIGURE 12:	Phase diagrams showing the stability of minerals in the Fe-O-S system as a function of $\log f_{\text{O}_2}$ and pH at 475°C for pressures of 1000 to 5000 bar.....	46
FIGURE 13:	Phase diagrams of the stability of minerals in the Fe-O-S system shown as a function of $\log f_{\text{O}_2}$ and $\log S_2$ at 475°C for pressures of 1000 to 5000 bars and a pH range of 4-7	47
FIGURE 14:	Comparison of the composition of hydrothermal fluid from ore stage quartz in Canadian Malartic to brine/sedimentary formation, metamorphic and magmatic waters	49

FIGURE 15: Interpreted oxygen and hydrogen isotope composition of the fluid responsible for formation of the South Barnat orebody compared to that of magmatic, metamorphic and meteoric water50

FIGURE 16: Phase diagram showing the stability fields of minerals in the Fe-O-S system as a function of $\log f_{O_2}$ and pH at 475°C and 3000 bar together with contours of $\delta^{34}S_{H_2S}$ based on the sulfur isotope composition of pyrite.....53

FIGURE 17: Stability fields of minerals in the Fe-O-S system as a function of $\log f_{O_2}$ and pH at 475°C and 3000 bar together with the predominance boundaries of gold species and gold solubility contours55

LIST OF TABLES

TABLE A:	Comparison of Canadian Malartic to major Archean gold deposit types.....	3
TABLE 1:	$\delta^{34}\text{S}$, $\delta^{34}\text{S}_{\text{fluid}}$ and $\Delta^{33}\text{S}$ values of pyrite and barite.....	35
TABLE 2:	Isotopic ratios for oxygen and hydrogen and corresponding $\delta^{18}\text{O}_{\text{fluid}}$ and $\delta\text{D}_{\text{fluid}}$ compositions	37
TABLE 3:	Titanium concentrations in hydrothermal quartz from mineralized veins.....	39
TABLE 4:	Concentrations of fluid inclusion leachates from hydrothermal quartz	42
TABLE 5:	Estimated temperature of gold mineralization calculated using stable isotope and trace element geothermometers	44

LIST OF APPENDICES

APPENDIX A: DESCRIPTION OF METHODS	81
APPENDIX B: BULK-ROCK CHEMICAL ANALYSES	90
APPENDIX C: ELECTRON MICROPROBE ANALYSES	101
APPENDIX D: MASS CHANGES ASSOCIATED WITH HYDROTHERMAL ALTERATION	115
APPENDIX E: SULFUR ISOTOPE ANALYSES	121
APPENDIX F: OXYGEN AND HYDROGEN ISOTOPE DATA	126
APPENDIX G: ISOTOPIC GEOTHERMOMETRY	129
APPENDIX H: FLUID INCLUSION LEACHATES.....	134
APPENDIX I: TITANIUM CONCENTRATIONS IN VEIN QUARTZ AND TITANIQ GEOTHERMOMETRY	148
APPENDIX J: PHASE EQUILIBRIUM MODELING.....	154

CHAPTER I: INTRODUCTION

MOTIVATION

Genetic models for Archean gold deposits can rarely be developed with confidence due to overprinting of the mineralization by metamorphism and deformation, and a general lack of preservation of primary evidence of ore-forming processes. In many cases, exploration models are adopted based on preliminary field observations to drive a project forward, and well-supported genetic models may emerge only after years or even decades of investigation (e.g., Dome, Pamour, Hollinger-McIntyre, Kirkland Lake, Hemlo, Bousquet: Robert and Poulsen, 1997).

Despite a mining legacy dating back to the 1930s, our understanding of the genesis of gold deposits in the Abitibi Greenstone Belt, one of the world's great mining districts, is still quite incomplete and is repeatedly confounded by the discovery of new deposits having characteristics that seem inconsistent with existing models. The world class (17.33 million ounces gold) Canadian Malartic gold deposit is one of these deposits. For practical reasons, Osisko Mining Corporation adopted an Archean porphyry-Au type model (Wares, 2005) in their open-pit operation based on voluminous, low-grade, disseminated gold mineralization, and a spatial association of the ores to a felsic to intermediate porphyritic intrusion and associated potassic alteration. Although this is an attractive model, some characteristics of the Canadian Malartic deposit are compatible with non-porphyry intrusion-related-Au and/or orogenic-Au deposit models (Table 1). Indeed, because the temporal relationships of gold mineralization to magmatism, deformation and metamorphism remain unresolved, researchers have previously described the Canadian Malartic deposit as being of porphyry-type (Issigonis, 1980), orogenic-type (Trudel and Sauvé, 1992), and syenite-associated-type (Robert, 2001).

Although there have been several published papers (Derry, 1939; Issigonis, 1980; Desrochers and Hubert, 1996; Robert, 2001), a M.Sc. thesis (Beaulieu, 2010) and geoscientific reports (Eakins, 1962; Sansfaçon, 1986; Sansfaçon and Trudel, 1987; Trudel et Sansfaçon, 1987; Trudel and Sauvé, 1992; Desrochers et al., 1996; Fallara et al. 2000) detailing the structure, deformational history, mineralization and alteration of gold deposits in the Canadian Malartic area, and several generalized models have been proposed to explain their genesis, none of the studies have tested these models by placing adequate constraints on the physicochemical conditions of gold mineralization ($T, f_{O_2}, m_{\Sigma S}, pH$). This is the subject of the present study.

Table A. Comparison of Canadian Malartic to major Archean gold deposit types. Deposits in the reduced intrusion-related class formed during much of the Phanerozoic although some Proterozoic and Archean deposits have also been proposed.

	Canadian Malartic	Porphyry-Au	Non-Porphyry Type Intrusion-Related-Au Oxidized	Reduced	Orogenic-Au
Metal signature	Au-Te-Ag-Mo-Bi-Sb-(W-Pb); depletion in Cu	Au ± Cu-Ag ± Bi-Te	Au ± As-Te-Mo ± Bi	Au ± Bi-W-As-Mo-Te ± Sb and low concentrations of base metals	Au-Ag ± As-B-Bi-Hg-Sb-Te-W
Alteration	Pervasive biotite-K-feldspar; biotite-K-feldspar haloes around quartz-pyrite-carbonate veinlets	Pervasive biotite-K-feldspar; biotite-K-feldspar haloes around quartz-pyrite veinlets; common sericite-pyrite overprinting; distal propylitic alteration	Pervasive biotite-K-feldspar; sericite-carbonate; albite surrounding variably developed stockworks of quartz-carbonate ± K-feldspar veinlets	Pervasive albite and/or K-feldspar alteration; weak, fracture-controlled sericite-carbonate-feldspar haloes on quartz veinlets	Albite-Fe-Mg carbonate vein haloes
Ore mineral association	Pyrite + minor to trace tellurides and hematite	Chalcopyrite, bornite, molybdenite	Pyrite, arsenopyrite + trace hematite, tellurides, molybdenite, magnetite	Arsenopyrite, pyrrhotite, pyrite; lacks magnetite or hematite	Pyrite, pyrrhotite, trace scheelite
Fluids	Oxidizing, CO ₂ -H ₂ O-bearing	Oxidizing, H ₂ O-NaCl-bearing	Oxidizing, CO ₂ -H ₂ O-bearing	Reducing, CO ₂ -H ₂ O ± CH ₄ bearing,	Reducing, H ₂ O-CO ₂ ± CH ₄ ± N ₂ bearing
Intrusion	Sub-alkalic to alkalic, felsic to intermediate, porphyritic, magnetite series	Calc-alkalic, intermediate, porphyritic, magnetite series	Sub-alkalic to alkalic, felsic to intermediate, porphyritic, magnetite series	Sub-alkalic to alkalic, felsic to intermediate; typically ilmenite series	Spatial association with granitoids of a variety of compositions
Timing	Mineralization broadly contemporaneous with intrusion? – overprinted by regional deformation	Mineralization genetically related to intrusion	Mineralization broadly contemporaneous with intrusion – overprinted by regional deformation	Mineralization coeval (± 2 Ma) with intrusion – mineralization post-regional peak metamorphism	Mineralization syn-kinematic with at least one stage of penetrative deformation of the country rocks
Crustal level of emplacement	Unknown	0.5 to 2 km	Unknown	4 to 6 km	5 to 10 km
Geologic Setting	Accretionary orogen (Abitibi Greenstone Belt), at the boundary between contrasting lithological domains	Continental- and island-arc settings; subduction-related but commonly associated with extensional environments	Accretionary orogen, commonly at or near the boundaries between contrasting lithological domains	Back-arc, foreland fold-thrust, collisional, post-collisional proposed but accretionary to collisional, subduction-related favored	Deformed metamorphic terranes/greenstone belts; spatially associated with large scale compressional to transpressional structures in accretionary and collisional orogens
P-T Conditions	> 3 kbar?, ~475°C	0.3-1 kbar, 300-700°C	Unknown	0.5-1.5 kbar, 200-400°C	1-6 kbar, 250-700°C
Example	Canadian Malartic	Boddington	Holt-McDermott, Beattie, Douay	Fort Knox, Donlin Creek, Kidston	Sigma-Lamaque, Siscoe, Golden Mile
References	This study	Sinclair, 2007; Seedorf et al., 2005; Fraser 1993 ; Mason and Melnik, 1982; Roth et al., 1982; Sillitoe, 1979	This study; Robert, 2001; Cameron and Hattori, 1987	Lang and Baker, 2001; Hart and Goldfarb, 2005; Thompson and Newberry, 2000; Thompson et al., 1999; Goldfarb et al, 2000	Goldfarb et al., 2001; Groves et al., 1998; Groves et al., 2003; Ridley and Diamond, 2000

BACKGROUND

The Superior Province is at the core of the Canadian Shield and represents the mining heartland of Canada. This geological province is world-renowned for its numerous precious metal and polymetallic deposits, but perhaps most of all for the Abitibi Greenstone Belt, in which the majority of Canada's world class gold deposits are located. The Abitibi is the largest, and among the richest Archean greenstone belts in the world. It is approximately 650 km long, 150 km wide and extends east-northeast from Wawa in central Ontario to Chibougamau in north-central Québec. An estimated 4,700 tons of gold has been extracted from the Abitibi and areas immediately adjacent, which represents over half of the 8,125 tons produced from the entire Superior Province (Spooner and Barrie, 1993; Robert and Poulsen, 1997). This gold has been derived from several different types of deposits, of which the major producers have been gold-bearing quartz \pm carbonate vein or orogenic deposits and volcanogenic massive sulphide deposits. However, a significant proportion of the gold has also come from intrusion-related deposits.

The term "intrusion-related" refers to deposits that are associated spatially and genetically to small intrusions of felsic to intermediate composition. These systems comprise an incoherent group of generally large tonnage, low grade deposits with diverse characteristics, but are often characterized by disseminations of gold and sulphide minerals and gold-sulphide-bearing quartz stockworks in and adjacent to intrusions. Sillitoe (1991) established a classification scheme for intrusion-related gold deposits based on a porphyry-copper model. He defined a spectrum of mineralization styles in epizonal to mesozonal environments and identified six interrelated styles, namely porphyry, skarn, intrusion-hosted, carbonate-replacement, breccia and vein. Although Sillitoe (1991) did not note this explicitly, his definition of intrusion-related gold deposits focuses on oxidized intrusions of calc-alkaline affinity that contain elevated concentrations of base metals, chiefly copper. Thompson et al. (1999) expanded the classification of Sillitoe (1991) to include gold deposits associated with reduced sub-alkaline to alkaline intrusions having a low concentration of Cu and other base metals, and enrichments in Bi, Te, As, Mo, Sb, W and in some cases Sn. These were subsequently re-classified by Thompson and Newberry (2000) and Lang and Baker (2001) as reduced intrusion-related deposits to emphasize the more reduced character of the intrusions relative to those of the

porphyry-related systems described by Sillitoe (1991). An additional family of gold deposits, genetically associated with intrusions, that fits neither of the classifications described above was recognized by Cameron and Hattori (1987) and Robert (1997). These deposits are associated with sub-alkaline to alkaline intrusions, have an oxidized mineral assemblage (hematite/magnetite \pm anhydrite and/or barite), are generally enriched in As-Te-Mo \pm Bi and occur at or near the boundaries between contrasting lithological domains. Robert (2001) termed these gold deposits occurring in the Abitibi Greenstone Belt as syenite-associated deposits.

From the preceding discussion, it is apparent that intrusion-related deposits vary greatly in the chemical affinity of the intrusions, their oxidation state, and the metal signature of the mineralization. The intrusion-related gold deposits of Sillitoe (1991) differ from the two other classes described above in the calc-alkaline affinity of the intrusions and the elevated concentrations of copper. By contrast, magmas associated with the reduced intrusion-related class of gold deposits of Thompson and Newberry (2000) and the syenite-associated family of Robert (2001) have a sub-alkaline to alkaline affinity, and the gold mineralization is associated with elevated concentrations of As-Te-Mo \pm Bi and a general deficiency in base metals (see descriptions in Dyer, 1936; Davidson and Banfield, 1944; Sinclair, 1982; Akande, 1985; Troop, 1985; Robert, 1997; Lunistra and Benn, 2001; Ropchan et al., 2002; Dupéré and Gagnon, 2011). In the interest of simplifying the terminology, it is therefore proposed that: 1) the term intrusion-related gold deposit (oxidized and reduced) be restricted to deposits associated with sub-alkaline to alkaline intrusions; 2) the reduced intrusion-related class of Thompson and Newberry (2000) be retained as originally defined, with the prefix reduced relating to the primary oxidation state of the magma; 3) gold deposits having characteristics nearly similar to the reduced-intrusion-related class, including deposits termed syenite-associated by Robert (2001) be re-classified as oxidized intrusion-related to distinguish a primary oxidized state of the magma; and 4) the intrusion-related class originally defined by Sillitoe (1991) be re-defined as the porphyry-associated class of gold deposits, in recognition of their genetic relationship to porphyry-copper deposits.

Although the classification proposed above removes some of the previous ambiguity, intrusion-related deposits, both oxidized and reduced, share characteristics common to orogenic-Au deposits, in particular, anomalously high concentrations of Bi, W and Te, low concentrations of Cu and other base metals, an apparent genetic association with CO₂-rich fluids, and a

spatial/temporal link with regional metamorphism and magmatism. These overlapping characteristics have led to a number of deposits formerly considered as orogenic to be re-classified as intrusion-related gold deposits (Hart and Goldfarb, 2005; Robert, 2001). Intrusion-related ore-forming systems can be distinguished from orogenic systems by: 1) an association with sub-alkaline to alkaline intrusives (these are uncommon in fore-arc settings where orogenic gold deposits are thought to be most common); and 2) broadly coeval timing of mineralization and magmatism subsequent to regional metamorphism and deformation of the host allochthons (Hart and Goldfarb, 2005).

The Canadian Malartic deposit in the Abitibi Greenstone Belt shows: 1) a spatial association with small felsic to intermediate porphyritic intrusions; 2) an enrichment of Te, Ag, Mo, Bi, Sb, with lesser W and Pb in addition to Au, a depletion in Cu and low concentrations of other base metals; 3) an oxidized ore assemblage including hematite and minor barite; 4) widespread potassic alteration; and 5) a remarkably consistent gold grade (~1-3g/t Au). Based on these characteristics, the Canadian Malartic deposit could represent a copper-poor variant of an Archean porphyry-Au system. However, most gold-rich porphyry deposits, including those of Archean age contain at least some copper, whereas the mineralization at Canadian Malartic is depleted in copper even in comparison to the unaltered host rocks. The Canadian Malartic deposit could also qualify as a reduced intrusion-related deposit of the type described by Thompson and Newberry (2000) and Lang and Baker (2001). The reduced nature of these deposits refers to the primary oxidation state of the associated magmas, and not that of a potentially evolved mineralizing fluid. Therefore, although the ore-related assemblage at Canadian Malartic is oxidized, this may have no implication regarding the primary oxidation state of the magma responsible for the host intrusions. Similarly, Canadian Malartic could be a disseminated variant of the typical orogenic type of deposit (in which gold mineralization is generally vein-hosted and accompanied by albite-carbonate alteration); such disseminated deposits have been described in the Superior Province (Grondin and Williams-Jones, 2004) as well as elsewhere (Bierlein and Maher, 2001).

A proper classification of the world class Canadian Malartic gold deposit is of paramount importance in guiding future exploration for similar deposits. In mature mining districts, such as the Abitibi, one of the keys to making new discoveries is to employ exploration models based on

an improved understanding of deposit genesis. The purpose of this thesis is to help furnish this understanding for deposits exemplified by Canadian Malartic.

OBJECTIVES

To understand the genesis of the Canadian Malartic deposit it is necessary to elucidate: i) the nature and distribution of alteration and mineralization; ii) the source and composition of the mineralizing fluids; iii) the physicochemical conditions of the hydrothermal system; and iv) the changes in conditions that led to the deposition of gold. Addressing these issues is essential in developing a genetic model for the deposit.

METHODOLOGY

The research objectives were pursued using a combination of:

- 1) Fieldwork at the Canadian Malartic mine, including drill core logging and sampling of rocks for geochemical, petrographic, stable isotope and fluid inclusion leachate analyses;
- 2) Major and trace element geochemical analyses to determine the affinity of the intrusive rocks and mass changes of elements accompanying hydrothermal alteration and mineralization;
- 3) Petrographic examination to identify the ore, gangue and alteration mineral assemblages and generate a paragenetic sequence;
- 4) Electron microprobe analyses of gold grains to determine fineness $[(Au \cdot 100)/(Au + Ag)]$, and of biotite grains to evaluate proportions of Mg and Fe and substitution of F and Cl for OH;
- 5) Stable isotopic analyses of sulfur, oxygen and hydrogen to assess the origin(s), evolution and temperature of ore fluid(s);
- 6) Laser ablation inductively coupled plasma mass spectrometry of quartz to evaluate temperature using the TitaniQ (Wark and Watson, 2006) geothermometer;
- 7) Analyses of fluid inclusion leachates for major element ratios;
- 8) Modeling of dissolved aqueous species, phase, and sulfur isotope equilibria using the computer program Unitherm (Shvarov and Bastrakov, 1999) and thermodynamic data

from Holland and Powell (1998); Johnson et al. (1992); Pal'yanova and Drebuschak (2002); Robie and Hemmingway (1995); Shock et al. (1997), Stefansson and Seward (2003a); Stefansson and Seward (2003b); Stefansson and Sward (2004); and Sverjensky et al. (1997) and equations of Ohmoto (1972) for the calculation of $\delta^{34}\text{S}_{\text{H}_2\text{S}}$ contours.

A detailed description of methods is presented in Appendix A.

THESIS ORGANIZATION

This thesis has been written in manuscript format. In addition to the manuscript, there are two supporting chapters and nine appendices. The introductory chapter explains the motivation behind the research, provides background information, presents the objectives of the study and refers to the methodology used to reach these objectives. The second chapter is a manuscript entitled “Constraints on the genesis of oxidized intrusion-related gold mineralization in the Archean, Canadian Malartic deposit, Québec, Canada” to be submitted to *Economic Geology*. The manuscript describes the geology and mineralogy of the Canadian Malartic deposit, presents whole rock and mineral chemical data, stable isotope data, bulk crush leachate data and analyses of aqueous fluid species, phase and sulfur isotope equilibria to constrain the conditions and controls on ore deposition ($T, f_{\text{O}_2}, m_{\Sigma\text{S}}, \text{pH}$) and uses this information to develop a genetic model for the Canadian Malartic deposit. Chapter Three summarizes the conclusions of this study, identifies the contributions to knowledge and makes recommendations for future work. The appendices comprise: A) a detailed description of methods; B) results of whole-rock chemical analyses; C) results of electron microprobe analyses of minerals; D) results of mass change calculations; E) sulfur isotope compositions; F) oxygen and hydrogen isotope compositions; G) fractionation equations with corresponding fractionation factors and temperatures used in calculating temperature from both sulfur and oxygen isotopic data; H) results of crush-leach analyses; I) concentrations of Ti in quartz using LA-ICP-MS and corresponding temperatures calculated using TitaniQ (Wark and Watson, 2006); and J) ΔG_f data of phase/aqueous species, reactions, equations for the calculation of sulfur isotope contours and diagrams of $\log f_{\text{O}_2}$ versus pH over a range of pressures and $\log a_{\Sigma\text{S}}$ versus $\log f_{\text{O}_2}$ over a range of pH at 475°C with sulfur isotope contours.

CHAPTER II: JOURNAL MANUSCRIPT

CONSTRAINTS ON THE GENESIS OF OXIDIZED INTRUSION-RELATED
GOLD MINERALIZATION IN THE ARCHEAN, CANADIAN MALARTIC
DEPOSIT, QUÉBEC, CANADA

Kayla M. Helt[†], Anthony E. Williams-Jones, James R. Clark* and Boswell A. Wing

Earth and Planetary Sciences, McGill University
3450 University Street, Montreal, QC
Canada H3A 0E8

[†]Corresponding author: e-mail, kayla.helt@mail.mcgill.ca

*also at Osisko Mining Corp., 2140 St.-Mathieu, Montreal, QC, Canada, H3H 2J4

Submitted to Economic Geology

ABSTRACT

The Canadian Malartic deposit, with a resource of 17.33 million ounces of gold, represents an increasingly important class of Archean gold deposits in which the ore is disseminated (or in fine veinlets) and is hosted largely by felsic intrusions. The deposit is located in the Abitibi greenstone belt, Québec, within and adjacent to the Cadillac-Larder Lake tectonic zone, and occurs in porphyritic monzodiorite intrusions and country rocks that comprise clastic metasedimentary rocks of the Pontiac Group in the south and mafic and ultramafic volcanics of the Piché Group in the north. These rocks have undergone pervasive potassic alteration, carbonatization, pyritization and local silicification. Mineralization is characterized by native gold and subordinate gold telluride minerals, accompanied by pyrite and minor chalcopyrite, galena, sphalerite, hematite, molybdenite and a suite of Ag-Pb-Bi-bearing telluride minerals. Gold is concentrated in two generations of thin, discontinuous veins, and as finely disseminated grains in associated alteration envelopes. Early veinlets contain the assemblage quartz-carbonate \pm biotite \pm albite and are surrounded by alteration haloes of K-feldspar-biotite \pm pyrite \pm calcite, whereas later veins contain quartz-pyrite-calcite \pm chlorite \pm muscovite \pm biotite. Alteration and mineralization was accompanied by large mass gains in K and S, extremely large mass gains in Ag, Te and Au and significant mass gains in Ba, Cd, W, Pb, As, Sb, Bi and Mo; Cu underwent a large mass loss. The composition of the mineralizing fluid determined from isotopic compositions of quartz, biotite, hematite and pyrite ($\delta^{18}\text{O}_{\text{fluid}}$ of +5.15 to +9.77‰, $\delta\text{D}_{\text{fluid}}$ of -52.00 to -45.00‰, $\delta^{34}\text{S}_{\text{fluid}}$ of -4.45 to +3.30‰ and small, positive $\Delta^{33}\text{S}$ values) is consistent with a dominantly magmatic source for both fluid and sulfur, with a small contribution of sulfur from sedimentary rocks. A dominantly magmatic source for the fluid is also indicated by the composition of fluid inclusion leachates from quartz. From stable isotope and titanium-in-quartz geothermometry, the deposit is interpreted to have formed at a temperature of $\sim 475^\circ\text{C}$.

Based on geochemical and thermodynamic considerations, we propose a model in which felsic to intermediate, borderline alkaline to sub-alkaline magmas emplaced at mid-crustal levels (≥ 10 km; ≥ 3 kbar) exsolved relatively oxidized ($\log f_{\text{O}_2} \sim 19$), CO_2 - and sulfur-rich ($\sum a_{\text{S}} \geq 0.1$), auriferous fluids. These fluids rose to higher levels, where they interacted with associated porphyritic monzodiorite intrusions, clastic Pontiac Group metasedimentary and Piché Group

mafic to ultramafic rocks. The porphyries and metasedimentary rocks buffered fluids to near neutral pH, whereas the mafic/ultramafic rocks buffered fluids to higher pH and lower f_{O_2} . Ore deposition resulted from pyritization of the host rocks and oxidation of the mineralizing fluid, which reduced a_{H_2S} and caused destabilization of gold bisulfide species, leading to precipitation of native gold and telluride minerals.

INTRODUCTION

Although much of the gold extracted from Archean greenstone belts is derived from orogenic (mesothermal) deposits, a significant and growing proportion of production is mined from intrusion-related deposits. The latter comprise a group of generally large tonnage, low grade deposits that are commonly characterized by disseminated gold and sulfide minerals in alteration zones and gold-sulfide-bearing quartz stockworks in and adjacent to intrusions of felsic to intermediate composition. These include copper-bearing deposits associated with calc-alkaline intrusions as well as deposits that are depleted in copper and other base metals, which are associated with sub-alkaline to alkaline intrusions. Examples of the former are the Hollinger-McIntyre Au-Cu deposit in the Abitibi greenstone belt, Canada, the Boddington Cu-Au deposit in the Saddleback greenstone belt, Australia, and the Troilus Au-Cu deposit in the Evans-Frotet greenstone belt, Canada (Mason and Melnik, 1986; Roth, 1992; Fraser, 1993), all of which have been cited as examples of Archean porphyry-related systems. Deposits in the Archean associated with sub-alkaline to alkaline intrusions have been classified by Robert (2001) as syenite-associated based on the characteristics of a number of such deposits in the Abitibi, including Young-Davidson, Ross and Holloway (see descriptions in Davidson and Banfield, 1944; Sinclair, 1982; Akande, 1985; Robert, 1997; Ropchan et al., 2002). The world-class Canadian Malartic deposit is the largest of these deposits (current resource of 12.23 million ounces plus 5.1 million ounces gold from previous production) and is the subject of this paper (Trudel and Sauvé, 1992; Osisko, 2012).

Several papers (Derry, 1939; Issigonis, 1980; Desrochers and Hubert, 1996; Robert, 2001), a M.Sc. thesis (Beaulieu, 2010) and reports (Eakins, 1962; Sansfaçon and Trudel, 1987; Sansfaçon et al., 1987; Trudel and Sansfaçon, 1987; Trudel and Sauvé, 1992; Desrochers et al., 1996; Fallara et al., 2000) have described the structure, deformational history, mineralization and alteration of the Canadian Malartic deposit. However, none of these studies has directly addressed the problem of the origin of the mineralization. Indeed, because temporal relationships of the gold mineralization to magmatism, deformation and metamorphism remain unresolved, researchers have variously described the Canadian Malartic deposit as being of porphyry-type (Issigonis, 1980), orogenic-type (Trudel and Sauvé, 1992), and most recently as syenite-associated (Robert, 2001). In this paper we place physicochemical ($T, f_{O_2}, m_{\Sigma S}, pH$) constraints

on the conditions of gold deposition at Canadian Malartic and use this information to develop a genetic model that can be applied to comparable deposits in the Abitibi and Archean greenstone belts elsewhere.

GEOLOGIC SETTING

REGIONAL GEOLOGY

The Malartic gold district is situated in the southeastern Superior Province at the boundary between the southern margin of the Abitibi and the Pontiac subprovinces, Québec (Fig. 1A). These subprovinces are separated by the Cadillac-Larder Lake tectonic zone, a domain of steeply dipping, east-west trending major faults, which also represent a lithologic boundary between metavolcanic-plutonic and metasedimentary rocks of the Abitibi greenstone belt to the north and metasedimentary rocks of the Pontiac Group to the south (Robert, 1989; Figs 1B and C). The metavolcanic rocks belong to the Malartic, Blake River and Piché groups (the Piché Group is confined to the Cadillac-Larder Lake tectonic zone), and range from ultramafic to felsic in composition and from tholeiitic to calc-alkaline in chemical affinity. Volcanic activity in the region occurred between 2747 and 2698 Ma (Corfu et al., 1989; Mortensen, 1993; Ayer et al., 2002) and was followed between 2686 and 2677 Ma by intrusion of diorite to tonalite-trondjemite plutons of tholeiitic to calc-alkaline affinity (Corfu et al., 1991; Sutcliffe et al., 1993). This plutonism was accompanied by a period of contractional deformation, D_1 (Robert, 2001). Subsequent uplift and erosion led to the deposition of sedimentary rocks composed mainly of graywacke and mudstone (Cadillac, Kewagama and Pontiac groups), which were deposited unconformably on the volcano-plutonic assemblages between 2692 and 2675 Ma (Ayer et al., 2002; Davis, 2002). Deposition of these sedimentary rocks was broadly contemporaneous with emplacement of syntectonic plutons between 2695 and 2670 Ma (Mortensen, 1987; Corfu et al., 1989). Compositionally, the plutonic rocks comprise an early, syntectonic calc-alkaline, tonalite-granodiorite-granite suite and a late sub-alkaline to alkaline, monzonite-monzogranodiorite-syenite suite that Sutcliffe et al. (1993) reported to be LILE-enriched. The younger suite was accompanied by small intrusions of diorite, gabbro, clinopyroxenite, hornblendite and lamprophyre (Ayer et al., 2002). The syntectonic plutonic rocks were emplaced during the main period of deformation responsible for the regional east-

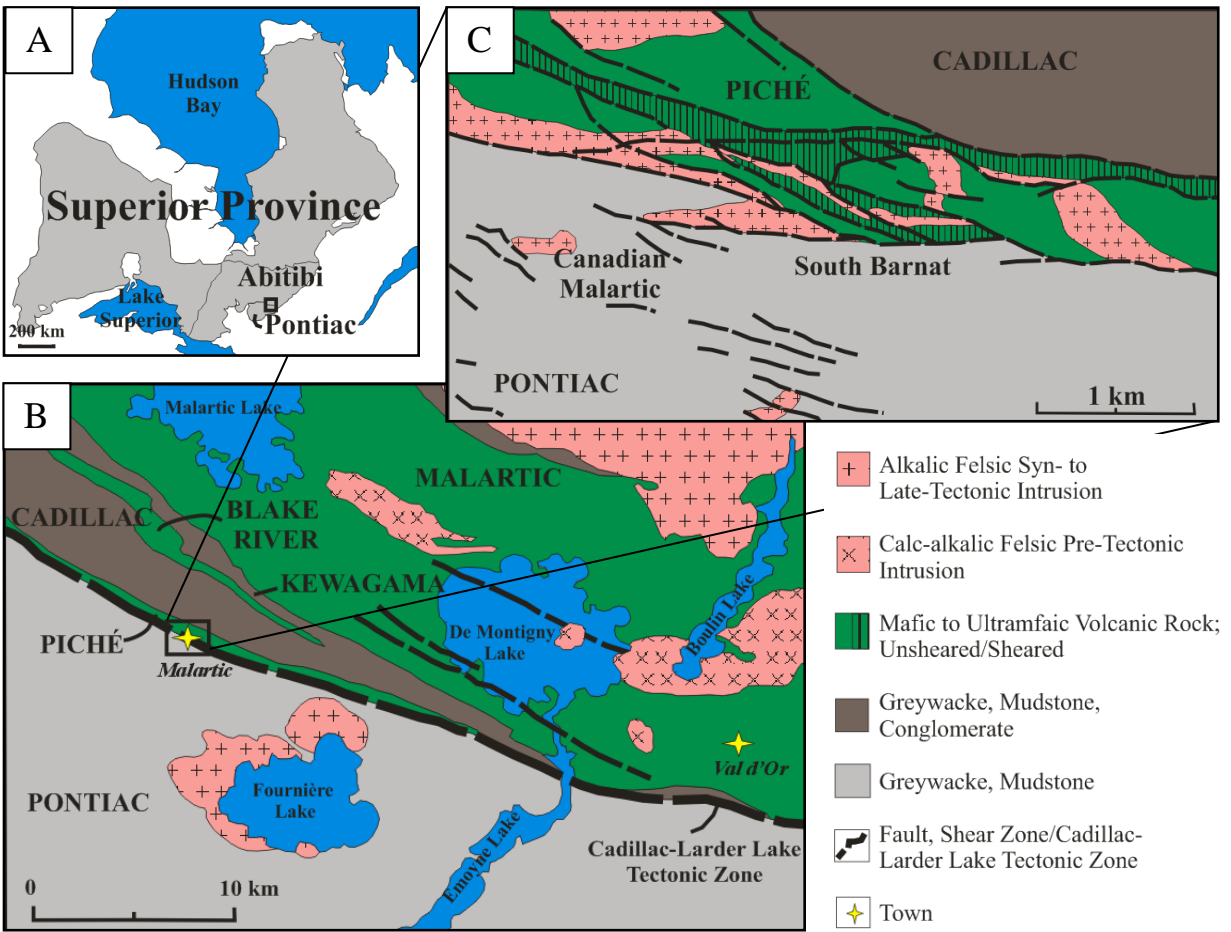


Fig. 1. A. Map showing the location of the Abitibi and Pontiac subprovinces in the southeastern Superior Province. B. Regional geological map. C. Local geology (inset map from A) showing the setting of the Canadian Malartic gold deposit hosted by rocks of the Piché and Pontiac groups. Modified from Robert (1989), Robert (2001) and Thurston et al., (2008).

west lithological trend, D₂, which involved north-south shortening (Robert, 2001). The D₂ event evolved into dextral transcurrent deformation along major fault zones, D₃, and was accompanied and post-dated by sub-alkaline to alkaline plutonism, which continued until approximately 2660 Ma (Robert, 2001). Post-tectonic biotite-granite-pegmatite intruded the regionally metamorphosed strata between 2665 and 2640 Ma (Feng and Kerrich, 1992; Ayer et al., 2002). The metamorphic grade in the region ranges from sub-greenschist to amphibolite facies (Dimroth et al., 1983; Powell et al., 1995). Retrograde metamorphism was largely restricted to the Cadillac-Larder-Lake tectonic zone, which was the locus of hydrothermal activity and related gold deposition, in second and third order shear zones.

LOCAL GEOLOGY

The Canadian Malartic deposit is located within and immediately adjacent to the Malartic tectonic zone (part of the Cadillac-Larder Lake tectonic zone; Fig 1). This structure dominates the local geology, and includes major east-west trending faults (the Sladen and Malartic faults) along with several northeast-southwest and northwest-southeast trending sub-vertical faults that together create lozenge-shaped fault blocks (Fallara et al., 2000). The Malartic tectonic zone is approximately 650 m wide, and is restricted to mafic-ultramafic rocks of the Piché Group, which comprise strongly deformed, biotitized and carbonatized, magnesian basaltic to komatiitic volcanics that are typically bluish-gray and pervasively foliated with numerous veinlets of talc-carbonate-chlorite (Sansfaçon and Hubert, 1990). These rocks do not outcrop on the Canadian Malartic property but underlie Pontiac Group rocks in the vicinity of the South Barnat orebody. Although gold mineralization occurs within the Piché Group, the bulk of the Canadian Malartic deposit is located south of the tectonic zone, where it is hosted by Pontiac Group sedimentary rocks and felsic to intermediate porphyritic intrusives that have undergone potassic, carbonate and silicic alteration. The Pontiac Group comprises graywackes, shales and minor conglomerates (turbiditic clastic sediments that in general are rhythmically layered with beds ranging from about one millimetre to one metre in thickness). These sediments typically have a well-developed foliation and are dark gray to black, locally exhibiting a brownish tint caused by development of metamorphic and/or hydrothermal biotite proximal to porphyritic intrusions. Porphyries intrude both Piché and Pontiac group rocks, and are feldspar-phyric with fine-grained to aphanitic matrices varying in color from light gray to reddish with progressive alteration.

Petrographically, the porphyries are monzodioritic and chemically range from sub-alkaline to alkaline based on their major element composition (Figs. 2A and B). The Pontiac Group has been shown to have a minimum age of 2682 ± 3 Ma (Davis, 2002) and the porphyritic monzodiorite has been dated at 2677-2679 Ma (zircon U-Pb ages; Clark et al., in prep). These latter ages are similar to those (2680 to 2676 Ma) reported previously for late tectonic alkalic, felsic to intermediate intrusions elsewhere in the southern Abitibi (Frerery and Krogh, 1986; Corfu et al., 1989; Jemielita et al., 1990; Davis et al., 2000).

DEFORMATION

Sansfaçon and Hubert (1990) identified three deformational events that affected rocks in the Malartic region. Their first event, D_1 , is manifested by a series of weakly to moderately dipping anticlines and synclines with northeast-southwest axial planes (F_1) and weak, penetrative schistosity (S_1). Folds associated with this deformation (F_1) are rare, but are observed locally in the hinges of F_2 folds, where S_1 is most easily recognized because of its orientation at a high angle to S_2 ; D_1 is commonly masked by D_2 . The D_2 event is manifested by a series of sub-vertical, sub-isoclinal folds (F_2) with northeast-oriented axial planes that refold D_1 structures, generating asymmetric S-folds that plunge 40 to 80° east. The northwest-southeast schistosity (S_2) produced by D_2 was much more penetrative (reflected by oriented biotite) than the weaker schistosity of D_1 , which it crenulated. Calc-alkaline intrusions in the Malartic region were deformed by D_2 and are therefore probably pre- D_2 and likely pre- to syn- D_1 in age. The final deformation event, D_3 , produced north-northwest trending, vertically dipping S_3 cleavages and fractures that are most conspicuous along the contact between the Piché and the Cadillac groups. Deformation produced a regional synclinal structure, the Malartic syncline, with a fold axis that trends west-northwest and plunges steeply to the north.

METAMORPHISM

The metamorphic grade increases in a southerly direction from sub-greenschist facies in rocks immediately north of the Malartic tectonic zone (Cadillac Group) to upper greenschist facies in Piché Group rocks within the tectonic zone and upper greenschist to amphibolites facies in Pontiac Group rocks south of this zone (Dimroth et al., 1983; Powell et al., 1995). The garnet-isograd occurs at the southern limit of the Canadian Malartic deposit and the staurolite-isograd is

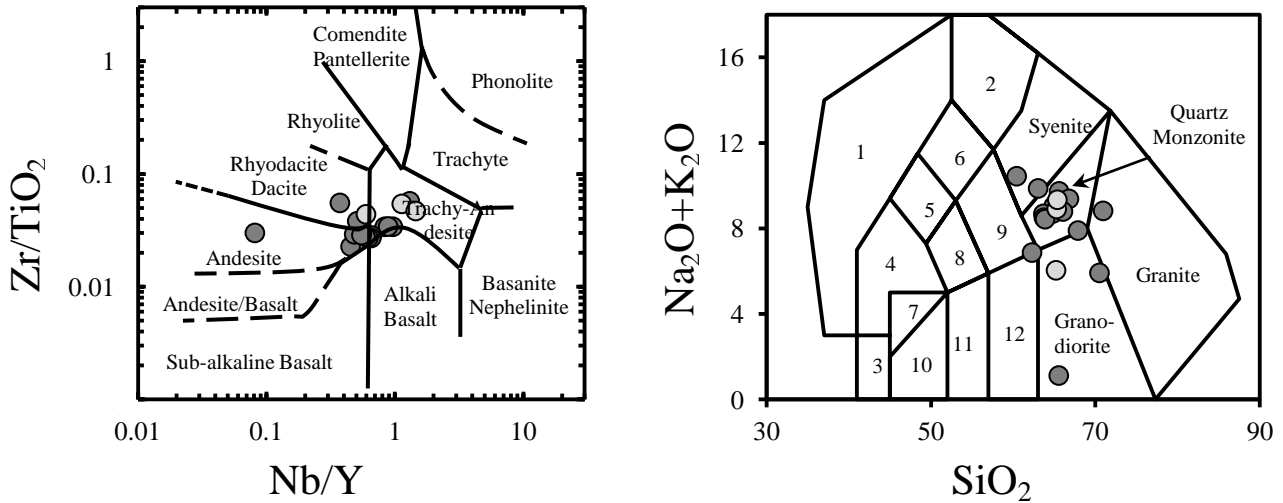


Fig. 2. A. A plot of Zr/TiO_2 vs. Nb/Y showing the composition and volcanic classification (Winchester and Floyd, 1977) of least altered porphyritic intrusive rocks from the Canadian Malartic (dark gray circles) and South Barnat orebodies (light gray circles). B. An alkali vs. silica plot showing the compositions of the least altered rocks represented in A and their classification using the fields of intrusive rocks of Middlemost (1994). Fields represented by numbers 1 to 12 correspond to foidolite (1), foid syenite (2), peridotgabbro (3), foid gabbro (4), foid monzodiorite (5), foid monzosyenite (6), monzogabbro (7), monzodiorite (8), monzonite (9), gabbro (10), gabbroic diorite (11) and diorite (12). As even the least altered rocks were subject to some alteration and as the alkalis and silica were mobile during this alteration, this diagram is considered to provide a less reliable classification of the Canadian Malartic porphyries than A. In the former diagram, these porphyries are identified mainly as diorites (andesites) and minzodiorites (trachy-andesites), reflecting lower alkali and silica contents than in the quartz monzonite classification of B. The plotted dataset comprises 20 samples.

crossed approximately 1.7 km further south (Sansfaçon, 1986). Rocks of the Piché Group have been subjected to retrograde metamorphism, evident in chloritization of biotite, formation of actinolite after hornblende and albitization of calcic plagioclase. This was likely a consequence of the extended, high flux of hydrothermal fluids through the Malartic tectonic zone.

CANADIAN MALARTIC AND SOUTH BARNAT OREBODIES

Osisko Mining Corporation started exploiting the Canadian Malartic deposit through an open-pit mining operation in May, 2011. This followed a forty-one year mining history (1938-1979), which included production of 5.1 million ounces of gold from three independent underground mines (Canadian Malartic, Barnat/Sladen and East Malartic; Trudel and Sauvé, 1992). The open-pit mine exploits ore remaining from these underground operations as well as more recently defined near-surface mineralized zones in and spatially associated with small porphyritic bodies, all of which are expressions of a much larger, low-grade mineralized system (Fig. 3). The current resource at Canadian Malartic is 12.23 million ounces of gold grading 1.02 g/t Au, making it one of the largest gold deposits in Canada (Osisko, 2012).

The Canadian Malartic deposit comprises two contiguous zones, the 3000 m long, east-west trending Canadian Malartic orebody and its eastern extension, the South Barnat orebody (global measured and indicated and inferred resources of 372.9 Mt at 1.02 g/t Au and 50.4 Mt at 0.71 g/t Au, respectively; Osisko, 2012). Whereas the Canadian Malartic orebody is hosted in Pontiac Group metasediments and monzodiorite porphyry intrusions, the South Barnat orebody, which straddles the southern edge of the Malartic tectonic zone, is also hosted by Piché Group rocks. However, hydrothermal alteration and gold mineralization are very similar in the two orebodies.

HYDROTHERMAL ALTERATION

Gold mineralization at both Canadian Malartic and South Barnat is associated with strongly altered rocks characterized by broadly similar mineral assemblages in both monzodiorite porphyry and graywacke. These assemblages are dominated by albite, quartz, carbonate (mainly calcite with lesser ankerite), K-feldspar and biotite (quartz and biotite are

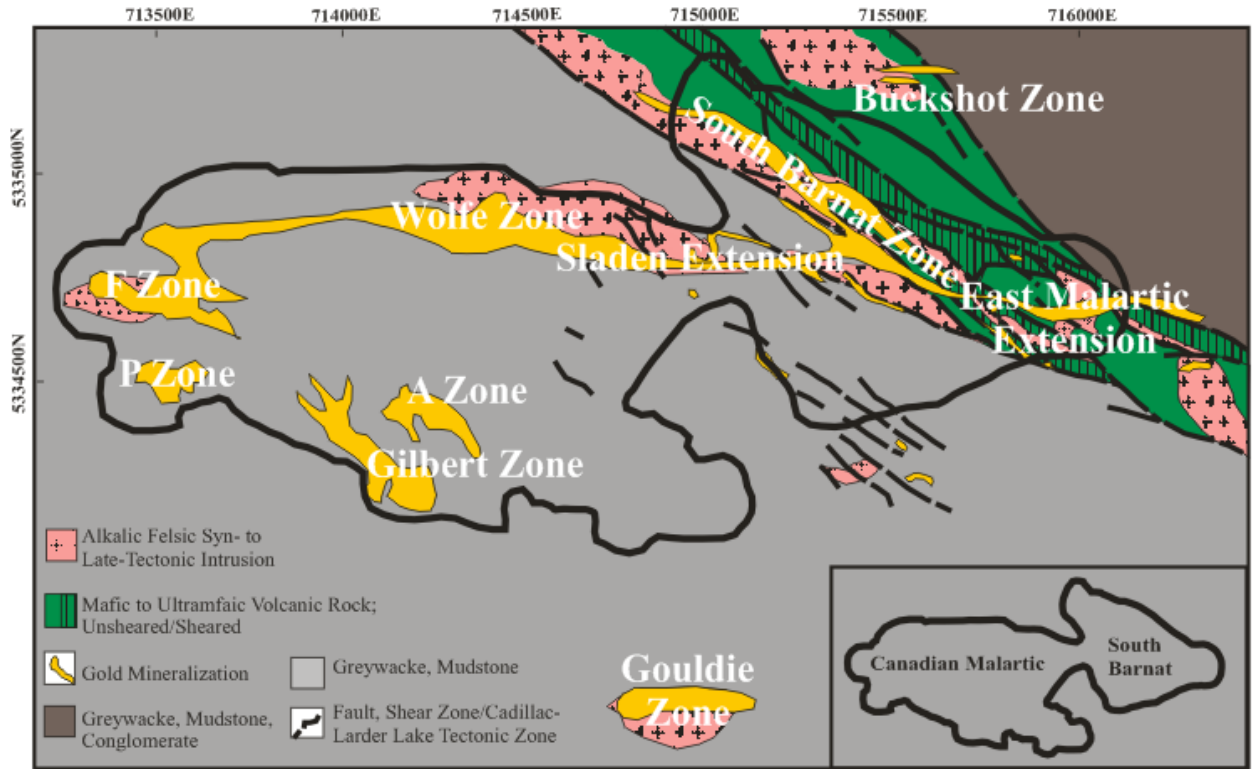


Fig. 3. Geological map of the Canadian Malartic deposit showing near-surface mineralized zones with inset outlining the main Canadian Malartic orebody in the Pontiac Group, and the South Barnat orebody along the southern margin of the Malartic tectonic zone. Modified from Robert (1989; 2001) and data provided by Osisko Mining Corp.

more abundant in graywacke), and include minor pyrite, sericite and chlorite plus traces of hematite (after magnetite; observed only in the porphyries), barite (only in the porphyries), rutile, titanite and scheelite. In addition to pyrite, the sulfides comprise chalcopyrite, galena, molybdenite, pyrrhotite and sphalerite. The sulfides are accompanied by traces of native gold, hessite (Ag_2Te), petzite (Ag_3AuTe_2), altaite (PbTe) and calaverite (AuTe_2), as well as rare bismuth and nickel tellurides. The main alteration minerals in the Piché Group rocks are biotite, plagioclase, actinolite and carbonate (calcite with lesser ankerite), which are accompanied by subordinate pyrite, magnetite and talc; the sulfide and telluride minerals are similar to those in porphyry and graywacke. The paragenesis for the above minerals is presented in Figures 4A and B, and is discussed in more detail below.

Early, pre-ore stage alteration is represented by quartz, generally accompanied by minor albite and carbonate (mainly calcite). This assemblage replaced matrix minerals of the monzodiorite porphyry intrusions and graywacke, and also occurs in first generation veinlets (≤ 1 cm diameter) and local stockworks that cut all lithotypes. In zones of replacement, quartz and albite are fine-grained, anhedral and intergrown, and in veinlets are anhedral to subhedral. Carbonate occurs as isolated subhedral crystals in veinlets as well as after quartz and albite in both veinlets and replacement zones, filling interstices between grains (Fig. 5A). Carbonate alteration is commonly accompanied by sericite, which is present in the cores of primary K-feldspar phenocrysts and throughout the matrix (Fig. 5B). The early alteration assemblage of quartz \pm albite \pm carbonate \pm sericite was overprinted by widespread pervasive and vein-related potassic alteration (Fig. 5C and D). Potassic alteration is intimately associated with gold mineralization and marks the onset of ore stage alteration. In monzodiorite porphyry intrusions, pervasive potassic alteration occurs as replacement of plagioclase by K-feldspar (commonly accompanied by finely disseminated hematite; Fig. 5E) and biotite. In graywacke, pervasive potassic alteration is evident from an increase in the abundance of biotite relative to that in unaltered graywacke (biotite is also an important metamorphic phase), and in Piché Group rocks from the replacement of mafic minerals by biotite. Vein-related potassic alteration produced biotite-K-feldspar-calcite \pm pyrite haloes around first generation veinlets (Fig. 5F and G). Pyrite was introduced concurrently with potassic alteration, and is ubiquitous in the deposit, occurring

Mineral	Sedimentary Assemblage	Igneous Assemblage	Hydrothermal Assemblage		
			Pre-Ore	Ore	Post-Ore
			V1	V1&V2	V3
Plagioclase	██████████	██████████	██████████	██████████	
Quartz	██████████	██████████	██████████	██████████	██████████
K-Feldspar		██████████		██████████	
Biotite	██████████	██████████		██████████	
Muscovite/sericite			██████████	██████████	
Calcite			██████████	██████████	
Pyrite			██████████	██████████	
Chlorite				██████████	
Magnetite	██████████	██████████		██████████	
Amphibole	██████████	██████████		██████████	
Monazite	██████████	██████████		██████████	
Apatite	██████████	██████████		██████████	
Zircon	██████████	██████████		██████████	
Allanite	██████████	██████████		██████████	
Epidote	██████████	██████████			██████████
Ankerite			██████████	██████████	
Hematite				██████████	
Pyrrhotite			██████████		
Ilmenite		██████████			
Barite			██████████	
Scheelite			██████████	
Titanite			██████████		
Chalcopyrite				██████████	
Galena				██████████	██████████
Molybdenite			██████████	██████████	
Sphalerite				██████████	
Rutile				██████████	
Native Gold				██████████	██████████
Electrum				██████████	██████████
Calaverite				██████████	
Hessite				██████████	
Petzite				██████████	
Altaite				██████████	
Tellurobismuthite				██████████	

Mineral	Igneous Assemblage	Hydrothermal Assemblage		
		Pre-Ore	Ore	Post-Ore
		V1	V1&V2	V3
Plagioclase(Ca-Na)	██████████	██████████	██████████	██████████
Quartz		██████████	██████████	
Biotite		██████████	
Amphibole		██████████	██████████	
Calcite		██████████	██████████	
Pyrite		██████████	██████████	
Magnetite	██████████	██████████	
Talc		██████████	██████████	
Chlorite			██████████	
Ankerite		██████████	██████████	
Ilmenite	██████████		
Hematite		██████████	██████████	
Monazite		██████████		
Pyrrhotite		██████████		
Scheelite		██████████	
Titanite		██████████		
Chalcopyrite			██████████	
Galena			██████████	██████████
Sphalerite			██████████	
Molybdenite		██████████	██████████	
Rutile			██████████	
Gold			██████████	██████████
Altaite			██████████	

Fig. 4. A. Paragenetic sequence for alteration/mineralization in monzodiorite porphyry and graywacke. B. Paragenetic sequence for alteration/mineralization in Piché Group rocks. Vein generations associated with alteration and mineralization are indicated by V1, V2 and V3.

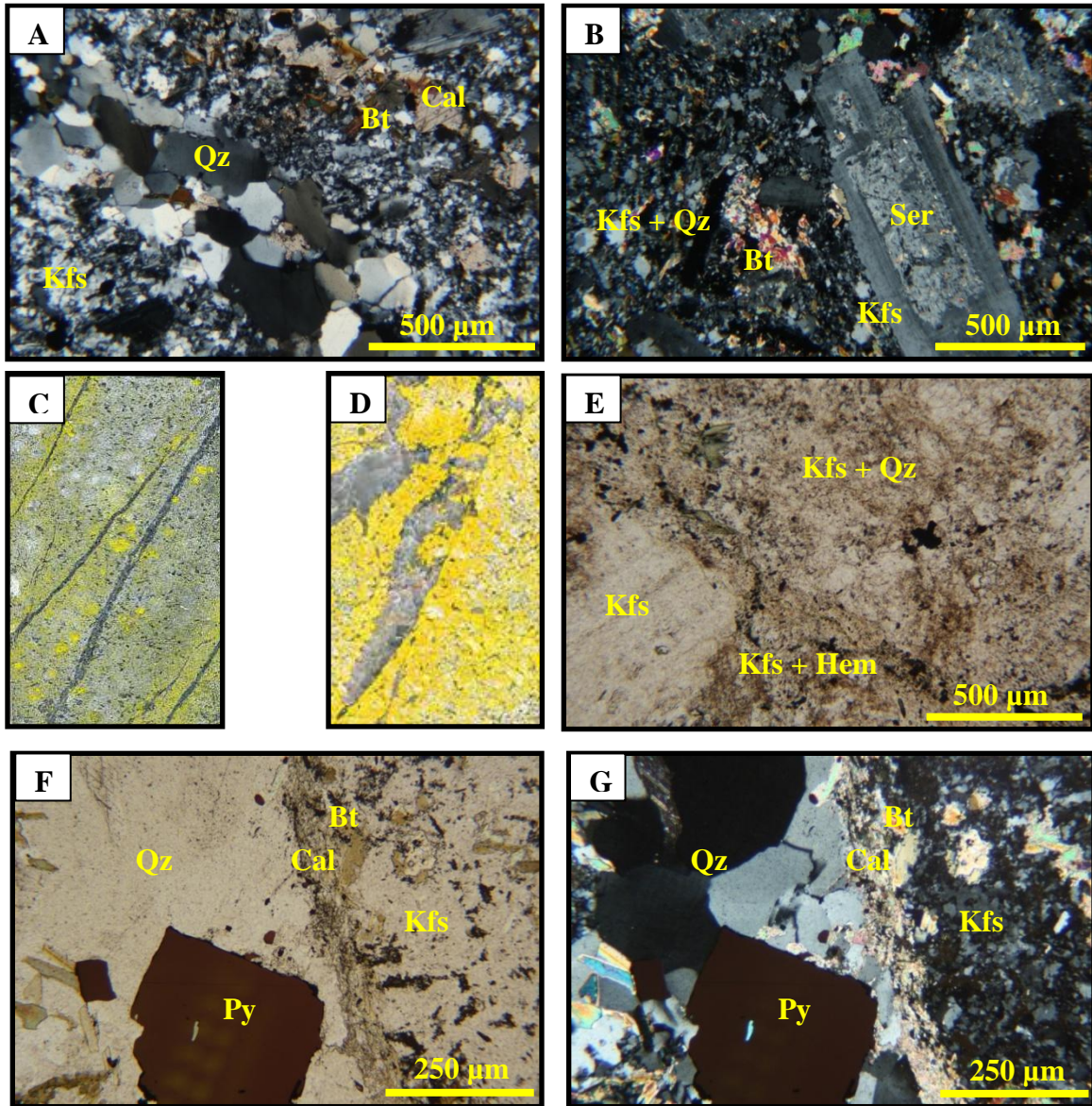


Fig. 5. Photomicrographs showing alteration minerals and their modes of occurrence. A-E show alteration in monzodiorite porphyry and F-G in Pontiac Group sediments. A. Early quartz-albite-calcite veinlets; crossed polars. B. Plagioclase phenocryst with core replaced by K-feldspar and minor sericite; crossed polars. C. Offcut block stained for K-feldspar (yellow) showing vein-related potassic alteration; block width ≈ 2.5 cm. D. Offcut block stained for K-feldspar (yellow) showing strong pervasive potassic alteration; block width ≈ 2.5 cm. E. Secondary K-feldspar associated with finely disseminated hematite; plane polarised light. F. Quartz-carbonate-pyrite veinlet (left) with an alteration halo of K-feldspar and biotite; plane polarised light. G. As in F, showing K-feldspar alteration halo; crossed polars. Py = pyrite, Au = native gold, Qz = quartz, Cal = calcite, Kfs = K-feldspar, Bt = biotite, Hem = hematite, Ser = sericite.

as disseminated grains and in mineralized veinlets. Potassic alteration was overprinted locally by massive silicification and quartz veining in the late ore stage. Second generation quartz veins are coarse-grained and commonly contain large muscovite and biotite crystals in addition to variable proportions of pyrite, calcite and chlorite. Minor chlorite replaced biotite formed during earlier stages of alteration and veining, and is most conspicuous in haloes around quartz \pm albite \pm carbonate veinlets. Carbonatization was extensive and long lived, outlasting ore stage alteration, and occurs as patchy aggregates of calcite, as well as third generation calcite-only veinlets that overprint and crosscut early quartz \pm albite \pm carbonate alteration, potassic alteration and later silicification.

VEINS

Three main generations of veins are observed in the deposit (in addition, hydrothermal breccias have been reported to occur in the Canadian Malartic orebody: Beaulieu, 2010). All are veinlets on the order of centimetres to metres in length and millimetres to centimetres in width, and are observed in all the main rock types. First and second generation veinlets are auriferous, whereas third generation veinlets post-date gold mineralization, overprinting first and second generation veinlets, as well as disseminated gold mineralization. First generation veinlets contain quartz, quartz-carbonate \pm biotite or quartz-carbonate-albite, and are generally <1 cm in diameter. They are commonly surrounded by alteration haloes containing K-feldspar, biotite, pyrite and calcite. Second generation veins average 1.5 cm in diameter, are composed of coarser-grained quartz and subordinate pyrite, calcite and chlorite. Some late second generation veins contain large muscovite and/or biotite grains. Although second generation veinlets are hosted in rocks that have experienced strong potassic alteration, they lack the potassic alteration haloes characteristic of early veinlets and generally have margins that are gradational with the host rocks. Third generation veinlets are composed only of calcite, have sharp contacts with the host rocks, and lack alteration haloes.

NATURE OF GOLD MINERALIZATION

The bulk of the gold mineralization occurs as fine-grained native gold with an average gold:silver weight ratio of 9:1, and is associated locally with subordinate gold telluride minerals, chiefly petzite and locally calaverite. The gold-bearing phases occur with pyrite and minor

(<0.1%) fine-grained chalcopyrite, galena, sphalerite, hematite (very fine disseminations of anhedral aggregates and fine- to medium-grained well-formed specularite crystals after magnetite), hessite, altaite and other telluride minerals. Native gold, tellurides, sulfides and hematite occur both as isolated grains and as complex intergrowths (Fig. 6A-G). The ore minerals occur in early veinlets (≤ 1 cm diameter) of quartz, quartz-carbonate and quartz-carbonate-biotite (first generation), later veins of quartz-pyrite-calcite-chlorite \pm muscovite \pm biotite (second generation), and as disseminated grains in the host rocks. In early veinlets, gold-bearing minerals display a strong spatial association with K-feldspar and biotite, a feature which is also evident in associated vein haloes and in the pervasively altered wall rocks. The gold-bearing phases have a very strong spatial association with pyrite, occurring most commonly as inclusions and to a somewhat lesser extent, along fractures within pyrite and at the margins of pyrite grains (Fig. 6H-J). Biotite in the altered haloes around early veinlets is foliated, suggesting that the gold mineralization was emplaced pre- or syn-deformation. In second generation mineralized veins, gold-bearing minerals occur as inclusions in pyrite and more commonly at the South Barnat orebody, along grain boundaries or fill fractures in pyrite, locally accompanied by carbonate and chlorite. These veins are associated with higher gold grades and are interpreted to be retrograde. At South Barnat, disseminated native gold and tellurides have a close spatial association with pyrite, K-feldspar and calcite in monzodiorite porphyry and graywacke, and with actinolite, pyrite and carbonate in mafic and ultramafic rocks (Fig. 6K). In rare cases, electrum occurs in the South Barnat orebody as blebby disseminated grains with native gold in association with calcite and chlorite (Fig. 6L).

MASS CHANGES ASSOCIATED WITH HYDROTHERMAL ALTERATION

Mass changes associated with hydrothermal alteration and gold mineralization were estimated using the methods of Gresens (1967), Grant (1986) and MacLean and Kranidiotis (1987). Bulk rock compositions were analyzed by Acme Analytical Laboratories Ltd., Vancouver, British Columbia, using a combination of ICP-OES and ICP-MS methods. The samples used in this evaluation were restricted to altered and unaltered graywacke from the Canadian Malartic and South Barnat orebodies. Although igneous rocks were also host to mineralization, primary compositional variability and a lack of unaltered examples preclude satisfactory analysis of associated mass changes.

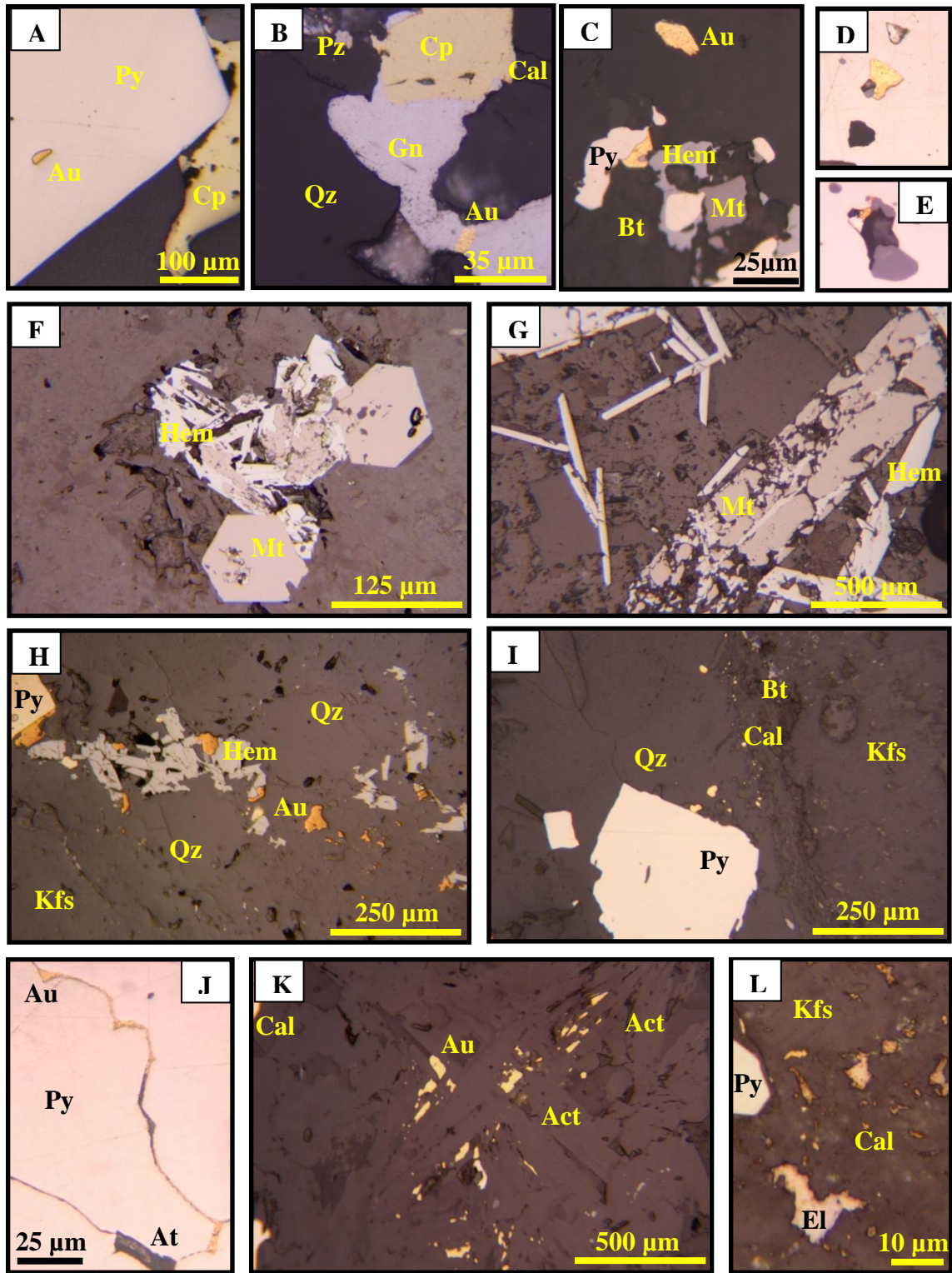


Fig. 6. Photomicrographs showing gold-bearing minerals and their modes of occurrence in reflected light. A-C, F-H, J and L show gold mineralization in monzodiorite porphyry, D and E in graywacke and K in ultramafic rock. A. Inclusion of native gold in pyrite. B. Intergrowth of galena and chalcopyrite with native gold and petzite in a quartz-biotite-carbonate veinlet. Also present in the vein is pyrite (photomicrograph A), sphalerite and hessite (not shown). C. Native gold with pyrite and adjacent hematite and magnetite. D. Inclusion of native gold in pyrite accompanied by tellurides (medium gray hessite; white altaite). E. Complex inclusion in pyrite containing native gold, calaverite (light yellow), rutile (medium gray) and ankerite (dark gray). F. Hematite replacing magnetite. G. Hematite replacing magnetite. H. Quartz-carbonate veinlet (right) with a halo of pyrite and K-feldspar, showing association of gold with pyrite and hematite. I. Quartz-pyrite veinlet (left) with K-feldspar halo, showing calcite with native gold near the margin of the veinlet. J. Native gold, calcite and altaite along a pyrite-pyrite grain boundary. K. Native gold within and along contacts of actinolite. L. Blebby grains of gold and electrum with pyrite, K-feldspar and minor calcite. Gn = galena, Py = pyrite, Cp = chalcopyrite, Au = native gold, Qz = quartz, Cal = calcite, Pz = petzite, Kfs = K-feldspar, Bt = biotite, Hem = hematite, Mt = magnetite, At = altaite, El = electrum. Act = actinolite.

A comparison of the composition of altered graywacke to that of a least-altered precursor indicates that aluminum, titanium, scandium, terbium and yttrium are linearly distributed. These elements are therefore considered to define isocons and to be immobile (Grant, 1986). Similarly, the distributions of pairs of these elements produce best fit lines that pass through the origin, indicating that they have constant ratios, providing further evidence of immobility during hydrothermal alteration. The tightest fit to a line was obtained for aluminum and titanium (Fig. 7), which was improved by screening for outliers determined by the fourth-spread method (Hoaglin et al., 1983). Although, the data set is dominated by samples from the Canadian Malartic orebody, it is evident from Figure 7 that the graywackes hosting both orebodies were similar. Aluminum and titanium are the elements in greatest abundance of those identified as immobile, and are therefore the least susceptible to nugget effects. As aluminum is distributed among the principal rock-forming minerals, mass changes were estimated by normalizing compositions of altered rocks to a constant aluminum concentration corresponding to that of the least-altered rock.

The least-altered rock composition is defined by the mean composition of six samples from the Canadian Malartic orebody and one from the South Barnat orebody. Least-altered compositions were compared to the median compositions of four types of altered rocks: 1) weakly altered; 2) weakly to moderately altered (early alteration); 3) moderately to strongly altered (dominantly potassic); and 4) strongly altered (dominantly silicic). Median compositions were based on sets of 16, 28, 24 and 13 samples for the Canadian Malartic orebody and of 0, 2, 4 and 2 for the South Barnat orebody. Consequently, reliable conclusions about mass changes during alteration are only possible for graywacke from the Canadian Malartic orebody (Fig. 8). However, where mass changes in the South Barnat orebody for particular elements appear to have been significantly different from those in the Canadian Malartic orebody, this is reported below. Nearly all the altered rocks underwent gains in K, Ca, and S (the latter almost entirely as pyrite) reaching +86, +63 and +1070 percent, respectively. Loss-on-ignition (LOI) increases with progressive alteration and relative gains were +50, +257, +429 and +478 percent, respectively, in the four alteration facies. The mass change for Si was negligible in most rocks, but reached +100 percent SiO₂ in the most strongly altered rocks of the Canadian Malartic orebody. The mass change for Na was negligible in all weakly altered rocks, and there were small gains (+19 to

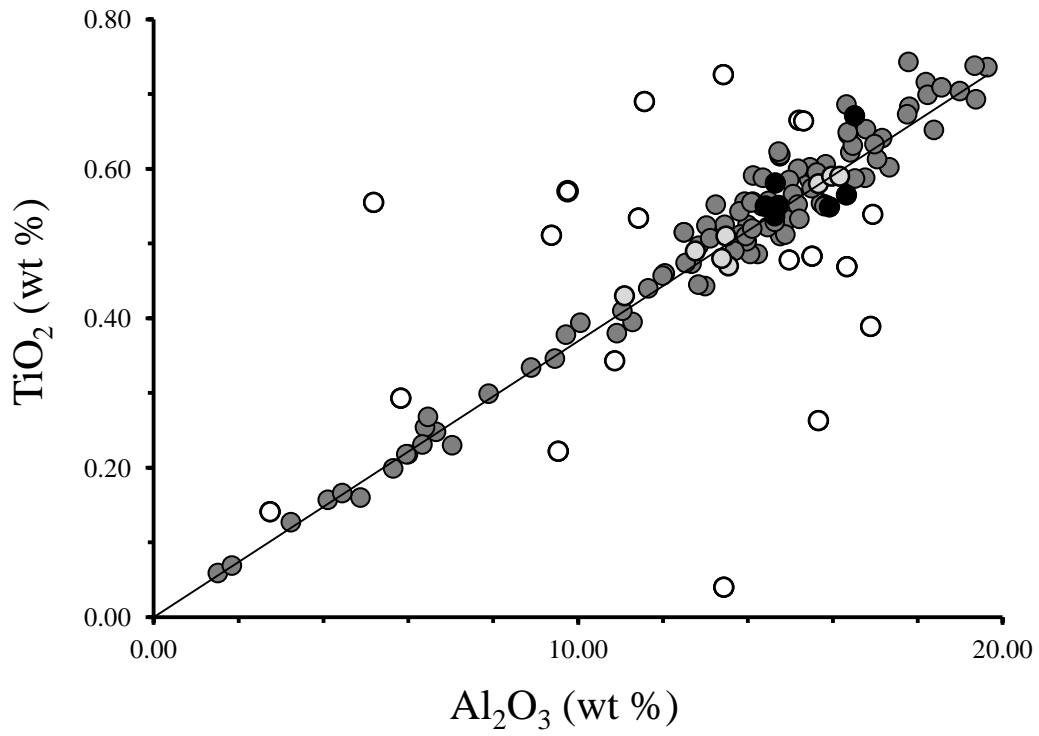


Fig. 7. Concentrations of alumina versus titania in graywacke from the Canadian Malartic (dark gray circles) and South Barnat (light gray circles) orebodies. Least altered samples are identified by black circles and outliers by white circles (see text for further detail).

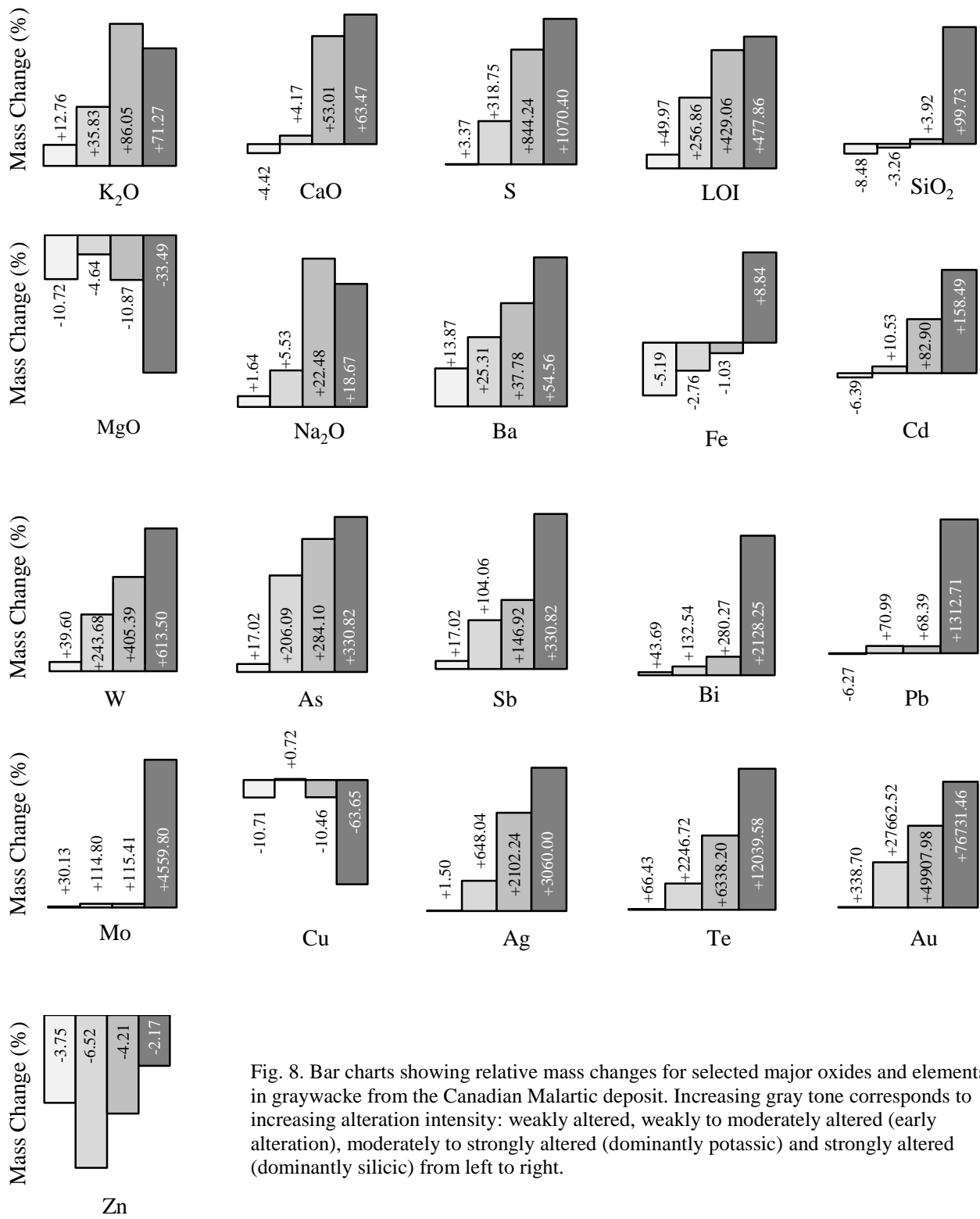


Fig. 8. Bar charts showing relative mass changes for selected major oxides and elements in graywacke from the Canadian Malartic deposit. Increasing gray tone corresponds to increasing alteration intensity: weakly altered, weakly to moderately altered (early alteration), moderately to strongly altered (dominantly potassic) and strongly altered (dominantly silicic) from left to right.

+22%) in moderately to strongly altered rocks. The mass change for Fe was negligible in all alteration facies. The only major element to show fairly consistent depletion was Mg (-11 to -33% MgO). Barium, Cd, W, Pb, As, Sb, Bi and Mo underwent large mass gains (+55% , +158%, +614%, +1313%, +331%, +331%, +2,128% and +4,560%, respectively) in the Canadian Malartic orebody and there were extremely large mass gains in Ag, Te and Au of +3,060, +12,040 and +76,731 percent, respectively, in the most strongly altered rocks.

Trace element behaviour was somewhat different in the South Barnat orebody. Barium underwent mass loss in all altered rocks (up to -27%) and Cd underwent the largest mass gain in moderately to strongly altered rocks. Molybdenum, As and Bi underwent fairly consistent gains in all alteration facies, albeit of a lesser magnitude than at Canadian Malartic (up to +324%, +124% and +155%, respectively). Tungsten, Pb and Sb all underwent similar mass gains to Canadian Malartic, with greatest gains in the most strongly altered rocks, although of lesser magnitude (+555%, +194% and +18%, respectively). There was a large mass gain in Ag of +5495 and an extremely large gain in Au of + 591,763% in the most strongly altered rocks in the South Barnat orebody. In addition, Te shows only relatively small mass gains (up to +136%).

In contrast to the trace metals listed above, Cu underwent mass loss in nearly all alteration facies in the Canadian Malartic orebody (-11 to -64%) and the South Barnat orebody (up to -78% in moderately to strongly altered rocks). Thus, although chalcopyrite is an important trace mineral in mineralized rocks, Cu was removed during alteration. Zinc behaved similarly to Cu in the Canadian Malartic orebody and underwent mass loss in all alteration facies, although very small (up to -7%), whereas at South Barnat zinc was slightly more depleted, up to -21 percent in weakly to moderately altered rocks.

TRACE ELEMENT CORRELATIONS WITH GOLD

Gold concentrations are characterized by a strongly positive correlation with Ag in both the Canadian Malartic and South Barnat orebodies (Fig. 9A). By contrast, two trends are evident in a plot of Au versus Te concentrations; there is a general trend of increasing gold with increasing tellurium, especially in the Canadian Malartic orebody, and a second steeper gold

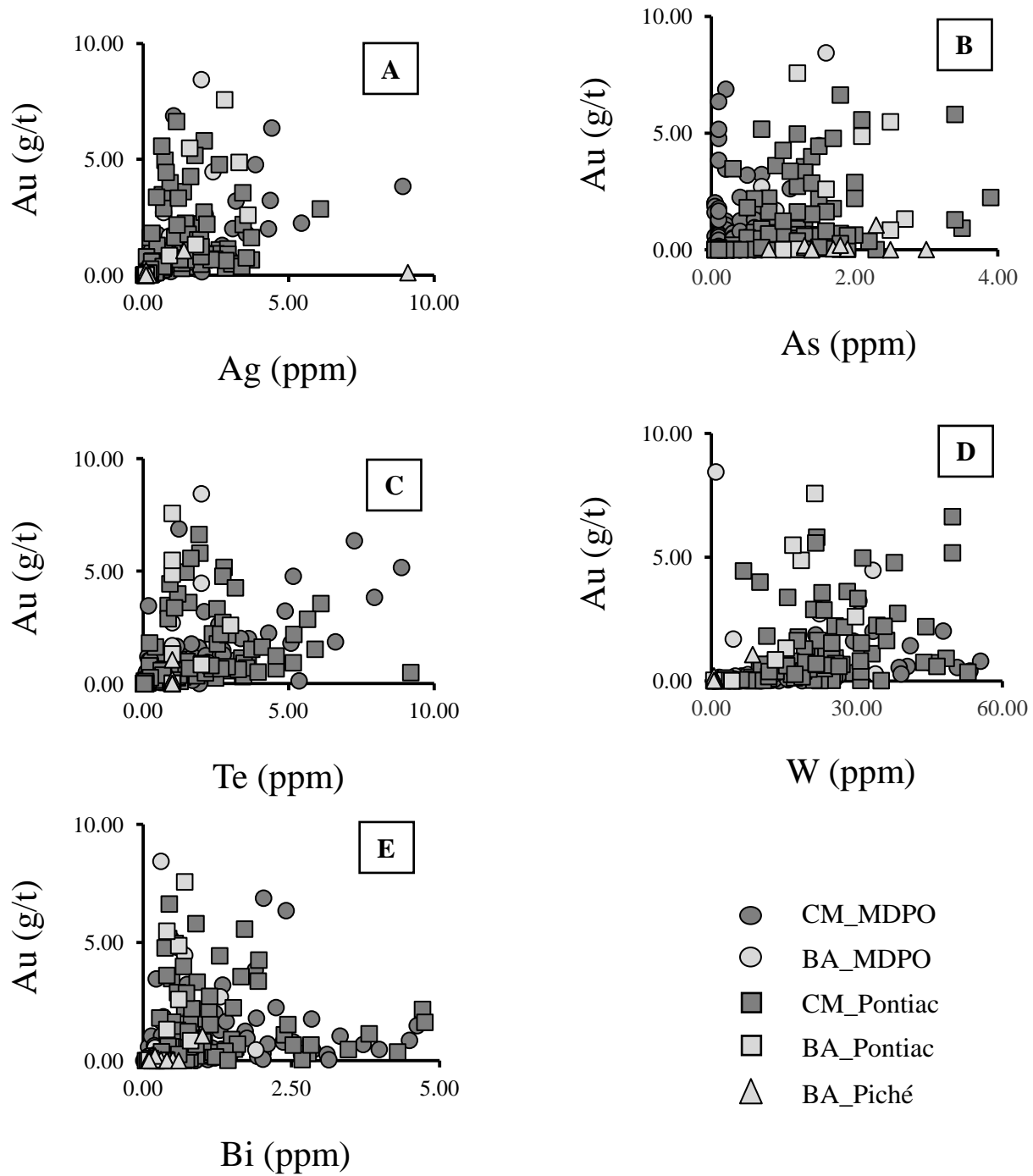


Fig. 9. Binary plots of bulk-rock gold versus the concentrations of other selected trace elements in graywacke from all lithotypes in both orebodies. CM = Canadian Malartic, BA = South Barnat, MDPO = monzodiorite porphyry.

trend with lower Te values in both orebodies (Fig. 9B). This suggests a heterogeneous distribution of native gold and telluride mineralization. A similar distribution is evident for Bi although the highest Bi values for the Canadian Malartic orebody correspond to rocks with low Au concentrations (Fig. 9C). Gold concentrations vary greatly with those of W, As, Pb, Cu, Zn, Mo, Sb and Cd in both orebodies. Arsenic concentrations are generally very low but are slightly higher in the South Barnat orebody; W concentrations are higher in the Canadian Malartic orebody (Figs. 9D and E)

STABLE ISOTOPES

Sulfur isotopic compositions of pyrite and barite were analyzed at McGill University in order to investigate the source of sulfur and estimate the temperature of gold mineralization. Ore-stage pyrite separates from crushed samples (23 of monzodiorite porphyry, 12 of Pontiac sediments, and 12 of Piché Group mafic/ultramafic rocks) were picked manually under a binocular microscope. For samples in which the pyrite grains were too small for hand picking, and in samples targeting barite (which is present only as very fine and sparse grains), rocks were pulverized to powder and the entire samples were analyzed. Powdered bulk samples and pyrite separates were reacted with chromium reduction solution (CRS) at ~100°C to liberate sulfur as hydrogen sulfide. The H₂S was then trapped using a zinc acetate solution and reacted with silver nitrate to produce silver sulfide (Canfield et al., 1986). In order to determine the sulfur isotopic composition of barite, the residue from the CRS extraction was washed and reacted with Thode solution (Thode et al., 1961) to liberate the remaining sulfur (as sulfate), which was converted to silver sulfide. Silver sulfide was in turn converted to sulfur hexafluoride by reaction with fluorine (Rumble et al., 1993) generated by heating hexafluoronickelate. The resulting solution was then purified using cryogenic traps and a gas chromatograph, and isotopic compositions were analyzed with a ThermoFinnigan MAT253 dual-inlet gas-source mass spectrometer. Results are reported relative to Vienna Cañon Diablo troilite (V-CDT), against which the international silver sulfide reference material, IAEA-S-1, has a $\delta^{34}\text{S}$ value of -0.30 per mil (Robinson, 1995). The analytical uncertainty (1 σ) was ± 0.02 per mil for both $\delta^{34}\text{S}$ and $\Delta^{33}\text{S}$ values.

The $\delta^{34}\text{S}$ values of pyrite from the monzodiorite porphyry, greywacke and mafic/ultramafic rocks have similar ranges of -3.35 to +3.20 ‰, -3.45 to +2.41 ‰, and -3.11 to

+4.30 ‰, respectively (Table 1). However, whereas the values for pyrite from monzodiorite porphyry and greywacke are fairly evenly distributed between positive and negative values, 75% of the values for pyrite from mafic and ultramafic rocks are positive. The pyrite $\Delta^{33}\text{S}$ values, with two exceptions, are positive and relatively small (<0.1 ‰); on average they are greater for greywacke and smaller for mafic and ultra-mafic rocks (Figure 10).

Separates of six pairs of minerals (four quartz-biotite and two quartz-hematite) from ore-stage veins and vein haloes were analyzed for their oxygen isotopic composition (biotite was also analyzed for hydrogen) at the Queen's University Facility for Isotope Research (QFIR), Kingston, Ontario, to estimate alteration/mineralization temperature and gain insights into the origin of the hydrothermal fluid. Oxygen was extracted from the separates by thermochemical conversion in the presence of bromine pentafluoride (Clayton and Mayeda, 1963), purified with liquid nitrogen cryotrap to remove volatile reaction products and then reacted over a hot carbon rod to convert oxygen gas to carbon dioxide. The isotopic composition of oxygen in this gas was analyzed using a Finnigan MAT252 stable isotope ratio mass spectrometer. Hydrogen was extracted using a thermal conversion elemental analyzer (TC/EA) interfaced with a ThermoFinnigan Delta^{Plus} XP stable isotope ratio mass spectrometer via continuous He flow, and analyzed as hydrogen gas.

Isotopic ratios for oxygen and hydrogen are reported as $\delta^{18}\text{O}$ and δD (V-SMOW), and have an analytical uncertainty (1σ) of ± 0.30 per mil (Table 2). The $\delta^{18}\text{O}$ values for quartz range from +8.8 to +13.4 per mil, for biotite from +5.9 to +8.9 per mil, and for hematite from +6.3 to +6.9 per mil. Values of δD for biotite range from -52 to -45 per mil, and the more negative δD values correspond to more positive $\delta^{18}\text{O}$ values.

TITANIUM CONCENTRATIONS IN VEIN QUARTZ

Twelve samples of hydrothermal vein quartz (first generation veinlets with potassic alteration haloes and second generation veins that contain coarse biotite and muscovite) were analyzed for titanium concentrations in order to apply the TitaniQ geothermometer of Wark and Watson (2006). The analyses were conducted at the University of Toronto, Ontario, using a Thermo Elemental (VG) PlasmaQuad PQ ExCell ICP-MS instrument coupled to a Nu-Wave UP-

Table 1. Values of $\delta^{34}\text{S}$, $\delta^{34}\text{S}_{\text{Fluid}}$ and $\Delta^{33}\text{S}$ for pyrite and barite

Sample ID	Lithology	Material	$\delta^{34}\text{S}$	$\delta^{34}\text{S}_{\text{Fluid}}$	$\Delta^{33}\text{S}$	Sample ID	Lithology	Material	$\delta^{34}\text{S}$	$\delta^{34}\text{S}_{\text{Fluid}}$	$\Delta^{33}\text{S}$
BA08_3008_189.6*	MDPO	Bulk	8.06	7.05	0.03	BA08_3040_362.5	Pontiac	Pyrite	2.41	1.41	0.08
BA08_3121_8	MDPO	Pyrite	2.75	1.75	0.02	BA08_3040_297.9	Pontiac	Bulk	2.12	1.12	0.07
BA08_3594_4	MDPO	Pyrite	2.05	1.05	0.09	BA08_3040_299.6	Pontiac	Pyrite	2.10	1.10	0.07
CM07_1499_201.0	MDPO	Bulk	2.03	1.03	0.10	BA08_3040_322.6	Pontiac	Pyrite	1.49	0.49	0.08
BA08_3040_180	MDPO	Bulk	1.78	0.78	0.08	BA08_3040_271.2	Pontiac	Pyrite	1.24	0.24	0.05
BA08_3068_27	MDPO	Pyrite	0.87	-0.13	0.03	BA08_3008_121.8	Pontiac	Pyrite	0.07	-0.94	0.08
CM05_667_256.3	MDPO	Bulk	0.79	-0.21	0.07	BA08_3008_116.9	Pontiac	Pyrite	-0.03	-1.03	0.09
BA08_3594_8	MDPO	Pyrite	0.56	-0.44	0.08	BA08_3121_10	Pontiac	Pyrite	-0.64	-1.64	0.04
BA08_3040_340.2	MDPO	Bulk	0.44	-0.56	0.08	BA08_3008_86.9	Pontiac	Pyrite	-0.78	-1.79	0.08
BA08_3008_250.5	MDPO	Pyrite	0.34	-0.66	0.04	CM06_719_200	Pontiac	Bulk	-1.07	-2.07	0.12
BA08_3040_241	MDPO	Pyrite	-0.39	-1.39	0.05	BA08_3008_126.9	Pontiac	Pyrite	-1.13	-2.13	0.09
BA08_3008_202.2	MDPO	Bulk	-0.47	-1.47	0.10	BA08_3121_11	Pontiac	Pyrite	-3.45	-4.45	0.04
CM06_701_298.5	MDPO	Bulk	-0.51	-1.51	0.10	BA08_3594_13	Piché	Pyrite	4.30	3.30	0.04
BA08_3008_230.7	MDPO	Pyrite	-0.79	-1.79	0.05	BA08_3594_11	Piché	Pyrite	3.67	2.67	-0.03
BA08_3068_17	MDPO	Pyrite	-0.88	-1.89	0.06	BA08_3594_15	Piché	Pyrite	3.01	2.01	0.03
BA08_3040_52.1	MDPO	Bulk	-0.93	-1.94	0.08	BA08_3594_14	Piché	Pyrite	2.51	1.51	0.02
BA08_3121_5	MDPO	Pyrite	-0.94	-1.94	0.00	BA08_3068_29	Piché	Pyrite	2.34	1.34	0.06
BA08_3121_1	MDPO	Pyrite	-1.07	-2.07	0.05	BA08_3119_9	Piché	Pyrite	1.46	0.46	0.04
BA08_3068_11	MDPO	Pyrite	-1.27	-2.27	0.03	BA08_3040_209.5	Piché	Pyrite	1.01	0.01	0.03
BA08_3008_186.6	MDPO	Bulk	-1.33	-2.33	0.07	BA08_3008_169.7	Piché	Pyrite	0.97	-0.03	0.04
BA08_3040_340.2	MDPO	Pyrite	-1.52	-2.52	0.09	BA08_3040_131.7	Piché	Pyrite	0.03	-0.97	0.04
BA08_3040_175.4	MDPO	Pyrite	-2.75	-3.75	0.07	BA08_3008_162.1	Piché	Pyrite	-0.15	-1.15	0.04
BA08_3008_189.6	MDPO	Bulk	-3.19	-4.19	0.06	BA08_3040_29.1	Piché	Pyrite	-1.59	-2.60	0.05
BA08_3040_30.5	MDPO	Pyrite	-3.35	-4.36	0.06	BA08_3068_2	Piché	Pyrite	-3.11	-4.11	0.03

¹All data are given in per mil (‰)

²Fluid compositions calculated using the fractionation equations of Ohmoto and Rye (1979) and Ohmoto and Lasaga (1982)

³BA indicates that the sample is from the South Barnat orebody and CM that it is from the Canadian Malartic orebody and MDPO = monzodiorite porphyry

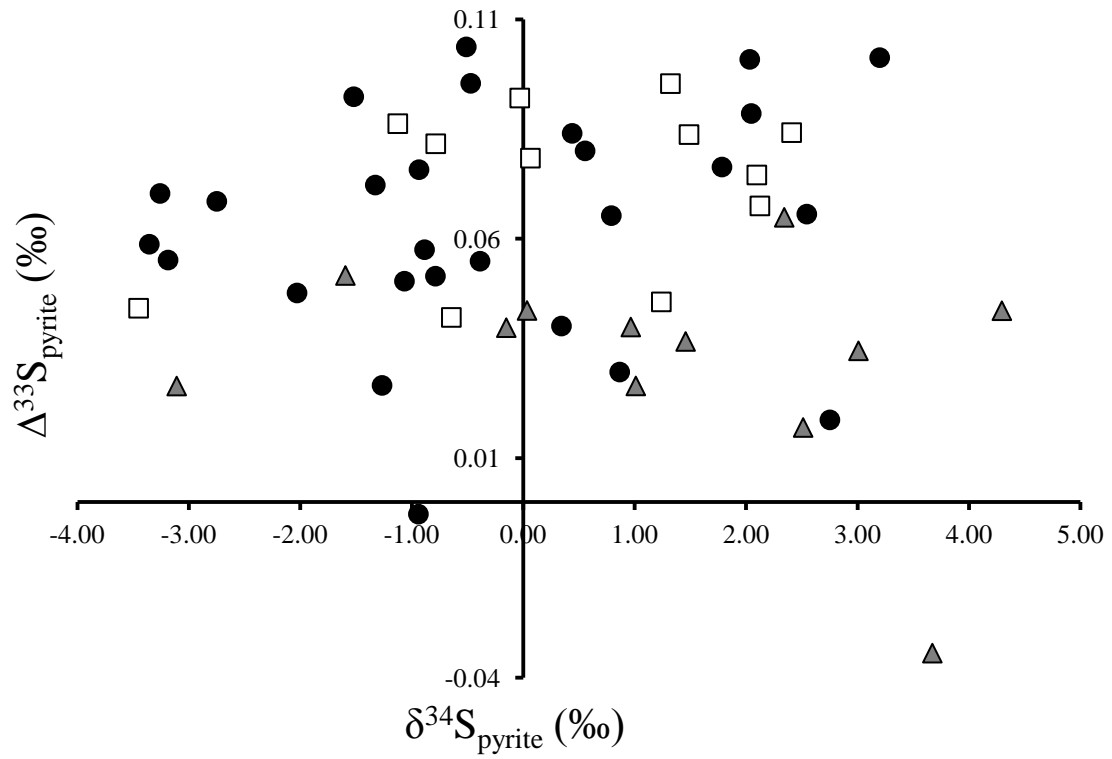


Fig. 10. A plot of $\delta^{34}\text{S}$ versus $\Delta^{33}\text{S}$ for pyrite from porphyritic monzodiorite (black circles), Pontiac graywackes (open squares) and mafic/ultramafic rocks (dark gray triangles) from the Piché Group. The gray ellipse shows the generally more positive range of isotopic compositions for Piché Group rocks.

Table 2. Isotopic ratios for oxygen (quartz, hematite, biotite), hydrogen (biotite) and corresponding estimated isotopic compositions of the ore fluid assuming 475°C

Sample ID	Lithology	Material	G.V	$\delta^{18}\text{O}$	$\delta^{18}\text{O}_{\text{Fluid}}$	δD	$\delta\text{D}_{\text{Fluid}}$
BA08_3040_249.6	MDPO	Quartz	2	11.9	8.19		
BA08_3040_249.6	MDPO	Biotite	2	6.8	6.36	-47.00	-47.00
BA08_3040_52.1	MDPO	Quartz	2	8.9*	5.26		
BA08_3040_52.1	MDPO	Biotite	2	8.9*	8.47	-49.00	-49.00
BA08_3121_2	MDPO	Quartz	2	12.0	8.36		
BA08_3121_2	MDPO	Biotite	2	6.9	6.43	-52.00	-52.00
BA08_3119_16	MDPO	Quartz	2	8.8*	5.15		
BA08_3119_16	MDPO	Biotite	2	5.9*	5.50	-45.00	-45.00
BA08_3121_5	MDPO	Quartz	1	11.8	8.17		
BA08_3121_5	MDPO	Hematite	1	6.3	8.18		
BA08_3040_189.8	MDPO	Quartz	1	13.4	9.77		
BA08_3040_189.8	MDPO	Hematite	1	6.9	8.74		

¹All data are given in per mil (‰)

²Samples are from mineral separates from mineralized veins and haloes in the South Barnat orebody (BA)

³Oxygen isotopic fluid compositions were calculated using the fractionation equations of Bottinga and Javoy (1975; 1973) and Clayton and Epstein (1961) for biotite, quartz and hematite respectively. The hydrogen isotopic fluid composition was calculated using the fractionation equation of Suzuoki and Epstein (1976) for biotite

⁴“*” indicates interpreted disequilibrium. MDPO = monzodiorite porphyry, G.V. = generation of veining

213 nm laser ablation microscope. The laser beam was fired at a 10 Hz repetition rate with an energy of $\sim 1.8 \text{ J/cm}^2$. The spot size was $75 \mu\text{m}$ and data acquisition was based on 50 ms point ablation. Data reduction and calculation of titanium concentrations were performed using the GLITTER! software package (Griffen et al., 2008); the analytical uncertainty (1σ) was calculated to be $\pm 0.19 \text{ ppm}$. The titanium concentration in the quartz ranges from 1.80 to 7.57 ppm, and averages 4.53 ppm for first generation veinlets and 5.45 ppm for second generation veins (Table 3).

FLUID INCLUSION LEACHATES

Fluid inclusions are fairly common in quartz veinlets at the Canadian Malartic deposit, but most are less than $1 \mu\text{m}$ in diameter. They contain liquid and vapour, and in some rare, larger inclusions (2 to $3 \mu\text{m}$ diameter) also contain halite daughter crystals (Figs. 11A and B). The fluid inclusions commonly define secondary trails, but most are of indeterminate origin (Fig. 11C). The small size of the inclusions precludes microthermometric and micro-quantitative analyses of individual inclusions, and thus analyses were limited to determination of the composition of inclusion leachates.

Fluid was extracted from ten samples of hydrothermal vein quartz similar to those used for the determination of titanium concentration. The extractions were conducted at McGill University using the methods of Botrell et al. (1988) and Halter and Williams-Jones (1995). Quartz grains (between 0.5 and 1 g per sample) were cleaned using a series of nitric acid and de-ionized water washes to dissolve impurities and create a strong positive charge on grain surfaces to repel singly- or doubly-charged cations. Once clean, samples were crushed to powder, split into two aliquots and leached, one split with 30 mL de-ionized water (for analyses of anions) and the other with 100 mL 1 M nitric acid solution containing 200 ppm lanthanum to prevent adsorption of highly charged cations on grain surfaces (for analyses of cations). Quartz powder was filtered from the leachates, which were analyzed by ion chromatography by Activation Laboratories Ltd., Ancaster, Ontario and ICP-MS and ICP-AES by Geolabs Geoscience Laboratories, Sudbury, Ontario, for anion and cation contents, respectively. Leachates from selected pre-crushed samples were analyzed to assess contamination from incompletely cleaned

Table 3. Titanium concentrations in hydrothermal quartz associated with gold mineralization in the Canadian Malartic deposit

Sample ID	Lithology	G.V.	Ti (ppm)
CM06_698_218.2	MDPO	1	7.57
CM06_698_218.2	MDPO	1	6.44
CM06_698_218.2	MDPO	1	7.17
BA08_3040_37.8	MDPO	1	2.53
BA08_3040_37.8	MDPO	1	1.80
BA08_3068_24	MDPO	1	5.99
BA08_3068_24	MDPO	1	6.62
BA08_3040_249.6	MDPO	2	4.34
BA08_3040_249.6	MDPO	2	3.51
CM07_1540_20.15	MDPO	2	4.66
CM07_1540_20.15	MDPO	2	4.71
SLADEN 2	MDPO	2	4.21
SLADEN 2	MDPO	2	4.72
CM05_665_31.5	Pontiac	2	5.24
CM05_665_31.5	Pontiac	2	4.89
CM06_794_40.9	Pontiac	2	5.64
CM06_794_40.9	Pontiac	2	5.65
CM06_794_40.9	Pontiac	2	5.96
CM08_1969_165.4	Pontiac	2	4.41
CM08_1969_165.4	Pontiac	2	4.30
BA08_3040_52.1	MDPO	2	4.10
BA08_3040_52.1	MDPO	2	5.88
CM07_1402_227	MDPO	2	2.10
CM07_1402_227	MDPO	2	2.62

¹ The data are reported in ppm

²CM indicates that the sample is from the Canadian Malartic orebody and BA indicates that it is from the South Barnat orebody

³MDPO = monzodiorite porphyry and G.V. = generation of vening

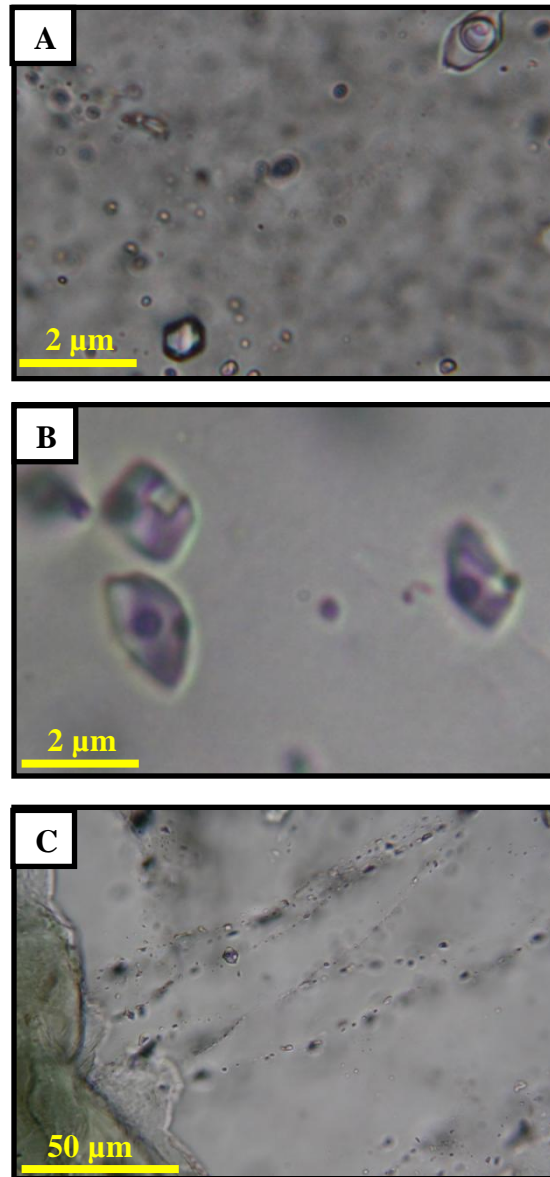


Fig. 11. Photomicrographs of fluid inclusions in hydrothermal quartz. A. Fluid inclusions from a second generation vein showing both liquid and vapour phases. B. Fluid inclusions from a first generation vein with halite daughter crystals. C. Secondary trails of fluid inclusions in a first generation vein.

grain surfaces, as was filtered leaching solution to assess the extent of incorporation of ions from filter paper. These constituted blank analyses (together with a leachate from 99.99% silica powder) to which the compositions of the leached inclusion fluids were compared and corrected by subtracting the blank compositions.

A total of 65 elements were analyzed in the leachates. Many elements were below the lower detection limit and others had concentrations similar to or greater than those in the blank solutions. A suite of 26 elements was determined to be in concentrations greater than those of the blank solutions: Ca, Na, Mg, Al, K, S, Si, Fe, Cl, S, N, Ti, Cu, W, Pb, Sn, Ba, Rb, Sr, Co, Cs, Tl, Cd, Li, V and Cr. Results are reported for the above elements in ratios with Ca as the denominator to permit comparison among samples (Table 4). The principal ions in the leachates are Ca, Na, Mg, Al, S, Cl and SO₄, and the important trace metals are Cu, Sr and Ba. The leachate compositions vary considerably, but average concentrations of Mg, Al, K, S, Fe, SO₄, Ti, Cu, Pb, Ba, Rb, Sr, Co, Li, V and Cr are greater in first generation veinlets, and Ca, Na, Si, Cl, NO₃, W, Sn and Cd greater in second generation veins.

DISCUSSION

TEMPERATURE-PRESSURE CONDITIONS

The temperature of gold mineralization at Canadian Malartic was estimated using a combination of stable isotope geothermometers and the titanium-in-quartz geothermometer. A temperature of equilibration for a single barite-pyrite pair from an ore sample was calculated using the measured sulfur isotope compositions (Table 1) and the fractionation equations of Ohmoto and Rye (1979) and Ohmoto and Lasaga (1982) for pyrite-H₂S and for barite-H₂S, respectively. Although bulk rock extraction methods had to be used to liberate the sulfur (barite could not be mechanically separated), textural relationships for this sample indicate that pyrite and barite formed contemporaneously. Furthermore, the observation that their $\Delta^{33}\text{S}$ values, within analytical uncertainty, are the same indicates that the two minerals were in isotopic equilibrium (Jamieson et al., 2006). The temperature calculated using the barite-pyrite geothermometer is $481 \pm 25^\circ\text{C}$. Two quartz-hematite pairs from first generation veins were selected for oxygen isotope contemporaneously. Temperatures were calculated using the

Table 4. Composition of fluid inclusion leachates from hydrothermal quartz associated with mineralization at the Canadian Malartic deposit

Analyte	Ca	Na	Mg	Al	K	S	Si	Fe	Cl	SO₄	NO₃	Ti	Cu	
DL (ppb)	30	100	10	50	50	135	15	30	30	30	10	1	2	
Sample ID	G.V.													
BA08_3121-5	1	57.000	5.263	1.456	1.579	1.579	15.807	-	0.930	7.544	25.614	-	0.032	0.719
BA08_3121-4	1	82.000	0.000	1.427	1.159	0.854	11.159	5.988	1.085	3.293	4.756	-	0.078	0.316
BA08_3040-189.8	1	193.000	-	0.394	0.306	0.311	-	3.119	0.420	2.124	3.575	-	0.010	0.026
CM07-1540-20.1	2	42.000	7.143	1.714	-	-	5.238	7.214	-	29.286	9.048	0.476	0.024	0.076
CM07-1540-20.1	2	140.000	-	0.207	0.464	-	4.450	-	0.214	1.857	1.214	0.571	0.011	0.107
CM08-1969-165.4	2	182.000	2.198	0.346	0.346	0.604	-	2.198	-	4.341	5.769	75.550	0.006	0.067
BA08_3040-249.6	2	214.000	0.000	0.720	0.598	0.514	5.509	2.136	0.748	1.963	4.673	0.327	0.062	0.039
CM06-799-40.9	2	63.000	4.762	0.794	0.000	0.952	-	12.619	-	5.397	5.556	-	0.019	0.087
BA08_3068-15	2	501.000	0.120	0.595	1.126	0.539	1.325	1.910	0.763	0.958	1.297	0.040	0.065	0.043

Analyte	W	Pb	Sn	Ba	Rb	Sr	Co	Cs	Tl	Cd	Li	V	Cr	
DL (ppb)	0.1	0.02	0.1	0.2	0.05	1	0.05	0.005	0.01	0.1	0.1	0.03	0.2	
Sample ID	G.V.													
BA08_3121-5	1	0.005	0.017	-	40.401	0.003	2.160	0.003	0.000	0.001	-	-	0.002	0.004
BA08_3121-4	1	0.002	0.023	-	0.911	0.003	0.078	-	0.000	0.000	0.012	0.002	0.005	-
BA08_3040-189.8	1	0.001	0.002	-	0.498	0.001	1.273	-	0.000	0.000	-	-	0.001	0.001
CM07-1540-20.1	2	0.006	0.037	-	0.827	0.002	0.179	-	0.000	-	-	-	0.002	-
CM07-1540-20.1	2	0.001	0.007	0.001	0.699	0.001	0.069	0.000	0.000	0.000	-	-	0.001	0.003
CM08-1969-165.4	2	0.001	0.009	0.001	0.018	0.001	0.015	-	0.000	0.000	0.045	0.001	0.000	0.002
BA08_3040-249.6	2	0.001	0.002	0.001	1.850	0.002	1.289	0.000	0.000	0.000	-	0.001	0.004	0.002
CM06-799-40.9	2	0.008	0.009	-	0.044	0.002	-	-	0.000	0.001	-	-	0.002	-
BA08_3068-15	2	0.002	0.004	0.000	0.418	0.002	0.026	0.001	0.000	0.000	-	0.001	0.002	0.001

¹BA indicates that the sample is from the South Barnat orebody and CM indicates that it is from the Canadian Malartic orebody

²“-“ indicates the element ratioed to Ca was below detection limit, DL = detection limit and GV. = generation of veining

fractionation equations of Bottinga and Javoy (1973) and Clayton and Epstein (1961) for quartz-H₂O and hematite-H₂O, respectively, and yielded values of $476 \pm 44^\circ\text{C}$ and $420 \pm 41^\circ\text{C}$. The first temperature is for a sample that contains native gold in association with quartz and hematite, thereby providing a direct estimate of the temperature of mineralization. The quartz-biotite oxygen isotope geothermometer was applied to four quartz-biotite pairs from second generation veins. These pairs yielded temperatures ranging from $630 \pm 23^\circ\text{C}$ to $2247 \pm 410^\circ\text{C}$ using the quartz-biotite fractionation equation of Bottinga and Javoy (1975) and clearly reflect disequilibrium. The titanium-in-quartz geothermometer, TitaniQ, of Wark and Watson (2006) was applied to 11 quartz samples, three from first generation veins and eight from second generation veins. Given the presence of rutile in altered wall-rock adjacent to the veins, the activity of titania was assumed to be unity. The mean temperature for first generation veins in the South Barnat orebody is $461 \pm 17^\circ\text{C}$, and for a first generation vein in the Canadian Malartic orebody is $505 \pm 3^\circ\text{C}$; second generation veins in both orebodies were estimated to have formed at $473 \pm 3^\circ\text{C}$. Based on the data reported above (excluding values calculated using the quartz-biotite geothermometer), the temperature estimated for formation of the Canadian Malartic deposit is $475 \pm 35^\circ\text{C}$ (Table 5).

Although pressure could not be estimated quantitatively, some insight about likely pressure conditions is provided by the association of carbonate minerals and gold mineralization, and the inference that the ore fluid contained significant CO₂. If, as is argued below, the source of the ore fluid was a magma, then it follows that the magma must have been emplaced at considerable depth. The reason for this is that the solubility of CO₂ in magmas is highly dependent on pressure and only becomes significant at pressures >3 kbar (at 3 kbar the solubility of CO₂ in a rhyolitic magma is approximately 1200 ppm, assuming a conservative water content of 5 wt%; Lowenstern, 2001). Although it is possible to produce a fluid with a high mole fraction of a CO₂ by greatly limiting the extent of degassing, generation of the amount of fluid required to produce the observed veining and alteration assumes substantial degassing and correspondingly low proportions of CO₂. Support for the notion that a magmatic source for the fluid was likely deep-seated is provided by the observation that CO₂-bearing fluid inclusions and carbonate alteration are rarely found in porphyry ore deposits; these are thought to be emplaced at depths of 1 to 4 km (≤ 1.2 kbar; Sillitoe, 2010). In contrast to typical porphyry deposits, Archean gold

Table 5. Estimated temperatures for mineralization at the Canadian Malartic deposit

Sample ID	G.V.	Geothermometer	T (°C)	±	Sample ID	V.G.	Geothermometer	T (°C)	±
BA08_3008_189.6	1	Barite-Pyrite	480.94	25.47	CM05_665_31.5	2	TitaniQ	484.44	2.39
BA08_3121_5	1	Quartz-Hematite	475.71	44.38	CM05_665_31.5	2	TitaniQ	479.90	2.35
BA08_3040_189.8	1	Quartz-Hematite	419.77	40.66	CM06_794_40.9	2	TitaniQ	489.34	2.39
BA08_3040_249.6	2	Quartz-Biotite	640.93	23.24	CM06_794_40.9	2	TitaniQ	489.46	2.39
BA08_3040_52.1	2	Quartz-Biotite	2246.63	410.28	CM06_794_40.9	2	TitaniQ	493.06	2.61
BA08_3121_2	2	Quartz-Biotite	631.11	23.02	CM08_1969_165.4	2	TitaniQ	473.20	2.34
BA08_3119_16	2	Quartz-Biotite	1003.81	30.77	CM08_1969_165.4	2	TitaniQ	471.58	2.35
BA08_3040_249.6	2	TitaniQ	472.17	5.59	BA08_3040_52.1	2	TitaniQ	468.55	2.36
BA08_3040_249.6	2	TitaniQ	458.82	2.37	BA08_3040_52.1	2	TitaniQ	492.15	2.45
CM07_1540_20.15	2	TitaniQ	476.76	2.34	CM07_1402_227	2	TitaniQ	428.41	2.24
CM07_1540_20.15	2	TitaniQ	477.45	2.37	CM07_1402_227	2	TitaniQ	441.19	2.30
CM05_698_218.2	1	TitaniQ	509.60	3.50					
CM05_698_218.2	1	TitaniQ	498.34	2.89					
CM05_698_218.2	1	TitaniQ	505.78	3.15	MINIMUM			419.77	40.66
BA08_3040_37.8	1	TitaniQ	439.14	2.27	MAXIMUM			509.60	3.50
BA08_3040_37.8	1	TitaniQ	419.77	2.24	MEAN			473.59	6.40
BA08_3068_24	1	TitaniQ	493.40	2.40					
BA08_3068_24	1	TitaniQ	500.24	2.41					
SLADEN 2	2	TitaniQ	470.23	2.35					
SLADEN 2	2	TitaniQ	477.59	2.37					

¹Isotope equilibrium fraction factors for barite-H₂S are taken from Ohmoto and Lasaga (1982), for pyrite-H₂S from Ohmoto and Rye (1979), for quartz-H₂O and for biotite-quartz from Bottinga and Javoy (1973; 1975), and for hematite-H₂O from Clayton and Epstein (1961)

²G.V. = generation of veining

³Minimum, maximum and mean temperatures exclude quartz-biotite data

mineralization is generally accompanied by carbonatization, and estimates for the pressure of emplacement are typically in the range 3 to 5 kbar (Brown and Lamb, 1986). For this reason and the reasons presented earlier, we therefore conclude that the Canadian Malartic deposit formed from fluids originating at a depth of ≥ 10 km (≥ 3 kbar). This fluid would have risen to shallower crustal levels, currently represented by the depth of emplacement of the monzodiorite porphyry, which hosts much of the gold mineralization. However, without information on the timing of mineralization relative to intrusion, the actual depth and thus pressure of mineralization cannot be known.

f_{O_2} , pH AND ΣaS

In order to constrain f_{O_2} , pH and sulfur activity, stability relationships were determined for minerals in the Fe-O-S system as a function of $\log f_{O_2}$ - pH, at 475°C and pressures of 1 to 5 kbar using the computer program Unitherm (Shvarov and Bastrakov, 1999); pH was established using the muscovite-K-feldspar buffer. Thermodynamic data for the calculations were taken from Johnson et al. (1992); Robie and Hemingway (1995); Shock et al. (1997); Sverjensky et al. (1997); Holland and Powell (1998); and Pal'yanova and Drebuschak (2002). In the absence of fluid inclusion microthermometric data, the chloride concentration of the fluid was assumed to be ~1 m (6 wt % NaCl) and the potassium concentration to be ~0.08 m, assuming equilibrium of the fluid with K-feldspar and albite (Fig. 12). The value of ΣaS was set at 0.1, which is the minimum value required for equilibrium between pyrite and hematite (Fig. 13). As formation of first generation, auriferous veins was marked by the coexistence of pyrite, hematite, K-feldspar and muscovite (Fig. 4), we conclude, based on Figure 12, that conditions of ore formation were relatively oxidising ($\log f_{O_2}$ approximately -19) and weakly acidic (pH 4.5).

SOURCE OF FLUIDS

Several lines of evidence suggest that the fluids responsible for the gold mineralization were of magmatic origin. The first of these is that, like magmatic-hydrothermal deposits of indisputable origin, e.g., porphyry deposits, the dominant alteration is potassic and this alteration is intimately associated with the deposition of the ore minerals. It could be argued that potassic

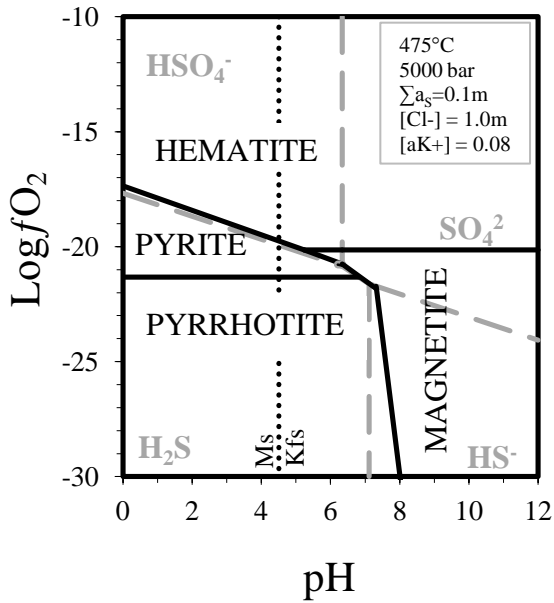
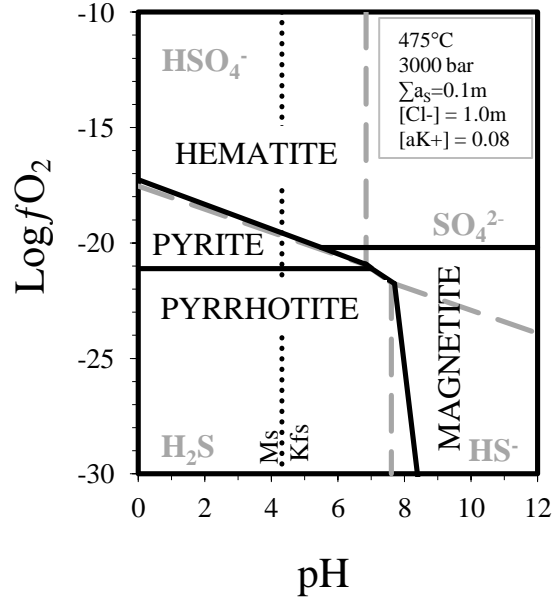
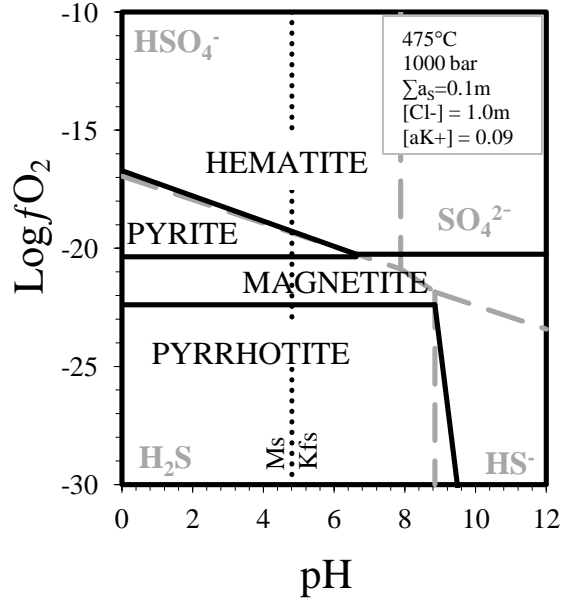


Fig. 12. Stability relationships of minerals in the Fe-O-S system as a function of $\log f_{O_2}$ and pH at 475°C and pressures 1 to 5 kbar. Also shown is the location of the muscovite-K-feldspar pH buffer (dotted line). Ms = muscovite, Kfs = K-feldspar. Phase boundaries were calculated using the computer program HCh (Shvarov and Bastrakov, 1999).

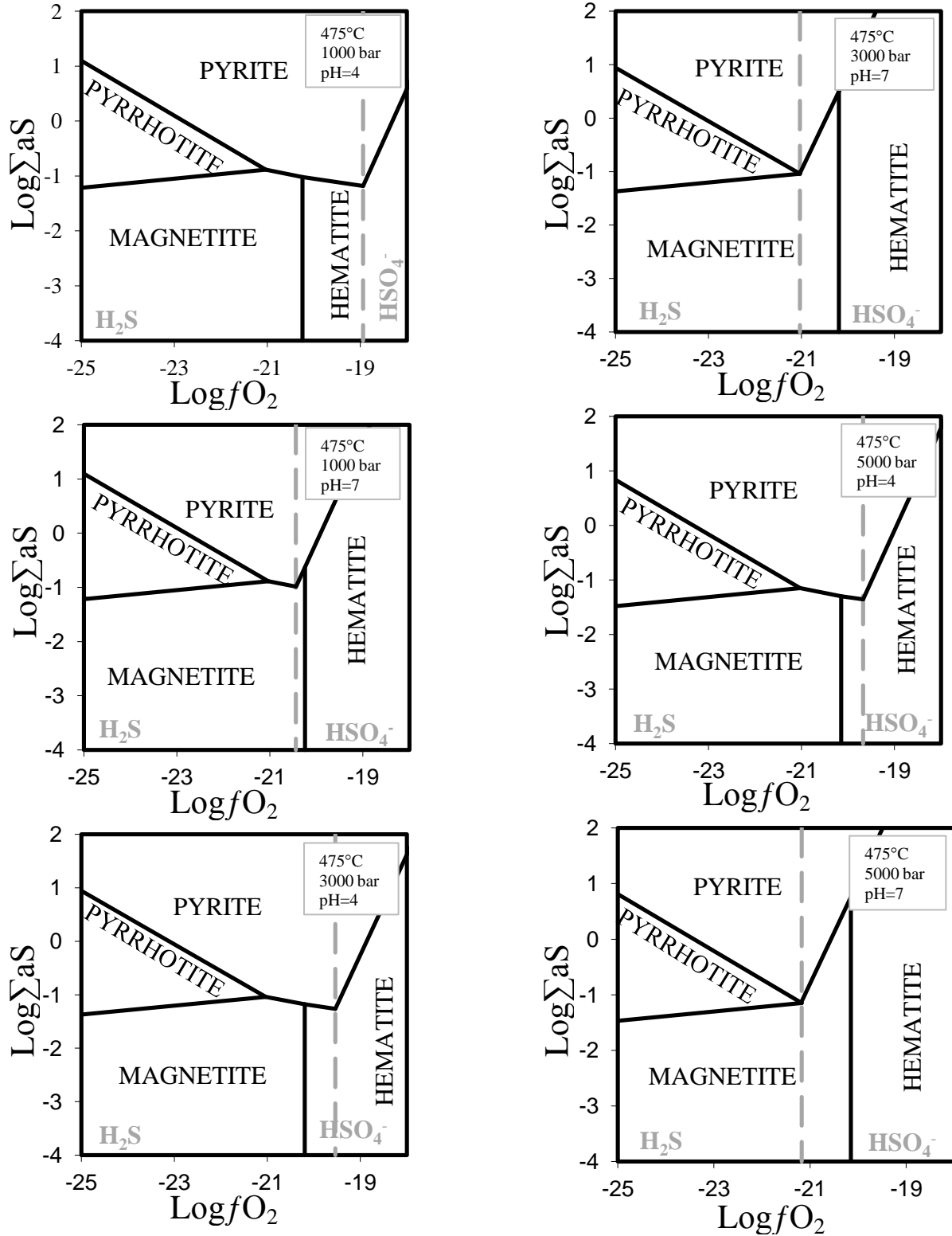


Fig. 13. Stability fields of minerals in the Fe-O-S system as a function of $\log \Sigma a_S$ and $\log f_{O_2}$ at 475°C, 1 to 5 kbar and pH conditions of 4-7. Phase boundaries were calculated using Hch (Sharov and Bastrakov, 1999).

alteration was produced by a fluid of meteoric or metamorphic origin that equilibrated with Pontiac sediments, but this seems unlikely given their composition (graywackes). Such fluids would likely have lower potassium contents and higher contents of elements like calcium and sodium than was apparently the case for the Malartic ore fluid (see below).

A second line of evidence is that the composition of the fluid inclusion leachates is very similar to that of typical magmatic-hydrothermal fluids. Figure 14 compares the compositions of the leachates to those of magmatic, metamorphic and brines/sedimentary formation waters. The Na/Ca, K/Ca, Fe/Ca, Li/Ca and Cl/Ca ratios of the Canadian Malartic leachates are all remarkably similar to those of magmatic water and quite different from those of brines/sedimentary formation waters. The Canadian Malartic leachates are also very different from metamorphic waters in respect to all of the above ratios except Fe/Ca. The leachate data therefore confirm that the potassic alteration could not have resulted from a fluid of metamorphic or formational origin that equilibrated with Pontiac sediments (see above).

Further evidence that the mineralizing fluid was magmatic is provided by the oxygen and hydrogen isotopic compositions estimated for this fluid (Fig. 15). The oxygen isotope composition of the fluid, $\delta^{18}\text{O}_{\text{fluid}}$, was calculated from the measured $\delta^{18}\text{O}$ values for quartz from first and second generation veins, for biotite from second generation veins, and for hematite from first generation veins. These calculations employed the fractionation equations of Bottinga and Javoy (1975; 1973) and Clayton and Epstein (1961), and assumed a temperature of 475°C. The value of $\delta\text{D}_{\text{fluid}}$ was calculated for biotite from second generation veins using the fractionation equation for biotite-H₂O of Suzuoki and Epstein (1976), assuming the same temperature. These calculations yielded $\delta^{18}\text{O}_{\text{fluid}}$ values for H₂O between +5.15 and +9.77 per mil and $\delta\text{D}_{\text{fluid}}$ values between -52.96 and -45.96 per mil. Although the quartz-biotite pairs yielded anomalously high temperatures, (see above), and isotopic compositions of H₂O calculated with these data, assuming a temperature of 475°C, should therefore be considered unreliable, in practice the errors introduced by this assumption are very small. For example, a 200°C increase in the assumed temperature of equilibration produced an increase of 0.08 per mil in the values of $\delta^{18}\text{O}_{\text{fluid}}$ and a negligible increase in the $\delta\text{D}_{\text{fluid}}$ values. The ranges of $\delta^{18}\text{O}_{\text{fluid}}$ (+5.15 to +9.77‰)

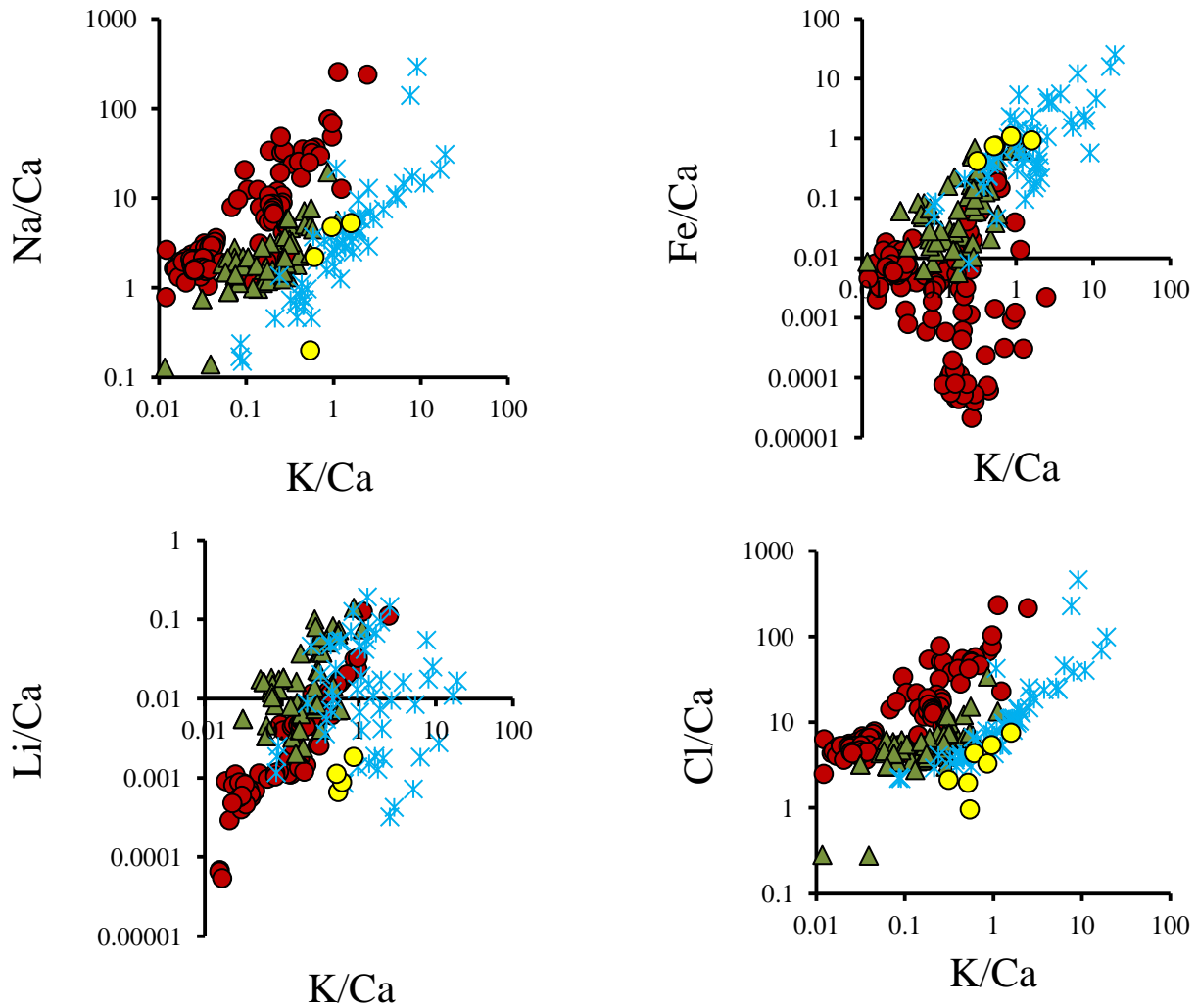


Fig. 14. Comparison of the compositions of hydrothermal fluid from ore stage quartz from Canadian Malartic (yellow circles) with those of typical brines/formation waters (red circles), metamorphic waters (green triangles) and magmatic waters (blue asterisks). The data for brines/formation waters are from Carpenter et al. (1974) and Connolly et al. (1990), for metamorphic waters are from Munz et al. (1995), Banks et al. (1999; 2000) and McCaig et al. (2000) and for magmatic waters are from Campbell et al. (1995), Smith et al. (1996) and Klemm et al. (2007). The Cl concentrations of magmatic fluids from Klemm et al., (2007) were calculated based on the reported salinities.

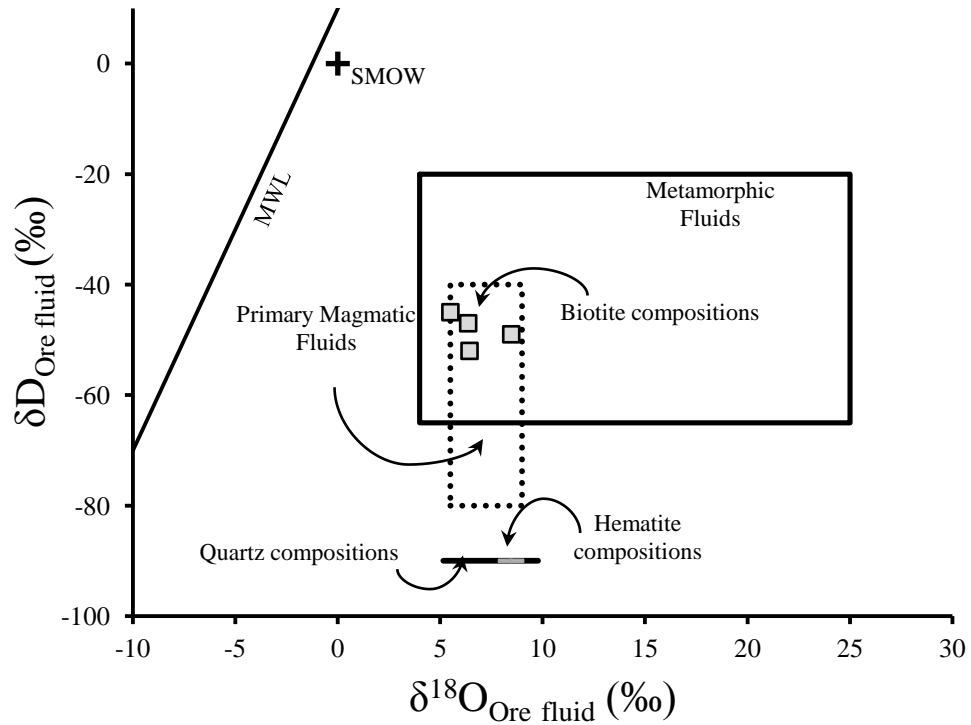


Fig. 15. Oxygen and hydrogen isotope compositions of fluids in the South Barnat orebody, interpreted from the biotite isotopic composition compared to those of typical magmatic, metamorphic and meteoric waters. Oxygen isotope compositions of fluids based on the compositions of quartz and hematite are shown below the fields of magmatic and metamorphic water and range from approximately +5.15 to +9.77‰. The fields for metamorphic and magmatic waters are from Taylor (1974) and the meteoric water line (MWL) is from Craig (1961). SMOW = standard mean ocean water.

and δD_{fluid} (-52.96 to -45.96‰), correspond to those of magmatic fluid and thus also to those of metamorphic fluids (the two fields partially overlap; Fig. 15). However, taken in conjunction with the evidence presented earlier, it seems more reasonable to conclude that they represent the signature of a gold mineralizing fluid that had a magmatic source.

SULFUR SOURCE

The sulfur isotopic composition of the mineralizing fluid, $\delta^{34}\text{S}_{\text{fluid}}$, calculated for equilibrium with pyrite using the fractionation equation of Ohmoto and Rye (1979) and the inferred temperature of 475°C (assuming $\delta^{34}\text{S}_{\text{fluid}} = \delta^{34}\text{S}_{\text{H}_2\text{S}}$), ranges between -4.45 and +3.30 per mil, with 85 percent of these values being within ± 3 of 0 per mil. This latter range of values coincides perfectly with that reported for magmatic sulfur (Ohmoto, 1986).

The only potential source for sulfur in the Canadian Malartic deposit, other than a magma or igneous rock (characterized by near zero $\delta^{34}\text{S}$ and $\Delta^{33}\text{S}$ values; Ohmoto, 1986; Mather et al., 2006) is sedimentary rock, i.e., diagenetic pyrite in the Pontiac metasedimentary rocks. Although the $\delta^{34}\text{S}$ signature for Archean sedimentary sulfur (sulfide and sulfate) is near 0 per mil (Lambert et al., 1978; Hattori et al., 1983), the contribution of sedimentary sulfur can be evaluated using $\Delta^{33}\text{S}$, which provides a unique, chemically conservative tracer of transfer in the Archean sulfur cycle (Jamieson et al., 2006). Non-zero $\Delta^{33}\text{S}$ values ($\Delta^{33}\text{S} = \delta^{33}\text{S}_{\text{measured}} - [(\delta^{34}\text{S}_{\text{measured}}/1000 + 1)^{0.515} - 1] \times 1000 \neq 0$) are attributed to photochemical reactions involving sulfur-bearing gases in which oxidized sulfur species produced in the atmosphere have negative $\Delta^{33}\text{S}$ values and reduced atmospheric sulfur species have positive values (Farquhar et al., 2000; 2001). The small positive $\Delta^{33}\text{S}$ values for pyrite in the Canadian Malartic deposit (0 to 0.12 ‰) indicate that a small component of reduced atmospheric sulfur was incorporated into the Canadian Malartic ore fluids. The most likely mechanism for this incorporation was transfer of the reduced sulfur to Pontiac Group sediments in the form of diagenetic pyrite, and subsequent acquisition of this sulfur by the fluids through dissolution of this pyrite.

FLUID EVOLUTION

The occurrence of magnetite in the pre-ore assemblage and its replacement by hematite provides clear evidence that f_{O_2} evolved to higher values during mineralization. Further support for this evolution of f_{O_2} is provided by negative $\delta^{34}S_{\text{fluid}}$ values. Significantly, the most negative values in this range (as low as -4.45 ‰) are for monzodiorite porphyry and Pontiac Group metasedimentary rocks, whereas fluids circulating in Piché Group rocks are interpreted to have had more positive $\delta^{34}S_{\text{fluid}}$ values (as high as +3.30 ‰). If, as discussed in the previous section, the source for the sulfur was magmatic, then $\Sigma\delta^{34}S$ would have been close to zero and, during oxidation, $\delta^{34}S_{\text{H}_2\text{S}}$ would have evolved to negative values, as a result of the preferential partitioning of ^{32}S into H_2S ; this would have resulted in an increase in the proportion of HSO_4^- relative to H_2S species in the ore fluid. As is evident from Figure 16, which was constructed at 475°C and 3000 bar (the effect of pressure on sulfur isotopic composition is negligible for most systems at pressures under 10 kbar; Ohmoto, 1972), changes in sulfur isotopic composition from -4.45 to +3.30 ‰ can be explained by a one log unit change in f_{O_2} for a wide range in pH around the pyrite/hematite phase boundary, assuming a $\Sigma\delta^{34}S$ value of zero. The deviation of $\delta^{34}S_{\text{H}_2\text{S}}$ to negative values in the porphyries and Pontiac group metasedimentary rocks (as low as -4.45 ‰) could therefore reflect oxidation and its deviation to values as high as +3.30 per mil in Piché Group rocks, could indicate reduction. The negative deviation is consistent with the local occurrence of hematite in the porphyries and Pontiac group rocks and the lack of this deviation in the Piché Group rocks by the absence of hematite. A likely explanation for the positive deviation in the latter rocks is their high content of magnetite (particularly the ultramafic rocks), and the reduction in f_{O_2} that accompanied replacement of this magnetite by pyrite. However, the high $\delta^{34}S_{\text{H}_2\text{S}}$ inferred for the ore fluid in Piché Group rocks could also reflect higher pH, predominance of HS^- and preferential partitioning of ^{34}S into this species. This is consistent with the observation that in pre-ore alteration assemblages, muscovite is common, whereas during the ore stage K-feldspar is dominant.

CONTROLS ON ORE DEPOSITION

At the physicochemical conditions estimated for ore formation, gold is present in solution predominantly as a bisulfide complex, as shown by the predominance fields of dissolved gold

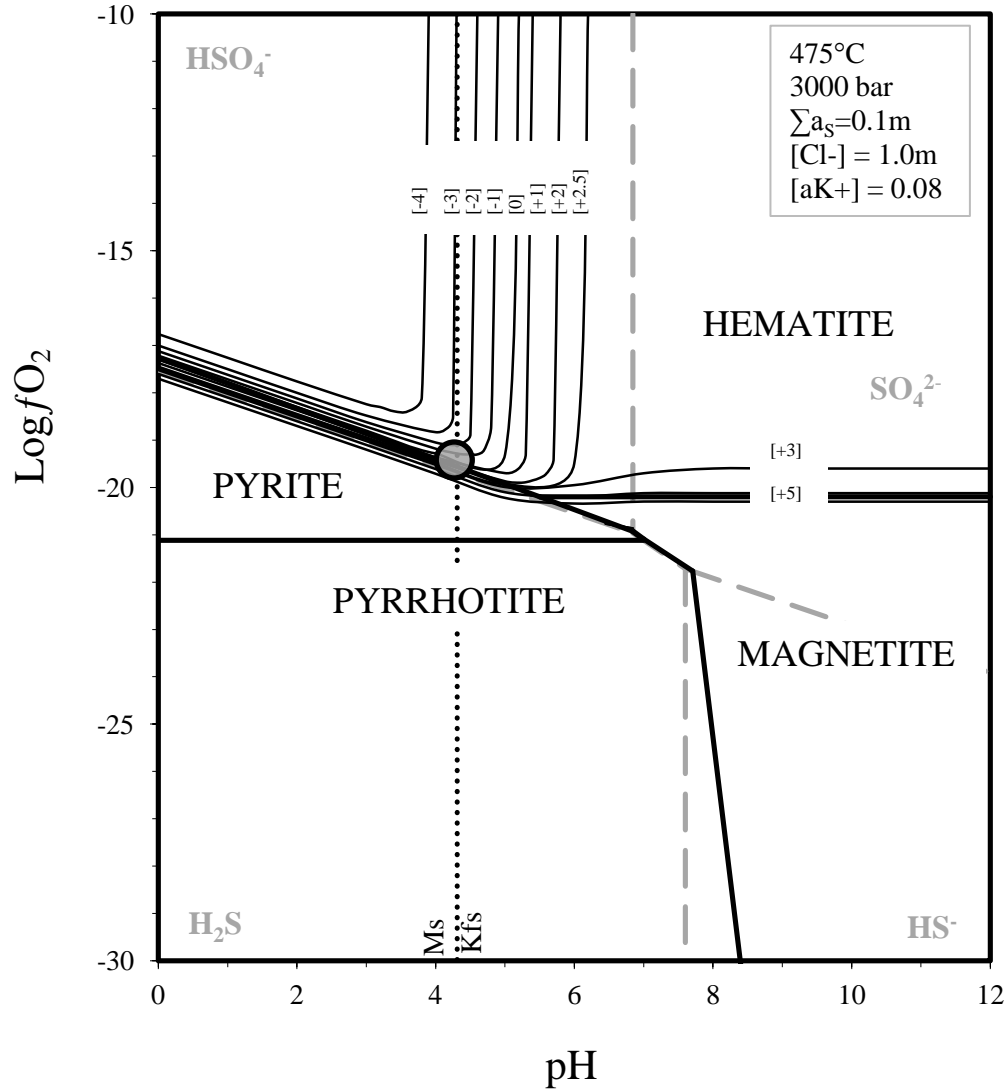


Fig. 16. Stability relationships in the Fe-O-S system and contours of $\delta^{34}\text{S}_{\text{H}_2\text{S}}$ as a function of $\log f_{\text{O}_2}$ and pH at 475°C and 3000 bar. Also shown is the location of the muscovite/K-feldspar pH buffer. The $\delta^{34}\text{S}_{\text{H}_2\text{S}}$ contours were calculated using the methods of Ohmoto (1972), assuming $\delta^{34}\text{S}_{\text{total}} = 0 \text{ ‰}$. The approximate conditions of Canadian Malartic mineralization are indicated by the gray circle.

species in Figure 17. Based on the preceding discussion, we propose that gold deposition at Canadian Malartic was triggered by sulfidation. Hydrothermal fluid reacting with the host rock would have replaced Fe-rich minerals such as magnetite and biotite with pyrite. This, in turn would have reduced H₂S activity and destabilized gold bisulfide complexes, causing precipitation of gold phases. Oxidation would also have been an effective mechanism for precipitation of gold. As shown in Figure 17, gold solubility contours (constructed with data from Stefansson and Seward, 2003a; 2003b, 2004) are stacked tightly near the pyrite-hematite boundary and their values decrease with increasing f_{O_2} . Consequently, even a small increase in f_{O_2} would lead to gold precipitation. Significantly, this would also increase the solubility of silver (which is transported dominantly as a chloride complex) and lead to the precipitation of silver-poor native gold (Gammons and Williams-Jones, 1995). The evidence for an increase in f_{O_2} during gold mineralization (e.g., the replacement of magnetite by hematite) and the high fineness of the native gold in the Canadian Malartic deposit therefore suggest that oxidation may also have been a factor in the formation of the deposit.

GENETIC MODEL

We propose a genetic model in which a CO₂- and SO₂-bearing felsic magma, emplaced at a depth of ≥ 10 km (corresponding to a pressure of ≥ 3 kbar), exsolved a relatively oxidized ($\log f_{O_2} \sim 19$), CO₂- and sulfur-rich ($\sum a_S \geq 0.1$) ore fluid. This fluid rose to shallower crustal levels where it altered genetically related porphyritic intrusions and their country rocks (Pontiac Group graywackes and Piché Group mafic to ultramafic volcanics) to an assemblage of biotite, K-feldspar, pyrite and carbonate minerals (calcite and lesser ankerite). Locally, the host rocks were silicified. The alteration and particularly the carbonatization (due to loss of CO₂ from the fluid) buffered pH to higher values. Carbonatization was strongest in the Piché Group rocks, consistent with the interpretation made earlier that the heavier $\delta^{34}S$ signature in Piché pyrite reflects predominance of HS⁻ and a correspondingly higher pH. Gold was transported as a bisulphide complex and was deposited at $\sim 475^\circ\text{C}$, mainly as a result of sulfidation of the host rocks, i.e., replacement of iron-bearing silicate minerals, which destabilized the gold-bisulfide complexes. The

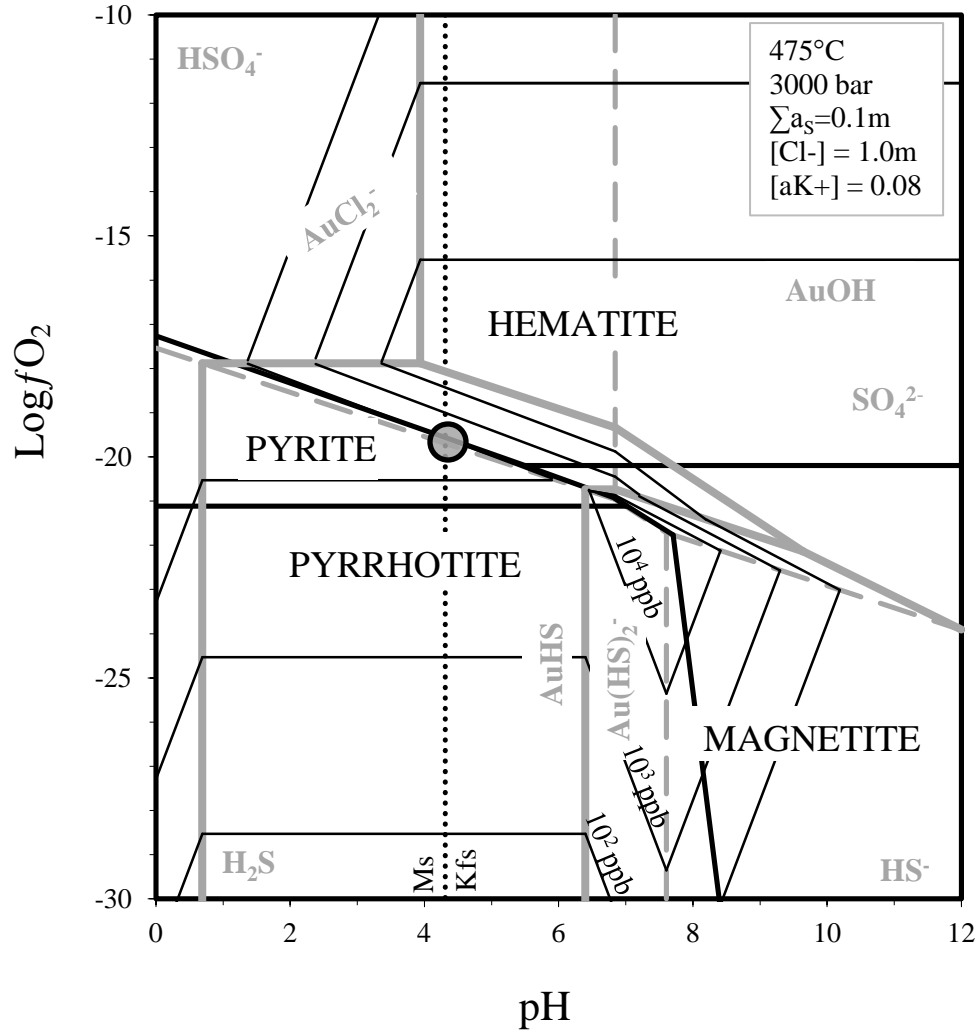


Fig. 17. Stability fields in the Fe-O-S system and the muscovite-K-feldspar alteration buffer shown as a function of $\log f_{O_2}$ and pH at 475°C and 3000 bar, with superimposed predominance boundaries of gold species and gold solubility contours. The approximate conditions of Canadian Malartic mineralization are indicated by the gray circle.

shift to higher f_{O_2} (inferred from deviations to low $\delta^{34}S$ of the host rocks) due perhaps to local mixing with meteoric water, and the small drop in temperature implied by the occurrence of gold in quartz veinlets also may have promoted deposition of gold (Fig. 17).

In summary, we embrace a magmatic-hydrothermal model for the genesis of the Canadian Malartic deposit that calls on the exsolution of an ore fluid from monzodioritic magma at depth, and deposition of gold at shallower crustal levels. Ascending fluids potassically altered, carbonated, sulfidized and locally silicified the host rocks and deposited the gold as a result of the accompanying loss of H_2S from the fluid, an increase in f_{O_2} , and possibly also a drop in temperature.

CLASSIFICATION OF THE CANADIAN MALARTIC DEPOSIT

From the genetic model developed above, it is clear that the Canadian Malartic deposit is intrusion-related in the sense that the gold mineralization is spatially related to porphyritic intrusions. However, the deposit is not typical of a porphyry-type system because the ore fluid does not appear to have been exsolved from these porphyries (see above). On the contrary, the coincidence of carbonatization and potassic alteration suggests strongly that the ore fluid exsolved from a magma at mid-crustal levels or perhaps even deeper. It is, however, likely that both the intrusives and the fluids exploited the same crustal conduits.

The term “intrusion-related” was originally introduced by Sillitoe (1991) and used by him to classify a spectrum of six interrelated styles of gold mineralization in epizonal to mesozonal environments based on a porphyry-copper model. Although Sillitoe (1991) did not note this explicitly, his definition of intrusion-related gold deposits was limited to intrusions of calc-alkaline affinity that contain elevated concentrations of base metals, chiefly copper. Thompson et al. (1999) subsequently coined the term “reduced intrusion-related” to refer to gold deposits genetically associated with reduced sub-alkaline to alkaline intrusions having a low Cu concentrations, and elevated concentrations of Bi, Te, As, Mo, Sb, W and some cases Sn (also see Thompson and

Newberry, 2000 and Lang and Baker, 2001). Another family of large tonnage, low grade gold deposits which are also associated with sub-alkaline to alkaline intrusions having low Cu concentrations was recognized by Robert (1997) and referred to him as syenite-associated (Robert, 2001). However, these deposits have an oxidized mineral assemblage (hematite/magnetite \pm anhydrite and/or barite).

We propose that large tonnage low grade gold deposits, including deposits termed syenite-associated by Robert (2001), having: 1) a genetic association with sub-alkaline to alkaline intrusions; 2) an oxidized ore mineral assemblage; 3) an enrichment in Te, Ag, Mo, Bi, Sb, with lesser W and Pb in addition to Au; 4) a depletion in Cu and low concentrations of other base metals, and; 5) widespread coincident potassic alteration, carbonatization, and sulfidation and lesser silicification, be re-classified as oxidized intrusion-related to distinguish them from the reduced intrusion-related gold deposits classified by Thompson et al. (1999). We further propose that the Canadian Malartic gold deposit be considered the type example of this new sub-class of intrusion-related deposits.

ACKNOWLEDGEMENTS

Financial support for the research was provided by a grant from the Osisko Mining Corporation and a matching grant from the NSERC Collaborative Research and Development Program, both to AEW-J, and a NSERC Discovery Grant to BAW. Osisko Mining Corporation provided access to the field area, drill core, internal reports and made company geologists Francois Bouchard and David Albert available for assistance and advice. The project was conceived by Robert Wares, Executive Vice President of Osisko, who secured company support and provided valuable advice on the geology of the deposit.

REFERENCES

- Akande, S.O., 1982, Mineralogy and genesis of three vein systems, Ross mine, Holtyre, Ontario, *in* Hodder, R.W. and Petruk, W., eds., *Geology of Canadian gold deposits*. Canadian Institute of Mining and Metallurgy, Special Volume 24, p. 94-97.
- Ayer, J., Amelin, Y., Corfu, F., Kamo, S., Ketchum, J., Kwok, K. and Trowell, N., 2002, Evolution of the southern Abitibi greenstone belt based on U-Pb geochronology: autochthonous volcanic construction followed by plutonism, regional deformation and sedimentation: *Precambrian Research*, v. 115, p. 63-95.
- Banks, D.A., Davies, G.R., Yardley, B.W.D., McCaig, A.M. and Grant, N.T., 1999, The chemistry of brines from an alpine thrust system in the Central Pyrenees: An application of fluid inclusion analysis to the study of fluid behavior in orogenesis: *Geochimica et Cosmochimica Acta*, v. 55, p. 1021-1030.
- Banks, D.A., Giuliani, G., Yardley, B.W.D. and Cheilletz, A., 2000, Emerald mineralization in Colombia: fluid chemistry and the role of brine mixing: *Mineralium Deposita*, v. 35, p. 699-713.
- Beaulieu, C., 2010, Le gisement aurifère péri-granitique de Canadian Malartic (Québec): Apport de la modélisation 3D à l'interprétation métallogénique: Unpublished M.Sc. thesis, Montréal, Canada, Université du Québec À Montréal, 70 p.
- Bottrell, S.H., Yardley, B. and Buckley, F., 1998, A modified crush-leach method for the analysis of fluid inclusion electrolytes: *Bulletin de Minéralogie*, v. 111, p. 279-290.
- Bottinga, Y., and Javoy, M., 1973, Comments on oxygen isotope geothermometry: *Earth and Planetary Science Letters*, v. 20, p. 250-265.
- Bottinga, Y. and Javoy, M., 1975, Oxygen isotope partitioning among the minerals and triplets in igneous and metamorphic rocks: *Reviews of Geophysics and Space Physics*, v. 13, p. 401-418.
- Brown, P.E. and Lamb, W.M. 1986. Mixing of H₂O-CO₂ in fluid inclusions; Geobarometry and Archean gold deposits. *Geochimica et Cosmochimica Acta*. 30: 847-852.
- Campbell, A.R., Banks, D.A., Phillips, R.S., and Yardley, B.W.D., 1995, Geochemistry of Th-U-REE mineralizing magmatic fluids, Captain Mountains, New Mexico: *Economic Geology*, v. 90, p. 1271-1287.
- Canfield, D.E., Raiswell, R., Westrich, J.T., Reaves, C.M. and Berner, R.A., 1986, The use of chromium reduction in the analysis of reduced inorganic sulfur in sediments and shales: *Chemical Geology*, v. 54, p. 149-155.

Carpenter, A.B., Trout, M.L. and Pickett, E.E., 1974, Preliminary report on the origin and chemical evolution of lead-and-zinc-rich oil field brines in Central Mississippi: *Economic Geology*, v. 69, p. 1191-1206.

Clayton, R.N. and Epstein, S., 1961, The use of oxygen isotopes in high-temperature geological thermometry: *The Journal of Geology*, v. 69, p. 447-452.

Clayton, R.N. and Mayeda, T.K., 1963, The use of bromine pentafluoride in the extraction of oxygen from oxides and silicates for isotopic analysis: *Geochimica et Cosmochimica Acta*, v. 27, p. 43-52.

Craig, H., 1961, Variations in meteoric waters: *Science*, v. 133, p. 1702-1703.

Connolly, C.A., Walter, L.M., Baadsgaard, H. And Longstaffe, F.J., 1990, Origin and evolution of formation waters, Alberta Basin, Western Canada Sedimentary Basin. I. Chemistry: *Applied Geochemistry*, v. 5, p. 375-395.

Corfu, F., Jackson, S.L. and Sutcliffe, R.H., 1991, U-Pb ages and tectonic significance of late alkali magmatism and non-marine sedimentation: Timiskaming Group, southern Abitibi belt, Ontario: *Canadian Journal of Earth Sciences*, v. 28, p. 489-503.

Corfu, F., Krogh, T.E., Kwok, Y.Y. and Jensen, L.S., 1989, U-Pb zircon geochronology in the southwestern Abitibi greenstone belt, Superior Province: *Canadian Journal of Earth Sciences*, v. 26, p. 1747-1763.

Davidson, S. and Banfield, A.F., 1944, Geology of the Beattie gold mine, Duparquet, Québec: *Economic Geology*, v. 39, p. 535-556.

Davis, D., 2002, U-Pb geochronology of Archean metasedimentary rocks in the Pontiac and Abitibi subprovinces, Québec, constraints on timing, provenance and regional tectonics: *Precambrian Research*, v. 115, p. 97-117.

Davis, W.J., Lacroix, S., Gariépy, C. and Machado, N., 2000, Geochronology and radiogenic isotope geochemistry of plutonic rocks from the central Abitibi subprovince: significance to the internal subdivision and plutono-tectonic evolution of the Abitibi belt: *Canadian Journal of Earth Sciences*, v. 37, p. 117-133.

Derry, D.R., 1939, The geology of the Canadian Malartic Gold Mine, N. Québec: *Economic Geology*, v. 34, p. 495-523.

Desrochers, J.P. and Hubert, C., 1996, Structural evolution and early accretion of the Archean Malartic composite block, southern Abitibi greenstone belt, Québec, Canada: *Canadian Journal of Earth Sciences*, v. 33, p. 1556-1569.

Desrochers, J.P., Hubert, C. and Pilote, P., 1996, Géologie de la région de Val-d'Or – Malartic: Québec Ministère des Ressources Naturelles, ET 96-01, 129 p.

Dimroth, E., Imreh, L., Goulet, N. and Rocheleau, M., 1983, Evolution of the south-central segment of the Archean Abitibi Belt, Québec. Part III: Plutonic and metamorphic evolution and geotectonic model: *Canadian Journal of Earth Sciences*, v. 20, p. 1374-1388.

Eatkins, P.R., 1962, Geological settings of the gold deposits of Malartic District, Abitibi east county: Québec Department of Natural Resources, Geological Report 99, 155 p.

Fallara, F., Ross, P.S and Sansfaçon, R., 2000, Caractérisation géochimique, pétrographique et structurale: nouveau modèle métallogénique du camp minier de Malartic: Québec Ministère des Ressources Naturelles, MB 2000-15, 155 p.

Farquhar, J., Bao, H.M. and Thiemens, M., 2000, Atmospheric influence of earth's earliest sulfur cycle: *Science*, v. 289, p. 756-758.

Farquhar, J., Savarino, J., Airieau, S. and Thiemens, M.H., 2001, Observation of wavelength-sensitive mass-independent sulfur isotope effects during SO₂ photolysis: Implications for the early atmosphere: *Journal of Geophysical Research – Planets*, v. 106, p. 829-839.

Feng, R. and Kerrich, R., 1992, Geochemical evolution of granitoids from the Archean Abitibi Southern Volcanic Zone and the Pontiac subprovince, Superior Province, Canada: Implications for tectonic history and source regions: *Chemical Geology*, v. 98, p. 23-70.

Frerery, M.J. and Krogh, T.E., 1986, U-Pb zircon ages of later internal plutons of the Abitibi and eastern Wawa Subprovinces, Ontario and Québec: Geological Survey of Canada Paper, 86-1A, p. 43-48.

Fraser, R.J., 1993, The Lac Troilus gold-copper deposit, northwestern Québec: A possible Archean porphyry system: *Economic Geology*, v. 88, p. 1685-1699.

Gammons, C.H. and Williams-Jones, A.E., 1995, Hydrothermal geochemistry of electrum: Thermodynamic constraints: *Economic Geology*, v. 90, p. 420-432.

Grant, J.A., 1986, The isocon diagram – A simple solution to Gresens' Equation for metasomatic alteration: *Economic Geology*, v. 81, p. 1976-1982.

Gresens, R.L., 1967, Composition-volume relationships of metasomatism: *Chemical Geology*, v. 2, p. 47-65.

Griffin, W.L., Pearson, N.J., Belousova, E.A. and Saeed, A., 2008, GLITTER: data reduction software for laser ablation ICP-MS. *in* Sylvester, P., ed., Mineralogical Association of Canadian Short Course Series, Volume 40, Vancouver, B.C. Appendix 2, p. 204-207.

- Halter, E.H. and Williams-Jones, A.E., 1995, Origin and evolution of the greisenizing fluid at the East Kemptville Tim Deposit, Nova Scotia, Canada: *Economic Geology*, v. 93, p. 1026-1051.
- Hattori, K., Krouse, H.R. and Campbell, F.A., 1983, The start of sulfur oxidation in continental environments: About 2.2×10^9 years ago: *Science*, v. 221, p. 549-551.
- Hoaglin, D.C., Mosteller, F. And Tukey, J.W., 1983, *Understanding robust and exploratory data analysis*, John Wiley and Sons, Inc., 447 p.
- Holland, T.J.B. and Powell, R., 1998, An internally consistent thermodynamic data set for phases of petrological interest: *Journal of Metamorphic Geology*, v. 16, p. 309-343.
- Issigonis, M.J., 1980, Occurrence of disseminated gold deposits in porphyries in Archean Abitibi belt, NW Quebec, Canada, *Institution of Mining and Metallurgy London, Transactions, Section B: Applied Earth Sciences*, v. 89, p. 157-158.
- Jamieson, J., Wing, B., Hannington, M., and Farquhar, J., 2006, Evaluating isotopic equilibrium among sulfide mineral pairs in Archean ore deposits: Case study from the Kidd Creek VMS deposit, Ontario, Canada: *Economic Geology*, v. 101, p. 1055-1061.
- Jemielita, R.A., Davis, D.W. and Krogh, T.E., 1990, U-Pb evidence for gold mineralization postdating greenstone magmatism and metamorphism: *Nature*, v. 346, p. 831-834.
- Johnson, J.W., Oelkers, E.H. and Helgeson, H.C., 1992, SUPCRT92: A software package for calculating the standard molal thermodynamic properties of minerals, gases, aqueous species, and reactions from 1 to 5000 bar and 0 to 1000 °C: *Computational Geoscience*, v. 18, p. 899-947.
- Klemm, L.M., Pettke, T. And Heinrich, C.A., 2007, Hydrothermal evolution of the El Teniente deposit, Chile: Porphyry Cu-Mo ore deposition from low salinity magmatic fluids: *Economic Geology*, v. 102, p. 1021-1045.
- Lambert, I.B., Donnelly, T.H., Dunlop, J.S.R. and Groves, D.I., 1978, Stable isotopic compositions of Early Archean sulphate deposits of probable evaporitic and volcanogenic origins: *Nature*, v. 276, p. 808-811.
- Lang, J.R. and Baker, T., 2001, Intrusion-related gold systems: the present level of understanding: *Mineralium Deposita*, v. 36, p. 477-489.
- Lowenstern, J.B., 2001, Carbon dioxide in magmas and implications for hydrothermal systems: *Mineralium Deposita*, v. 36, p. 490-502.

MacLean, W.H. and Kranidiotis, P., 1987, Immobile elements as monitors of mass transfer in hydrothermal alteration: Phelps Dodge massive sulphide deposit, Matagami, Québec: *Economic Geology*, v. 82, p. 951-962.

Mason, R. And Melnik, N., 1986, The McIntyre-Hollinger investigation, Timmins, Ontario: A gold dominated porphyry copper system: Canada Geological Survey Paper, 86-1B, p. 577-583.

Mather, T.A., McCabe, J.R., Rai, V.K., Thiemens, M., Pyle, D.M., Heaton, T.H.E., Sloane, H.J. and Fern, G.R., 2006, Oxygen and sulfur isotopic compositions of volcanic sulfate aerosol at the point of emission: *Journal of Geophysical Research*, v. 111, D18205.

McCaig, A.M., Tritlla, J. and Banks, D.A., 2000, Fluid mixing and recycling during Pyrenean thrusting: Evidence from fluid inclusion halogen ratios: *Geochimica et Cosmochimica Acta*, v. 64, p. 3395-3412.

Middlemost, E., 1994, Naming materials in the magma/igneous rock system: *Earth Science Reviews*, v. 37, p. 215-224.

Mortensen, J.K., 1987, Preliminary U-Pb zircon ages for volcanic and plutonic rocks of the Noranda – Lac Abitibi area, Abitibi Subprovince, Québec: Geological Survey of Canada Paper, 87-1A, p. 581-590.

Mortensen, J.K., 1993, U-Pb geochronology of the eastern Abitibi Subprovince, Part 2: Noranda – Kirkland Lake area: *Canadian Journal of Earth Sciences*, v. 30, p. 29-41.

Munz, I.A., Yardley, B.W.D., Banks, D.A. and Wayne, D., 1995, Deep penetration of sedimentary fluids in basement rocks from southern Norway: Evidence from hydrocarbon and brine inclusions in quartz veins: *Geochimica et Cosmochimica Acta*, v. 59, p. 239-254.

Ohmoto, H., 1972, Systematics of sulfur and carbon isotopes in hydrothermal ore deposits: *Economic Geology*, v. 67, p. 551-578

Ohmoto, H., 1986, Stable isotope geochemistry of ore deposits, *in* Valley, J.W., Taylor, Jr., H.P., and O'Neil, J.R., eds., *Stable Isotopes in High Temperature Geological Processes*, 16th ed.: Mineralogical Society of America, p. 491-560.

Ohmoto, H., and Lasaga, A.C., 1982, Kinetics of reactions between aqueous sulfates and sulfides in hydrothermal systems: *Geochimica et Cosmochimica Acta*, v. 46, p. 1727-1745.

Ohmoto, H., and Rye, R., 1979, *Isotopes of Sulfur and Carbon*. *in* Barnes, H., ed., *Geochemistry of Hydrothermal deposits*, 2nd ed.: New York, Wiley, p. 509-567.

Osisko Mining Corporation, 2012, Corporate document, (http://www.osisko.com/pdfs/OSK_Corp_EN_mar2012.pdf).

Outline of new whittle pit, Canadian Malartic Project [map]. 2009. Osisko. <<http://www.osisko.com/en/press/2009/12/14/465/osisko-releases-new-resource-estimate-for-canadian-malartic-project.html>> (12 Dec 2009).

Pal'yanova, G.A. and Drebuschak, V.A., 2002, Standard thermodynamic properties of high-grade gold, electrum, kustelite, and native silver: *Geochemistry International*, v. 40, p. 1222-1224.

Powell, W.G., Carmichael, D.M. and Hodgson, C.J., 1995, Conditions and timing of metamorphism in the southern Abitibi greenstone belt, Québec: *Canadian Journal of Earth Sciences*, v. 32, p. 787-805.

Robert, F., 1997, A preliminary geological model for syenite-associated disseminated gold deposits in the Abitibi belt, Ontario and Quebec: *Geological Survey of Canada Paper, Current Research*, p. 201-210.

Robert, F., 1989, Internal structure of the Cadillac tectonic zone southeast of Val d'Or, Abitibi greenstone belt, Québec: *Canadian Journal of Earth Sciences*, v. 26, p. 2661-2675.

Robert, F., 2001, Syenite-associated disseminated gold deposits in the Abitibi greenstone belt, Canada: *Mineralium Deposita*, v. 36, p. 503-516.

Robie, R.A., and Hemingway, B.S., 1995, Thermodynamic properties of minerals and related substances at 298.15 K and 1 Bar (105 Pascals) pressure and at higher temperatures: *U.S. Geological Survey Bulletin*, v. 2131, 461 pp.

Robinson, B. W., 1995, Sulfur isotope standards, *in* *Proceedings of a consultants' meeting held in Vienna, 1-3 December, 1993. IAEA-TECDOC-825*, p. 39-45.

Ropchan, R.J., 2002, Host-rock and structural controls on the nature and timing of gold mineralization at the Hollaway Mine, Abitibi Subprovince, Ontario: *Economic Geology*, v. 97, p. 291-309.

Roth, E., 1992, The nature and genesis of Archean porphyry-style Cu-Au-Mo mineralization at the Boddington gold mine, Western Australia: Unpublished Ph.D. thesis, Perth, Australia, University of Western Australia, 126 p.

Rumble, D., Hoering, T.C. and Palin, J.M., 1993, Preparation of SF₆ for sulfur isotope analysis by laser heating sulfide minerals in the presence of F₂ gas: *Geochimica et Cosmochimica Acta*, v. 57, p. 4499-4512.

Sansfaçon, R., 1986, Le district de Malartic: Structure et or, de Rouyn à Val d'Or, Québec *in* Pirie, J., and Downes, M.J., eds.: Réunion annuelle conjointe de l'Association Géologique du Canada et de l'Association Minéralogique du Canada, livret-guide de l'excursion, p. 28-43.

Sansfaçon, R., Hubert, C., 1990, The Malartic Gold District, Abitibi Greenstone Belt, Québec: Geological Setting, Structure and Timing of Gold Emplacement Barnat, East-Malartic, Canadian Malartic and Sladen Mines, *in* Rive, M., and Verpaelst, P., eds., The Northwestern Québec Polymetallic Belt: A summary of 60 years of mining exploration, Canadian Institute of Mining and Metallurgy, Special Volume 43, p. 221 - 235.

Sansfaçon, R. and Trudel, P., 1987, Géologie de la mine Canadian Malartic, District de Val-d'Or: Québec Ministère de l'Énergie et des Ressources, MB 87-26, 49 p.

Sansfaçon, R., Grant, M. and Trudel, P., 1987, Géologie de la mine Barnat – Sladen Malartic, District de Val-d'Or: Québec Ministère de l'Énergie et des Ressources, MB 87-41, 73 p.

Shock, E.L., Sassani, D.C., Willis, M. and Sverjensky, D.A., 1997, Inorganic species in geological fluids: Correlations among standard molal thermodynamic properties of aqueous ions and hydroxide complexes: *Geochimica et Cosmochimica Acta*, v. 6, p. 907-950.

Shvarov, Y.V. and Bastrakov, E.N., 1999, HCh: A software package for geochemical equilibrium modeling, user's guide: Australian Geological Survey Organisation Record 1999/25, 60 p.

Sillitoe, R.H., 1991, Intrusion-related gold deposits, *in* Foster, R.P., ed., *Gold Metallogeny and Exploration*, Glasgow, Blackie, p. 165-209.

Sillitoe, R.H., 2010, Porphyry copper systems: *Economic Geology*, v. 105, p. 3-41.

Sinclair, W.D., 1982, Gold deposits of the Matachewan area, Ontario, *in* Hodder, R.W., and Petruk, W., eds., *Geology of Canadian gold deposits*: Canadian Institute of Mining and Metallurgy, Special Volume 24, p. 83-93.

Smith, M., Banks, D.A., Yardley, B.W.D. and Boyce, A., 1996, Fluid inclusion and stable isotope constraints on the genesis of the Cligga Head Sn-W deposit, S.W. England: *European Journal of Mineralogy*, v. 8, p. 961-974.

Stefánsson, A. and Seward, T. M., 2003a, The hydrolysis of gold(I) in aqueous solutions to 600°C and 1500 bar: *Geochimica et Cosmochimica Acta*, v. 67, p. 1677-1688.

Stefánsson, A. and Seward, T. M., 2003b, Stability of chloridogold (I) complexes in aqueous solutions from 300 to 600 C and from 500 to 1800 bar: *Geochimica et Cosmochimica Acta*, v. 67, p. 4559–4576.

- Stefánsson, A. and Seward, T. M., 2004, Gold(I) complexing in aqueous sulphide solutions to 500°C at 500 bar: *Geochimica et Cosmochimica Acta*, v. 68, p. 4121-4143.
- Sutcliffe, R.H., Barrie, C.T., Burrows., D.R. and Beakhouse, G.P., 1993, Plutonism in the Southern Abitibi Subprovince: A tectonic and petrogenetic framework: *Economic Geology*, v. 88, p. 1359-1375.
- Suzuoki, T. and Epstein, S., 1976, Hydrogen isotope fractionation between OH-bearing minerals and water: *Geochimica et Cosmochimica Acta*, v. 40, p. 1229-1240.
- Sverjensky, D.A., Shock, E.L. and Helgeson, H.C., 1997, Prediction of the thermodynamic properties of aqueous metal complexes to 1000 °C and 5 kb: *Geochimica et Cosmochimica Acta*, v. 6, p. 1359-1412.
- Taylor, H.P., 1974, The application of oxygen and hydrogen isotope studies to problems of hydrothermal alteration and ore deposition: *Economic Geology*, v. 69, p. 843-883.
- Thode, H.G., Monster, J. and Dunford, H.B., 1961, Sulfur isotope geochemistry: *Geochimica et Cosmochimica Acta*, v. 25, p. 159-174.
- Thompson, J.F.H. and Newberry, R.J., 2000, Gold deposits related to reduced granitic intrusions: *Reviews in Economic Geology*, v. 13, p. 377-400.
- Thompson, J.F.H, Sillitoe, R.H., Baker, T., Lang, J.R. and Mortensen, J.K., 1999, Intrusion-related gold deposits associated with tungsten-tin provinces: *Mineralium Deposita*, v. 34, p. 197-217.
- Thurston, P.C., Ayer, J.A., Goutier, J. and Hamilton, M.A., 2008, Depositional gaps in Abitibi Greenstone Belt stratigraphy: A key to exploration for syngenetic mineralization: *Economic Geology*, v, 103, p. 1097-1134.
- Trudel, P. and Sansfaçon, R., 1987, Géologie de la mine East Malartic, Région de Val-d'Or: Québec Ministère de l'Énergie et des Ressources, MB 87-25, 64 p.
- Trudel, P. and Sauvé, P., 1992, Synthèse des caractéristiques géologiques des gisements d'or du district de Malartic: Québec Ministère de l'Énergie et des Ressources, MM 89-04, 126 p.
- Wark, D.A., and Watson, E.B., 2006, TitaniQ: a titanium-in-quartz geothermometer: *Contributions to Mineralogy and Petrology*, v. 152, p. 743-754.
- Winchester, J.A. and Floyd, P.A., 1977, Geochemical discrimination of different magma series and their differentiation products using immobile elements: *Chemical Geology*, v. 20, p. 325-343.

CHAPTER III: CONCLUSIONS AND CONTRIBUTIONS TO KNOWLEDGE

CONCLUSIONS

The large tonnage, low grade Canadian Malartic gold deposit in the Pontiac subprovince of Québec shows: 1) a spatial association with small felsic to intermediate porphyritic intrusions of sub-alkaline to alkaline affinity; 2) an enrichment of Te, Ag, Mo, Bi, Sb, with lesser W and Pb in addition to Au, a depletion in Cu and low concentrations of other base metals; 3) an oxidized ore assemblage including hematite and minor barite; 4) a close spatial association of the gold (native gold and later telluride minerals) with pyrite; and 5) widespread coincident potassic alteration, carbonatization, and sulfidation and lesser silicification. These deposit characteristics are explained by a genetic model in which a CO₂- and SO₂-bearing felsic magma, emplaced at a depth of ≥ 10 km (corresponding to a pressure of ≥ 3 kbar), exsolved a relatively oxidized ($\log f_{\text{O}_2} \sim 19$), CO₂ and sulfur-rich ($\sum a_S \geq 0.1$) ore fluid. This fluid rose to shallower crustal levels where it altered associated porphyritic intrusions and their country rocks (Pontiac metagreywackes and Piché Group mafic to ultramafic metavolcanics) to an assemblage of biotite, K-feldspar, pyrite and carbonate minerals (calcite and lesser ankerite). Locally, the host rocks were silicified. The alteration, particularly the carbonatization, buffered pH to higher values (due to loss of CO₂ from the fluid). Carbonatization was strongest in the Piché Group rocks, consistent with an interpretation that the heavier $\delta^{34}\text{S}$ signature in pyrite hosted by Piché Group rocks reflects predominance of HS⁻ and a correspondingly higher pH. Gold was transported as a bisulphide complex and was deposited at 475°C, mainly as a result of sulfidation of the rocks, i.e., replacement of iron-bearing oxide and silicate minerals, which destabilized the gold-bisulphide complexes. The shift to higher f_{O_2} (inferred from the deviations to low $\delta^{34}\text{S}$ of the host rocks) due perhaps to local mixing with meteoric water, and the small drop in temperature implied by the occurrence of gold in quartz veinlets also may have promoted deposition of gold.

This study provides a detailed description of the first clearly demonstrable example of a large tonnage, low-grade intrusion-related gold system in the Archean of Québec. Based on the characteristics of the deposit, Canadian Malartic and other similar deposits elsewhere having these characteristics represent an important but poorly

described family of deposits that is most appropriately classified as oxidized intrusion-related to distinguish them from the reduced intrusion-related class of gold deposits.

CONTRIBUTIONS TO KNOWLEDGE

Research on the Malartic gold camp has been limited to a few papers (Derry, 1939; Issigonis, 1980; Desrochers and Hubert, 1996; Robert, 2001) and reports (Eakins, 1962; Sansfaçon et al., 1987; Sansfaçon and Trudel, 1987; Trudel et Sansfaçon, 1987; Trudel and Sauvé, 1992; Desrochers et al., 1996; Fallara et al. 2000) detailing the structure, deformational history, mineralization and alteration of the district. Several generalized models have been proposed to explain their genesis, however, none of the studies have tested these models by placing adequate physical constraints on the physicochemical conditions of gold mineralization ($T, f_{O_2}, m_{\Sigma S}, pH$). This study has constrained these conditions. In particular, the study has shown that the ore fluid was oxidized, potassic and CO_2 -rich, and that the conditions of gold deposition were a temperature of ~ 475 °C, a $\log f_{O_2}$ of ~ -19 , $\Sigma aS \geq 0.1$ and pH of ~ 4.5 . The research also has shown that although the gold is spatially associated with felsic intrusions, the fluids were not exsolved from the corresponding magma. Instead, their characteristics (isotopic and chemical composition) indicate that they were exsolved from a related magma at mid or deep crustal levels. The Canadian Malartic deposit is therefore not a porphyry deposit. Instead it is an intrusion-related deposit in the sense that the gold mineralization is spatially associated with felsic intrusions but the magmatic-hydrothermal ore fluids originated from deeper crustal levels. This study has considerably enhanced our understanding of the genesis of deposits of the type represented by Canadian Malartic and as a corollary, has helped clarify the classification of intrusion-related gold systems. The results of the research presented in this thesis will aid in the exploration for similar deposits elsewhere and could lead to the discovery and exploitation of other world class Archean oxidized intrusion-related gold deposits.

REFERENCES

- Akande, S.O., 1982, Mineralogy and genesis of three vein systems, Ross mine, Holtyre, Ontario, *in* Hodder, R.W. and Petruk, W., eds., *Geology of Canadian gold deposits*. Canadian Institute of Mining and Metallurgy, Special Volume 24, p. 94-97.
- Ayer, J., Amelin, Y., Corfu, F., Kamo, S., Ketchum, J., Kwok, K. and Trowell, N., 2002, Evolution of the southern Abitibi greenstone belt based on U-Pb geochronology: autochthonous volcanic construction followed by plutonism, regional deformation and sedimentation: *Precambrian Research*, v. 115, p. 63-95.
- Banks, D.A., Davies, G.R., Yardley, B.W.D., McCaig, A.M. and Grant, N.T., 1999, The chemistry of brines from an alpine thrust system in the Central Pyrenees: An application of fluid inclusion analysis to the study of fluid behavior in orogenesis: *Geochimica et Cosmochimica Acta*, v. 55, p. 1021-1030.
- Banks, D.A., Giuliani, G., Yardley, B.W.D. and Cheilletz, A., 2000, Emerald mineralization in Colombia: fluid chemistry and the role of brine mixing: *Mineralium Deposita*, v. 35, p. 699-713.
- Beaulieu, C., 2010, Le gisement aurifère péri-granitique de Canadian Malartic (Québec): Apport de la modélisation 3D à l'interprétation métallogénique: Unpublished M.Sc. thesis, Montréal, Canada, Université du Québec À Montréal, 70 p.
- Bierlein, F.P., and Maher, S, 2001, Orogenic disseminated gold in Phanerozoic fold belts – examples from Victoria, Australia and elsewhere, *Ore Geology Reviews*, v. 18, p. 113-148.
- Bottrell, S.H., Yardley, B. and Buckley, F., 1998, A modified crush-leach method for the analysis of fluid inclusion electrolytes: *Bulletin de Minéralogie*, v. 111, p. 279-290.
- Bottinga, Y., and Javoy, M., 1973, Comments on oxygen isotope geothermometry: *Earth and Planetary Science Letters*, v. 20, p. 250-265.
- Bottinga, Y. and Javoy, M., 1975, Oxygen isotope partitioning among the minerals and triplets in igneous and metamorphic rocks: *Reviews of Geophysics and Space Physics*, v. 13, p. 401-418.
- Brown, P.E. and Lamb, W.M. 1986. Mixing of H₂O-CO₂ in fluid inclusions; Geobarometry and Archean gold deposits. *Geochimica et Cosmochimica Acta*. 30: 847-852.
- Campbell, A.R., Banks, D.A., Phillips, R.S., and Yardley, B.W.D., 1995, Geochemistry of Th-U-REE mineralizing magmatic fluids, Captain Mountains, New Mexico: *Economic Geology*, v. 90, p. 1271-1287.

- Canfield, D.E., Raiswell, R., Westrich, J.T., Reaves, C.M. and Berner, R.A., 1986, The use of chromium reduction in the analysis of reduced inorganic sulfur in sediments and shales: *Chemical Geology*, v. 54, p. 149-155.
- Carpenter, A.B., Trout, M.L. and Pickett, E.E., 1974, Preliminary report on the origin and chemical evolution of lead-and-zinc-rich oil field brines in Central Mississippi: *Economic Geology*, v. 69, p. 1191-1206.
- Clayton, R.N. and Epstein, S., 1961, The use of oxygen isotopes in high-temperature geological thermometry: *The Journal of Geology*, v. 69, p. 447-452.
- Clayton, R.N. and Mayeda, T.K., 1963, The use of bromine pentafluoride in the extraction of oxygen from oxides and silicates for isotopic analysis: *Geochimica et Cosmochimica Acta*, v. 27, p. 43-52.
- Craig, H., 1961, Variations in meteoric waters: *Science*, v. 133, p. 1702-1703.
- Connolly, C.A., Walter, L.M., Baadsgaard, H. And Longstaffe, F.J., 1990, Origin and evolution of formation waters, Alberta Basin, Western Canada Sedimentary Basin. I. Chemistry: *Applied Geochemistry*, v. 5, p. 375-395.
- Corfu, F., Jackson, S.L. and Sutcliffe, R.H., 1991, U-Pb ages and tectonic significance of late alkali magmatism and non-marine sedimentation: Timiskaming Group, southern Abitibi belt, Ontario: *Canadian Journal of Earth Sciences*, v. 28, p. 489-503.
- Corfu, F., Krogh, T.E., Kwok, Y.Y. and Jensen, L.S., 1989, U-Pb zircon geochronology in the southwestern Abitibi greenstone belt, Superior Province: *Canadian Journal of Earth Sciences*, v. 26, p. 1747-1763.
- Davidson, S. and Banfield, A.F., 1944, Geology of the Beattie gold mine, Duparquet, Québec: *Economic Geology*, v. 39, p. 535-556.
- Davis, D., 2002, U-Pb geochronology of Archean metasedimentary rocks in the Pontiac and Abitibi subprovinces, Québec, constraints on timing, provenance and regional tectonics: *Precambrian Research*, v. 115, p. 97-117.
- Davis, W.J., Lacroix, S., Gariépy, C. and Machado, N., 2000, Geochronology and radiogenic isotope geochemistry of plutonic rocks from the central Abitibi subprovince: significance to the internal subdivision and plutono-tectonic evolution of the Abitibi belt: *Canadian Journal of Earth Sciences*, v. 37, p. 117-133.
- Derry, D.R., 1939, The geology of the Canadian Malartic Gold Mine, N. Québec: *Economic Geology*, v. 34, p. 495-523.

- Desrochers, J.P. and Hubert, C., 1996, Structural evolution and early accretion of the Archean Malartic composite block, southern Abitibi greenstone belt, Québec, Canada: *Canadian Journal of Earth Sciences*, v. 33, p. 1556-1569.
- Desrochers, J.P., Hubert, C. and Pilote, P., 1996, *Géologie de la région de Val-d'Or – Malartic*: Québec Ministère des Ressources Naturelles, ET 96-01, 129 p.
- Dimroth, E., Imreh, L., Goulet, N. and Rocheleau, M., 1983, Evolution of the south-central segment of the Archean Abitibi Belt, Québec. Part III: Plutonic and metamorphic evolution and geotectonic model: *Canadian Journal of Earth Sciences*, v. 20, p. 1374-1388.
- Ding, T., Valkiers, S., Kipphardt, H., De Bièvre, P., Taylor, P.D.P., Gonfiantini, R., and Krouse, R., 2001, Calibrated sulfur isotope abundance ratios of three IAEA sulfur isotope reference materials and V-CDT with a reassessment of the atomic weight of sulfur, *Geochimica et Cosmochimica Acta*, v. 65, p. 2433-2437.
- Dupéré, M., and Gagnon, G., 2011, Resources update of the Douay property and preliminary economic assessment of the Douay West mineral deposit, Northern Abitibi, Québec, NI-43-101 Technical Report for Aurvista Gold Corporation, 214 pp.
- Dyer, W.S., 1936, Geology and ore deposits of the Matachewan-Kenogami area, Ontario Department of Mines, Forty-fourth Annual Report, XLIV, Part II 1935.
- Eatkins, P.R., 1962, Geological settings of the gold deposits of Malartic District, Abitibi east county: Québec Department of Natural Resources, Geological Report 99, 155 p.
- Fallara, F., Ross, P.S and Sansfaçon, R., 2000, Caractérisation géochimique, pétrographique et structurale: nouveau modèle métallogénique du camp minier de Malartic: Québec Ministère des Ressources Naturelles, MB 2000-15, 155 p.
- Farquhar, J., Chacko, T., and Frost, B.R., 1993, Strategies for high-temperature oxygen isotope thermometry: a worked example from the Laramie Anorthosite Complex, Wyoming, USA, *Earth and Planetary Science Letters*, v. 117, p. 407-422.
- Farquhar, J., Bao, H.M. and Thiemens, M., 2000, Atmospheric influence of earth's earliest sulfur cycle: *Science*, v. 289, p. 756-758.
- Farquhar, J., Savarino, J., Airieau, S. and Thiemens, M.H., 2001, Observation of wavelength-sensitive mass-independent sulfur isotope effects during SO₂ photolysis: Implications for the early atmosphere: *Journal of Geophysical Research – Planets*, v. 106, p. 829-839.
- Feng, R. and Kerrich, R., 1992, Geochemical evolution of granitoids from the Archean Abitibi Southern Volcanic Zone and the Pontiac subprovince, Superior Province, Canada: Implications for tectonic history and source regions: *Chemical Geology*, v. 98, p. 23-70.

Fraser, M.J. and Krogh, T.E., 1986, U-Pb zircon ages of later internal plutons of the Abitibi and eastern Wawa Subprovinces, Ontario and Québec: Geological Survey of Canada Paper, 86-1A, p. 43-48.

Fraser, R.J., 1993, The Lac Troilus gold-copper deposit, northwestern Québec: A possible Archean porphyry system: *Economic Geology*, v. 88, p. 1685-1699.

Gammons, C.H. and Williams-Jones, A.E., 1995, Hydrothermal geochemistry of electrum: Thermodynamic constraints: *Economic Geology*, v. 90, p. 420-432.

Goldfarb, R.J., Hart, C.J.R., Miller, M., Miller, L., Farmer, G.L. and Groves, D.I., 2000, The Tintina Gold Belt: A global perspective. *British Columbia and Yukon Chamber of Mines, Special Volume 2*, pp. 5-34.

Goldfarb, R.J., Groves, D.I., and Gardoll, S., 2001, Orogenic gold and geologic time: a global synthesis, *Ore Geology Reviews*, v. 18, p. 1-75.

Grant, J.A., 1986, The isocon diagram – A simple solution to Gresens' Equation for metasomatic alteration: *Economic Geology*, v. 81, p. 1976-1982.

Gresens, R.L., 1967, Composition-volume relationships of metasomatism: *Chemical Geology*, v. 2, p. 47-65.

Griffin, W.L., Pearson, N.J., Belousova, E.A. and Saeed, A., 2008, GLITTER: data reduction software for laser ablation ICP-MS. *in* Sylvester, P., ed., *Mineralogical Association of Canadian Short Course Series, Volume 40*, Vancouver, B.C. Appendix 2, p. 204-207.

Grondin, O., and Williams-Jones, A.E., 2004, The Onaman prospect, Ontario: An unusual occurrence of Cu-bearing Au mineralization in a shear zone, *Economic Geology*, v. 99, p. 141-156.

Halter, E.H. and Williams-Jones, A.E., 1995, Origin and evolution of the greisenizing fluid at the East Kemptville Tim Deposit, Nova Scotia, Canada: *Economic Geology*, v. 93, p. 1026-1051.

Groves, D.I., Goldfarb, R.J., Gebre-Mariam, M., Hagemann, S.G., and Robert, F., 1998, Orogenic gold deposits: A proposed classification in the context of their crustal distribution and relationships to other gold deposit types, *Ore Geology Reviews*, v. 13, p. 7-27.

Groves, D.I., Goldfarb, R.J., Robert, F., and Hart, C.J.R., 2003, Gold deposits in metamorphic belts: Overview of current understanding, outstanding problems, future research, and exploration significance, *Economic Geology*, v. 98, p. 1-29.

Hart, C.J.R., and Goldfarb, R.J., 2005, Distinguishing intrusion-related from orogenic gold systems: New Zealand Minerals Conference: Realising New Zealand's Mineral Potential, New Zealand, Proceedings, Australasian Institute of Mining and Metallurgy, p. 125-133.

Hattori, K., Krouse, H.R. and Campbell, F.A., 1983, The start of sulfur oxidation in continental environments: About 2.2×10^9 years ago: *Science*, v. 221, p. 549-551.

Hoaglin, D.C., Mosteller, F. and Tukey, J.W., 1983, Understanding robust and exploratory data analysis, John Wiley and Sons, Inc., 447 p.

Holland, T.J.B. and Powell, R., 1998, An internally consistent thermodynamic data set for phases of petrological interest: *Journal of Metamorphic Geology*, v. 16, p. 309-343.

Issigonis, M.J., 1980, Occurrence of disseminated gold deposits in porphyries in Archean Abitibi belt, NW Quebec, Canada, Institution of Mining and Metallurgy London, Transactions, Section B: Applied Earth Sciences, v. 89, p. 157-158.

Jamieson, J., Wing, B., Hannington, M., and Farquhar, J., 2006, Evaluating isotopic equilibrium among sulfide mineral pairs in Archean ore deposits: Case study from the Kidd Creek VMS deposit, Ontario, Canada: *Economic Geology*, v. 101, p. 1055-1061.

Jemielita, R.A., Davis, D.W. and Krogh, T.E., 1990, U-Pb evidence for gold mineralization postdating greenstone magmatism and metamorphism: *Nature*, v. 346, p. 831-834.

Johnson, J.W., Oelkers, E.H. and Helgeson, H.C., 1992, SUPCRT92: A software package for calculating the standard molal thermodynamic properties of minerals, gases, aqueous species, and reactions from 1 to 5000 bar and 0 to 1000 °C: *Computational Geoscience*, v. 18, p. 899-947.

Klemm, L.M., Pettke, T. And Heinrich, C.A., 2007, Hydrothermal evolution of the El Teniente deposit, Chile: Porphyry Cu-Mo ore deposition from low salinity magmatic fluids: *Economic Geology*, v. 102, p. 1021-1045.

Lambert, I.B., Donnelly, T.H., Dunlop, J.S.R. and Groves, D.I., 1978, Stable isotopic compositions of Early Archean sulphate deposits of probable evaporitic and volcanogenic origins: *Nature*, v. 276, p. 808-811.

Lang, J.R. and Baker, T., 2001, Intrusion-related gold systems: the present level of understanding: *Mineralium Deposita*, v. 36, p. 477-489.

Lowenstern, J.B., 2001, Carbon dioxide in magmas and implications for hydrothermal systems: *Mineralium Deposita*, v. 36, p. 490-502.

- Lunistra, B., and Benn, K., 2001, Structural geology of the Holloway Mine, Abitibi Greenstone Belt, Ontario, Ontario Geological Survey, Open File Report 6045, 36 pp.
- MacLean, W.H. and Kranidiotis, P., 1987, Immobile elements as monitors of mass transfer in hydrothermal alteration: Phelps Dodge massive sulphide deposit, Matagami, Québec: Economic Geology, v. 82, p. 951-962.
- Mason, R. And Melnik, N., 1986, The McIntyre-Hollinger investigation, Timmins, Ontario: A gold dominated porphyry copper system: Canada Geological Survey Paper, 86-1B, p. 577-583.
- Mather, T.A., McCabe, J.R., Rai, V.K., Thiemens, M., Pyle, D.M., Heaton, T.H.E., Sloane, H.J. and Fern, G.R., 2006, Oxygen and sulfur isotopic compositions of volcanic sulfate aerosol at the point of emission: Journal of Geophysical Research, v. 111, D18205.
- McCaig, A.M., Tritlla, J. and Banks, D.A., 2000, Fluid mixing and recycling during Pyrenean thrusting: Evidence from fluid inclusion halogen ratios: Geochimica et Cosmochimica Acta, v. 64, p. 3395-3412.
- Middlemost, E., 1994, Naming materials in the magma/igneous rock system: Earth Science Reviews, v. 37, p. 215-224.
- Mortensen, J.K., 1987, Preliminary U-Pb zircon ages for volcanic and plutonic rocks of the Noranda – Lac Abitibi area, Abitibi Subprovince, Québec: Geological Survey of Canada Paper, 87-1A, p. 581-590.
- Mortensen, J.K., 1993, U-Pb geochronology of the eastern Abitibi Subprovince, Part 2: Noranda – Kirkland Lake area: Canadian Journal of Earth Sciences, v. 30, p. 29-41.
- Munz, I.A., Yardley, B.W.D., Banks, D.A. and Wayne, D., 1995, Deep penetration of sedimentary fluids in basement rocks from southern Norway: Evidence from hydrocarbon and brine inclusions in quartz veins: Geochimica et Cosmochimica Acta, v. 59, p. 239-254.
- Ohmoto, H., 1972, Systematics of sulfur and carbon isotopes in hydrothermal ore deposits: Economic Geology, v. 67, p. 551-578
- Ohmoto, H., 1986, Stable isotope geochemistry of ore deposits, in Valley, J.W., Taylor, Jr., H.P., and O'Neil, J.R., eds., Stable Isotopes in High Temperature Geological Processes, 16th ed.: Mineralogical Society of America, p. 491-560.
- Ohmoto, H., and Lasaga, A.C., 1982, Kinetics of reactions between aqueous sulfates and sulfides in hydrothermal systems: Geochimica et Cosmochimica Acta, v. 46, p. 1727-1745.

Ohmoto, H., and Rye, R., 1979, Isotopes of Sulfur and Carbon. *in* Barnes, H., ed., *Geochemistry of Hydrothermal deposits*, 2nd ed.: New York, Wiley, p. 509-567.

Osisko Mining Corporation, 2012, Corporate document, (http://www.osisko.com/pdfs/OSK_Corp_EN_mar2012.pdf).

Outline of new whittle pit, Canadian Malartic Project [map]. 2009. Osisko. <<http://www.osisko.com/en/press/2009/12/14/465/osisko-releases-new-resource-estimate-for-canadian-malartic-project.html>> (12 Dec 2009).

Pal'yanova, G.A. and Drebuschak, V.A., 2002, Standard thermodynamic properties of high-grade gold, electrum, kustelite, and native silver: *Geochemistry International*, v. 40, p. 1222-1224.

Powell, W.G., Carmichael, D.M. and Hodgson, C.J., 1995, Conditions and timing of metamorphism in the southern Abitibi greenstone belt, Québec: *Canadian Journal of Earth Sciences*, v. 32, p. 787-805.

Robert, F., 1997, A preliminary geological model for syenite-associated disseminated gold deposits in the Abitibi belt, Ontario and Quebec: *Geological Survey of Canada Paper, Current Research*, p. 201-210.

Robert, F., 1989, Internal structure of the Cadillac tectonic zone southeast of Val d'Or, Abitibi greenstone belt, Québec: *Canadian Journal of Earth Sciences*, v. 26, p. 2661-2675.

Robert, F., 2001, Syenite-associated disseminated gold deposits in the Abitibi greenstone belt, Canada: *Mineralium Deposita*, v. 36, p. 503-516.

Robert, F., and Poulsen, K.H. 1997, World-class Archean gold deposits in Canada: an overview: *Canadian Journal of Earth Sciences*, v. 44, p. 329-351.

Robie, R.A., and Hemingway, B.S., 1995, Thermodynamic properties of minerals and related substances at 298.15 K and 1 Bar (105 Pascals) pressure and at higher temperatures: *U.S. Geological Survey Bulletin*, v. 2131, 461 pp.

Robinson, B. W., 1995, Sulfur isotope standards, *in* *Proceedings of a consultants' meeting held in Vienna, 1-3 December, 1993*. IAEA-TECDOC-825, p. 39-45.

Ropchan, R.J., 2002, Host-rock and structural controls on the nature and timing of gold mineralization at the Hollaway Mine, Abitibi Subprovince, Ontario: *Economic Geology*, v. 97, p. 291-309.

Roth, E., 1992, The nature and genesis of Archean porphyry-style Cu-Au-Mo mineralization at the Boddington gold mine, Western Australia: Unpublished Ph.D. thesis, Perth, Australia, University of Western Australia, 126 p.

Rumble, D., Hoering, T.C. and Palin, J.M., 1993, Preparation of SF₆ for sulfur isotope analysis by laser heating sulfide minerals in the presence of F₂ gas: *Geochimica et Cosmochimica Acta*, v. 57, p. 4499-4512.

Sansfaçon, R., 1986, Le district de Malartic: Structure et or, de Rouyn à Val d'Or, Québec *in* Pirie, J., and Downes, M.J., eds.: Réunion annuelle conjointe de l'Association Géologique du Canada et de l'Association Minéralogique du Canada, livret-guide de l'excursion, p. 28-43.

Sansfaçon, R., Hubert, C., 1990, The Malartic Gold District, Abitibi Greenstone Belt, Québec: Geological Setting, Structure and Timing of Gold Emplacement Barnat, East-Malartic, Canadian Malartic and Sladen Mines, *in* Rive, M., and Verpaelst, P., eds., The Northwestern Québec Polymetallic Belt: A summary of 60 years of mining exploration, Canadian Institute of Mining and Metallurgy, Special Volume 43, p. 221 - 235.

Sansfaçon, R. and Trudel, P., 1987, Géologie de la mine Canadian Malartic, District de Val-d'Or: Québec Ministère de l'Énergie et des Ressources, MB 87-26, 49 p.

Sansfaçon, R., Grant, M. and Trudel, P., 1987, Géologie de la mine Barnat – Sladen Malartic, District de Val-d'Or: Québec Ministère de l'Énergie et des Ressources, MB 87-41, 73 p.

Seedorf, E., Dilles, J.H., Proffett, J.M., Einaudi, M.T., Zurciier, L., Stavast, W.J.A., Johnson, D.A., and Barton, M.D., 2005, Porphyry deposits: Characteristics and origin of hypogene features: *Economic Geology*, 100th Anniversary volume, p. 251-298.

Shock, E.L., Sassani, D.C., Willis, M. and Sverjensky, D.A., 1997, Inorganic species in geological fluids: Correlations among standard molal thermodynamic properties of aqueous ions and hydroxide complexes: *Geochimica et Cosmochimica Acta*, v. 6, p. 907-950.

Shock, E.L., Sassani, D.C., Willis, M. and Sverjensky, D.A., 1997, Inorganic species in geological fluids: Correlations among standard molal thermodynamic properties of aqueous ions and hydroxide complexes: *Geochimica et Cosmochimica Acta*, v. 6, p. 907-950.

Shvarov, Y.V. and Bastrakov, E.N., 1999, HCh: A software package for geochemical equilibrium modeling, user's guide: Australian Geological Survey Organisation Record 1999/25, 60 p.

Sillitoe, R.H., 1979, Some thoughts on gold-rich porphyry copper deposits: *Mineralium Deposita*, v. 14, p. 161-174.

Sillitoe, R.H., 1991, Intrusion-related gold deposits, *in* Foster, R.P., ed., *Gold Metallogeny and Exploration*, Glasgow, Blackie, p. 165-209.

Sillitoe, R.H., 2010, Porphyry copper systems: *Economic Geology*, v. 105, p. 3-41.

- Sinclair, W.D., 1982, Gold deposits of the Matachewan area, Ontario, *in* Hodder, R.W., and Petruk, W., eds., *Geology of Canadian gold deposits: Canadian Institute of Mining and Metallurgy, Special Volume 24*, p. 83-93.
- Smith, M., Banks, D.A., Yardley, B.W.D. and Boyce, A., 1996, Fluid inclusion and stable isotope constraints on the genesis of the Cligga Head Sn-W deposit, S.W. England: *European Journal of Mineralogy*, v. 8, p. 961-974.
- Spooner, E.T.C., and Barrie, C.T., 1993, A special issue devoted to Abitibi ore deposits in a modern context; preface, *Economic Geology*, v. 88, p. 1307-1322.
- Stefánsson, A. and Seward, T. M., 2003a, The hydrolysis of gold(I) in aqueous solutions to 600°C and 1500 bar: *Geochimica et Cosmochimica Acta*, v. 67, p. 1677-1688.
- Stefánsson, A. and Seward, T. M., 2003b, Stability of chloridogold (I) complexes in aqueous solutions from 300 to 600 C and from 500 to 1800 bar: *Geochimica et Cosmochimica Acta*, v. 67, p. 4559-4576.
- Stefánsson, A. and Seward, T. M., 2004, Gold(I) complexing in aqueous sulphide solutions to 500°C at 500 bar: *Geochimica et Cosmochimica Acta*, v. 68, p. 4121-4143.
- Sutcliffe, R.H., Barrie, C.T., Burrows., D.R. and Beakhouse, G.P., 1993, Plutonism in the Southern Abitibi Subprovince: A tectonic and petrogenetic framework: *Economic Geology*, v. 88, p. 1359-1375.
- Suzuoki, T. and Epstein, S., 1976, Hydrogen isotope fractionation between OH-bearing minerals and water: *Geochimica et Cosmochimica Acta*, v. 40, p. 1229-1240.
- Sverjensky, D.A., Shock, E.L. and Helgeson, H.C., 1997, Prediction of the thermodynamic properties of aqueous metal complexes to 1000 °C and 5 kb: *Geochimica et Cosmochimica Acta*, v. 61, p. 1359-1412.
- Taylor, H.P., 1974, The application of oxygen and hydrogen isotope studies to problems of hydrothermal alteration and ore deposition: *Economic Geology*, v. 69, p. 843-883.
- Thode, H.G., Monster, J. and Dunford, H.B., 1961, Sulfur isotope geochemistry: *Geochimica et Cosmochimica Acta*, v. 25, p. 159-174.
- Thompson, J.F.H. and Newberry, R.J., 2000, Gold deposits related to reduced granitic intrusions: *Reviews in Economic Geology*, v. 13, p. 377-400.
- Thompson, J.F.H, Sillitoe, R.H., Baker, T., Lang, J.R. and Mortensen, J.K., 1999, Intrusion-related gold deposits associated with tungsten-tin provinces: *Mineralium Deposita*, v. 34, p. 197-217.

Thurston, P.C., Ayer, J.A., Goutier, J. and Hamilton, M.A., 2008, Depositional gaps in Abitibi Greenstone Belt stratigraphy: A key to exploration for syngenetic mineralization: *Economic Geology*, v, 103, p. 1097-1134.

Troop, D.G., 1985, Preliminary report on geology and metasomatism at the Ross mine and vicinity, District of Cochrane, *in* Wood, J., White, O.L., Barlow, R.B. and Colvine, A.C., eds., Summary of field work and other activities 1985, Ontario Geological Survey Miscellaneous Paper 126, pp. 320-325.

Trudel, P. and Sansfaçon, R., 1987, Géologie de la mine East Malartic, Région de Val-d'Or: Québec Ministère de l'Énergie et des Ressources, MB 87-25, 64 p.

Trudel, P. and Sauvé, P., 1992, Synthèse des caractéristiques géologiques des gisements d'or du district de Malartic: Québec Ministère de l'Énergie et des Ressources, MM 89-04, 126 p.

Wark, D.A., and Watson, E.B., 2006, TitaniQ: a titanium-in-quartz geothermometer: *Contributions to Mineralogy and Petrology*, v. 152, p. 743-754.

Wares, R., 2005, Canadian Malartic Gold Deposit, Quebec – Three to four million ounce gold potential, <http://www.osisko.com/pdfs/media_art_osisko_malartic_summary.pdf>.

Winchester, J.A. and Floyd, P.A., 1977, Geochemical discrimination of different magma series and their differentiation products using immobile elements: *Chemical Geology*, v. 20, p. 325-343.

APPENDICES

APPENDIX A: DESCRIPTION OF METHODS

CORE LOGGING

A total of 880 m of diamond drill core from four selected holes at the South Barnat Zone were logged and sampled in July 2009. Diamond drill holes were selected based on inspection of geological maps, sections and drill core logs with gold assays. Logging included descriptions of the dominant color of the rock and associated mineralogy, overall alteration strength and degree of magnetization, K-feldspathization, biotitization, carbonitization, silicification and pyritization. Descriptions of pyrite occurrence and veining were made and a lithological code assigned. Seventy-nine samples of halved NQ core were collected to represent variations in alteration type and intensity in the three main lithologies as well as the sulphide and gold mineralization. These samples were subsequently subjected to petrographic, whole rock geochemical and isotopic analyses. Additional diamond drill core samples previously collected from the Canadian Malartic deposit were also analyzed.

LITHOGEOCHEMISTRY

A suite of 36 halved NQ core samples of least altered to strongly altered porphyry, greywacke, mafic and ultramafic rock were analyzed for whole rock chemistry by Acme Analytical Laboratories Ltd., located in Vancouver, British Columbia, Canada to add to the Canadian Malartic deposit geochemical database. Major oxide, several minor element and rare earth element concentrations were analyzed using a combination of induced coupled plasma emission spectrometry (ICP-ES) following a lithium metaborate/tetraborate fusion and dilute nitric acid digestion; total carbon and sulfur contents were analyzed with a Leco combustion elemental analyzer. Precious and base metal concentrations were analyzed by induced coupled plasma mass spectrometry (ICP-MS) following an aqua regia digestion. Blanks, duplicates and standard reference materials were inserted as a measure of sample preparation quality, analytical precision, sub-sampling variation, background noise and accuracy. Uncertainty for major oxides, LOI, and elements Ba, C and S are between ± 2 and $\pm 5\%$ or better and are ± 10 to $\pm 15\%$ for all other elements. Results are listed in Appendix B and include the minimum detection limit for each analyte.

PETROGRAPHY

Fifty one standard polished thin sections (30 μ m) and ten fluid inclusion sections (120 μ m) were prepared from cut blocks of core samples by Vancouver Petrographics, Langley, British Columbia. Petrography was carried out using an Olympus BH2 microscope equipped for transmitted and reflected light.

ELECTRON MICROPROBE ANALYSES (EMPA)

Elemental analysis of native gold and biotite was carried out using a JEOL 8900L Electron Probe Microanalyzer, equipped with five wavelength dispersive spectrometers at McGill University. Instrument calibration was performed on standard reference materials. Forty point analyses over seven thin sections were conducted on grains of native gold. Preliminary analyses (28 points) for Au, Ag, Bi, Cu, Hg, Fe, and Pd showed only Au, Ag, Bi, and Cu to be present in detectable concentrations. The operating conditions were a 20kV accelerating voltage, a 20nA beam current and a beam focussed to approximately 1 μ m. Standard deviations for the analyzed elements are 0.8%, 0.5%, 2.5% and 0.9% respectively. One hundred thirteen point analyses over twelve thin sections were conducted on biotite grains. These grains were analyzed for Na₂O, K₂O, MgO, FeO, Al₂O₃, SiO₂, F, Cl, MnO, TiO₂, Cr₂O₃, BaO, V₂O₃ and CaO. The operating conditions were a 15kV accelerating voltage, a 20nA beam current and a beam diameter of 5 μ m. Standard deviations for the analyzed elements are 1.8%, 1.5%, 1.3%, 0.7%, 1.1%, 0.6%, 1.9%, 5.1%, 1.5%, 0.7%, 1.6%, 5.4%, 2.5% and 1.2%, respectively. Results of the analyses of native gold and biotite analyses are listed in Appendix C. Also reported in this appendix are the minimum detection limit for each element analyzed, information on the standards used and the counting times.

MASS CHANGE CALCULATIONS

Mass change calculations were conducted using data from Appendix B, combined with whole rock data from previous analyses, to evaluate chemical changes associated with hydrothermal alteration and mineralization. Formulas for these calculations are given in Appendix D as are the mean compositions of least altered and altered samples.

MINERAL SEPARATION

Mineral separation was conducted by the author at McGill University. Separates were obtained for stable isotope, crush leachate and laser ablation induced coupled plasma mass spectrometry (LA-ICPMS) analyses. Pyrite separates for stable isotope analysis were obtained by using a compression mortar to coarsely crush selected pieces of NQ diamond drill core. Most pyrite grains were sufficiently large for hand picking and, in samples in which they were not, whole rock samples were crushed powder-fine by Glenna Keating of the Trace Element Analytical Laboratories, McGill University and the whole rock was used for stable isotope analysis. The minimum amount of pyrite needed for successful sulfur extraction is 0.5 mg. In most cases, several tens of milligrams were obtained, and 2-3 mg used for extraction. Biotite, quartz and hematite separates (10-20 mg minimum) for oxygen (and hydrogen in the case of biotite) isotope analyses (and quartz separates for crush leachate analyses; 70 mg minimum) and LA-ICPMS analyses (a few grains) were carefully selected from vein material and isolated from diamond drill core using a hammer and chisel. In some cases, a compression mortar was used for further crushing. These grains were then handpicked, avoiding those with inclusions and/or intergrowths of other minerals. Separates of muscovite and biotite (50-100 mg minimum) and amphibole (100-150 mg minimum) were also prepared for $^{39}\text{Ar}/^{40}\text{Ar}$ age determinations using a Frantz isodynamic magnetic separator and subsequent handpicking. This work is not incorporated into the thesis. The amounts of the various mineral separates for the different types of analyses are given in the appropriate appendices.

STABLE ISOTOPIC ANALYSES AND GEOTHERMOMETRY

Sulfur

Sulfur isotopic analyses were conducted by the author at McGill University, using a combination of sulfur extraction techniques and mass spectrometry. To obtain sulfur isotopic data from sulfide minerals, powdered whole rock samples and pyrite separates were reacted with chromium reduction solution (CRS). This solution contains chromic chloride hexahydrate and concentrated hydrochloric acid and was reduced from the chromic (III) to the chromous (II) state by reacting it with zinc granules (a Jones

reductor) under vacuum. The sample and CRS were reacted at ~100°C to liberate sulfur as H₂S. The gas was then trapped using a zinc acetate solution and reacted with silver nitrate to produce silver sulfide (Canfield et al., 1986). In order to obtain sulfur isotopic compositions of the sulfate minerals (only barite was observed), the rock residue from the CRS extraction was thoroughly washed and reacted with Thode solution, a mixture of hydroiodic, hydrochloric and hypophosphorous acids (Thode et al., 1961), to liberate all the sulfur from the sulfate minerals. The sulfate was reduced to H₂S, captured with zinc acetate and reacted with silver nitrate to produce silver sulfide.

The silver sulfide was converted to sulfur hexafluoride by reacting it with fluorine (Rumble et al., 1993) generated from heating hexafluoronickelate. The resulting solution was then purified with several cryogenic traps and a gas chromatograph (to isolate the sulfur hexafluoride) before being introduced into a ThermoFinnigan MAT253 dual-inlet gas-source mass spectrometer. Sulfur isotope abundances were measured at a mass/charge ratio of 127-129 and are reported using δ notation standardized to the Vienna-Canyon Diablo Troilite (Ding et al., 2001). Accuracy and precision were checked by the random insertion of standard reference material (mss_1). The quantities of sample and reagent employed for sulfur extraction and the quantities of silver sulfide produced from the extraction process are reported in Appendix E together with sulfur isotopic compositions, $\delta^{33}\text{S}$, $\delta^{34}\text{S}$, $\delta^{36}\text{S}$, $\Delta^{33}\text{S}$, $\Delta^{36}\text{S}$, of the pyrite and barite and the analytical errors incurred during mass spectrometry.

The $\delta^{34}\text{S}$ values from sulfide-sulfate mineral pairs (when formed contemporaneously at equilibrium, and not subjected to re-equilibration at conditions different from those of their formation) can be used for geothermometry with a high degree of sensitivity, and are particularly useful in high-temperature magmatic hydrothermal systems due to factors affecting the kinetics of sulfur isotope exchange between SO_4^{2-} and H₂S (Ohmoto and Lasaga, 1982). The barite-pyrite geothermometer was employed in this study and temperatures calculated from sulfur isotope fractionation between barite and pyrite are presented in Appendix G together with the corresponding fractionation equations.

Oxygen and Hydrogen

Oxygen isotopic compositions of quartz, hematite and biotite and the hydrogen isotopic composition of biotite were analyzed by Kerry Klassen at the Queen's University Facility for Isotope Research (QFIR), Kingston, Ontario. Oxygen was extracted from the mineral separates by thermochemical conversion in the presence of bromine pentafluoride, then dehydrated and purified with liquid nitrogen cryotrap and reacted over a carbon rod to convert O₂ to CO₂ for measurement with a dual-inlet gas source mass spectrometer. Hydrogen was extracted using a thermal conversion elemental analyzer (TC/EA) interfaced to a gas source mass spectrometer and analyzed as H₂. The quantities of mineral separates, as well as Oxygen, $\delta^{18}\text{O}$, and hydrogen, δD , isotope compositions are listed in Appendix F. Temperatures calculated from fractionation of quartz-biotite and quartz-hematite mineral pairs together with the corresponding fractionation equations are reported in Appendix G.

CRUSH LEACHATE ANALYSES

The composition of the bulk included fluid in 10 samples of hydrothermal vein quartz was determined by crushing the samples, leaching the fluids and analysing the leachates using a combination of ICP-MS and ICP-AES (cations) and ion chromatography (anions). The fluid extraction was carried out by the author in the Hydrothermal Geochemistry Laboratory at McGill University, using the methods of Botrell et al., 1988 and Halter and Williams-Jones (1995). Between 0.5 and 1 g quartz was used in each extraction. Quartz grains were washed in hot, concentrated, trace metal grade nitric acid for two hours to dissolve carbonate and sulphide impurities and to create a strong positive charge on the surfaces of the grains to repel most singly-or doubly-charged cations which could contaminate the leachate (Halter and Williams-Jones, 1995). Samples were then washed in de-ionized water using an ultrasonic bath; this procedure was repeated several times. Since more highly charged cations can still be adsorbed onto grain surfaces after an acid wash, samples were washed with a 1M nitric acid solution containing 200 ppm lanthanum (prepared from lanthanum (III) chloride heptahydrate) for one hour as this has been shown to be effective in preventing adsorption of highly charge cations to grain surfaces (Botrell et al, 1988). Samples were then washed with de-ionized water for one

hour in an ultrasonic bath. After cleaning, each sample was rinsed repeatedly (20 times) in de-ionized water to remove traces of nitric acid, and dried in an oven at 100°C for three hours. The rinsed samples were crushed in an agate mortar to a fine powder, split into two aliquots and leached. One split was leached with 30 mL de-ionized water for determination of the anion content and the other with 100 mL 1 M nitric acid solution containing 200 ppm lanthanum for determination of the cation content. Quartz powder was filtered from the leachates, which were collected in HDPE bottles (anion leachate was stored at 4°C). Leachates from selected pre-crushed samples were also analyzed to assess contamination from incompletely cleaned grain surfaces, as was filtered leaching solution to assess the extent of incorporation of ions from the filter paper. These constituted blank analyses, in addition to a leachate from 99.99 % silica powder, to which the analyzed compositions of the inclusion fluids could be compared and corrected.

The ion chromatographic analyses (anions) were conducted by Activation Laboratories Ltd., Ancaster, Ontario and the ICP-MS and ICP-AES (cations) by Geolabs Geoscience Laboratories, Sudbury, Ontario. The results for Na were higher than those of the blank solution, so this element was re-analyzed using leachate employed for anion analyses by Activation Laboratories Ltd. In addition to Na, K and Ca were also re-analyzed as an additional check, as the anion leachate solution was analyzed by ICP-OES, whereas all other cation analyses had been analyzed by ICP-MS (as well as ICP-AES for Ca, K, Mg, Na, S, Si although results reported for these elements are from ICP-MS or ICP-OES due to lower detection limits). Also, as the anion leachate was not treated to avoid adsorption on the walls of the HDPE bottles, there was concern that some Na may have been adsorbed. Many of the elements analyzed in the leachate solutions were below the limit of detection (F, NO₂, Br, PO₄, Be, B, Sc, Mn, As, Se, Zr, Nb, Mo, Ag, Sb, Te, Au, Bi, Th, Hf, Ga) and others had contents similar to or greater than those in the blank solutions. Since lanthanum (III) chloride heptahydrate was used to prepare the cation leaching solution, Cl, as well as La and all other REE results were disregarded from ICP-MS analyses. As salinity was unknown (inclusions were too small for microthermometric analyses) the leachate data are reported in ratios with Ca as the denominator and have been corrected for addition of ions from the filter paper (Cl, NO₃, Na, Mg, Ca, S, Si, Cu, Sr, Ba, Pb, U). The leachate data are presented in Appendix H as

are leachate datasets representing brine/formation, metamorphic and magmatic waters for comparison.

LASER ABLATION INDUCED COUPLED MASS SPECTROMETRY (LA-ICPMS)

A composite grain mount was created from twelve samples of hydrothermal vein quartz and each sample analyzed for its titanium concentration using Laser Ablation Induced Coupled Mass Spectrometry. Samples of the larger quartz veinlets with intergrown biotite and muscovite were selected as well as narrower quartz veinlets with K-feldspar alteration haloes. Analyses were conducted using a Thermo Elemental (VG) PlasmaQuad PQ ExCell ICP-MS instrument coupled to a Nu-Wave UP-213nm Laser Ablation Microscope at the University of Toronto, Toronto, Ontario. The laser beam was fired at a 10Hz repetition rate with the laser energy in the range of $1.8\text{J}/\text{cm}^2$. A spot size of $75\ \mu\text{m}$ was used and data acquisition was based on a 50 ms point ablation. Data reduction and calculation of concentrations were performed using the GLITTER software package and analytical errors calculated as 1σ . The titanium concentrations and details on the standard are reported in Appendix I as are temperatures calculated with the TitaniQ geothermometer (Wark and Watson, 2006) and the algorithm used for the calculation of temperature.

PHASE EQUILIBRIA CALCULATIONS

Binary phase diagrams showing stability relationships among aqueous sulfur species (HSO_4^- , SO_4^{2-} , H_2S and HS^-), minerals in the Fe-S-O system (hematite, magnetite, pyrite and pyrrhotite), predominance fields of gold complexes (AuCl_2^- , AuOH , $\text{Au}(\text{HS})_2^-$ and AuHS) and gold solubility contours at 10^4 , 10^3 and 10^2 ppb were constructed at $475\ ^\circ\text{C}$ and 1000 to 5000 bar as a function of $\log f_{\text{O}_2}$ and pH, and $\log \Sigma a_s$ and $\log f_{\text{O}_2}$ over a range of pH values from 4-7. Unitherm, a computer program for evaluating chemical equilibria (Shvarov and Bastrakov, 1999), was used to obtain ΔG_r for the reactions determining phase boundaries, speciation predominance boundaries and gold saturation contours at the above temperatures and pressures (the values and references for these parameters are listed in Appendix J along with a list of reactions used); the $\log K_r$ values for the reactions were calculated manually and plotted using Microsoft Excel. Also shown in Appendix J

are calculations used to construct sulfur isotope contours in $\log f_{\text{O}_2}$ and pH space and an example diagram showing these contours at 475 °C and 3000 bar.

APPENDIX B: BULK-ROCK CHEMICAL ANALYSES

Analyte	Litho.	Weight	SiO₂	Al₂O₃	Fe₂O₃	MgO	CaO	Na₂O	K₂O	TiO₂	P₂O₅	MnO	Cr₂O₃	Ni	Sc
Unit		kg	Wt %	Wt %	Wt %	Wt %	Wt %	Wt %	Wt %	Wt %	Wt %	Wt %	Wt %	ppm	ppm
MDL		0.01	0.01	0.01	0.04	0.01	0.01	0.01	0.01	0.01	0.01	0.01	0.00	20.00	1.00
Sample (BA08)															
3008-116.9	Pontiac	0.17	60.67	16.16	5.35	2.61	2.20	5.51	3.21	0.59	0.13	0.06	0.03	87.00	16.00
3008-121.8	Pontiac	0.17	66.42	11.09	5.88	2.07	2.41	3.63	3.35	0.43	0.14	0.06	0.02	69.00	11.00
3008-126.9	Pontiac	0.14	60.56	13.54	4.84	2.25	3.68	5.40	3.53	0.47	0.08	0.07	0.02	68.00	12.00
3008-162.1	Piché	0.16	39.73	5.19	9.12	22.95	7.47	0.06	0.62	0.23	0.02	0.17	0.29	1191.00	19.00
3008-169.7	Piché	0.18	37.18	5.48	9.53	22.38	8.86	0.07	0.50	0.27	0.03	0.20	0.28	1095.00	20.00
3008-230.7	MDPO	0.12	61.05	16.52	4.20	1.68	2.69	8.31	0.83	0.59	0.28	0.04	0.01	34.00	4.00
3008-250.5	MDPO	0.24	67.32	16.38	1.51	0.47	2.07	8.88	0.77	0.28	0.11	0.02	0.00	BDL	1.00
3008-86.9	Pontiac	0.11	56.92	15.97	5.51	3.08	3.33	5.43	3.81	0.59	0.12	0.08	0.03	84.00	17.00
3040-131.7	Piché	0.13	41.85	6.35	10.20	22.49	4.45	0.04	3.45	0.30	0.03	0.12	0.35	1323.00	23.00
3040-175.4	MDPO	0.20	70.51	12.10	2.16	1.33	2.43	5.49	2.05	0.36	0.35	0.03	0.01	24.00	2.00
3040-209.5	Piché	0.13	44.06	4.82	9.75	20.99	7.66	0.16	2.73	0.32	0.03	0.17	0.27	1161.00	19.00
3040-241	MDPO	0.14	67.70	17.21	1.11	0.42	1.43	8.42	1.42	0.16	0.06	0.01	0.00	BDL	BDL
3040-271.2	Pontiac	0.24	66.82	13.38	4.89	2.21	1.90	5.70	1.52	0.48	0.10	0.05	0.02	78.00	10.00
3040-29.1	Piché	0.22	42.90	8.46	10.58	10.64	10.39	0.04	5.06	0.70	0.07	0.17	0.10	328.00	26.00
3040-299.6	Pontiac	0.11	64.76	13.48	5.79	3.63	0.83	3.07	4.49	0.51	0.07	0.03	0.03	86.00	14.00
3040-30.5	MDPO	0.17	65.29	15.93	1.39	0.59	1.62	6.39	2.52	0.25	0.10	0.01	0.00	BDL	1.00
3040-322.6	Pontiac	0.13	62.55	12.76	5.63	3.21	3.92	1.91	7.10	0.49	0.09	0.08	0.03	78.00	15.00
3040-340.2	MDPO	0.13	68.09	15.40	1.46	0.91	1.75	6.07	3.49	0.32	0.14	0.01	BDL	BDL	2.00
3040-362.5	Pontiac	0.16	53.90	15.66	6.27	3.07	4.05	4.62	5.75	0.58	0.08	0.08	0.02	87.00	16.00
3068-11	MDPO	0.13	64.20	16.19	2.98	0.85	2.43	6.02	3.88	0.49	0.22	0.02	BDL	BDL	2.00
3068-17	MDPO	0.14	62.70	14.72	3.16	0.80	3.99	5.12	3.83	0.45	0.23	0.04	BDL	BDL	2.00
3068-2	Piché	0.19	36.02	10.96	16.30	19.11	1.92	0.15	8.80	1.34	0.17	0.12	0.15	678.00	40.00
3068-27	MDPO	0.12	65.37	15.89	2.54	0.98	2.55	6.38	2.96	0.40	0.18	0.02	0.01	BDL	2.00
3068-29	Piché	0.20	50.21	12.74	9.79	7.21	6.51	3.05	3.79	0.91	0.48	0.13	0.04	53.00	32.00

Analyte	Litho.	Weight	SiO₂	Al₂O₃	Fe₂O₃	MgO	CaO	Na₂O	K₂O	TiO₂	P₂O₅	MnO	Cr₂O₃	Ni	Sc
Unit		kg	Wt %	Wt %	Wt %	Wt %	Wt %	Wt %	Wt %	Wt %	Wt %	Wt %	Wt %	ppm	ppm
MDL		0.01	0.01	0.01	0.04	0.01	0.01	0.01	0.01	0.01	0.01	0.01	0.00	20.00	1.00
Sample (BA08)															
3119-10	Pontiac	0.15	38.75	9.75	14.48	19.92	4.22	0.08	6.65	0.57	0.04	0.14	0.34	676.00	36.00
3119-9	Piché	0.19	45.91	7.15	9.98	22.15	7.37	0.16	1.07	0.29	0.02	0.15	0.31	1465.00	19.00
3121-1	MDPO	0.15	60.73	16.19	4.80	1.83	3.38	8.26	0.99	0.78	0.34	0.04	0.01	32.00	6.00
3121-11	Pontiac	0.12	65.50	14.41	5.87	2.97	2.63	3.75	2.17	0.55	0.17	0.06	0.03	100.00	14.00
3121-5	MDPO	0.07	61.81	16.95	3.81	0.86	1.89	6.72	3.93	0.51	0.23	0.02	0.00	28.00	2.00
3121-8	MDPO	0.25	62.65	14.47	3.62	1.35	4.18	7.97	0.66	0.62	0.30	0.04	0.00	20.00	4.00
3594-11	Piché	0.16	51.91	8.89	9.09	7.01	10.62	4.96	0.30	0.70	0.14	0.17	0.05	107.00	22.00
3594-13	Piché	0.21	48.23	12.54	14.24	5.35	8.28	6.01	0.17	1.43	0.11	0.23	0.01	49.00	45.00
3594-14	Piché	0.15	47.29	7.33	12.26	17.55	7.94	1.20	2.48	0.45	0.04	0.17	0.33	692.00	27.00
3594-15	Piché	0.14	46.39	6.00	10.12	20.31	7.68	0.65	4.38	0.34	0.02	0.18	0.31	939.00	22.00
3594-4	MDPO	0.19	73.90	2.69	4.21	8.71	2.62	0.03	2.06	0.13	BDL	0.06	0.12	468.00	8.00
3594-8	MDPO	0.13	58.34	8.25	10.33	4.43	3.66	2.42	3.40	1.15	0.04	0.08	0.02	77.00	25.00

Analyte	Litho.	Weight	LOI	Sum	Ba	Be	Co	Cs	Ga	Hf	Nb	Rb	Sn	Sr	Ta
Unit		kg	%	%	ppm										
MDL		0.01	-5.10	0.01	1.00	1.00	0.20	0.10	0.50	0.10	0.10	0.10	1.00	0.50	0.10
Sample (BA08)															
3008-116.9	Pontiac	0.17	3.30	99.82	358.00	2.00	19.80	1.70	17.80	3.10	6.00	85.50	BDL	403.10	0.50
3008-121.8	Pontiac	0.17	4.30	99.80	596.00	1.00	20.60	1.60	14.60	2.90	4.40	56.50	1.00	500.30	0.30
3008-126.9	Pontiac	0.14	5.40	99.85	320.00	1.00	17.80	0.50	17.60	3.10	4.80	34.20	BDL	431.30	0.30
3008-162.1	Piché	0.16	13.60	99.57	34.00	1.00	78.90	1.80	7.80	0.30	0.30	26.80	BDL	204.50	BDL
3008-169.7	Piché	0.18	14.70	99.58	46.00	BDL	79.50	1.30	6.10	0.40	0.30	20.50	BDL	165.60	BDL
3008-230.7	MDPO	0.12	3.50	99.69	1072.00	2.00	10.10	0.50	27.30	5.40	5.40	16.60	2.00	840.20	0.30
3008-250.5	MDPO	0.24	1.90	99.67	1564.00	2.00	3.00	0.30	22.70	3.90	3.00	12.00	1.00	1066.50	0.20
3008-86.9	Pontiac	0.11	4.90	99.77	629.00	3.00	19.10	2.80	20.60	3.10	5.60	69.60	1.00	440.70	0.40
3040-131.7	Piché	0.13	9.80	99.57	118.00	BDL	98.20	7.50	8.70	0.40	0.30	129.10	BDL	113.50	BDL
3040-175.4	MDPO	0.20	3.00	99.78	746.00	2.00	4.80	0.30	23.60	3.30	3.20	23.60	1.00	793.30	0.10
3040-209.5	Piché	0.13	8.50	99.60	61.00	2.00	76.90	10.80	7.40	0.50	0.60	120.40	BDL	114.40	BDL
3040-241	MDPO	0.14	1.80	99.75	909.00	2.00	1.70	0.30	20.00	3.00	1.70	20.30	BDL	1119.40	0.10
3040-271.2	Pontiac	0.24	2.80	99.88	216.00	2.00	17.80	2.50	14.80	2.90	4.80	47.20	BDL	307.40	0.40
3040-29.1	Piché	0.22	10.40	99.60	287.00	2.00	53.20	6.00	12.40	1.10	2.50	132.30	BDL	515.20	0.20
3040-299.6	Pontiac	0.11	3.10	99.77	756.00	1.00	23.90	1.20	18.30	2.80	4.60	46.70	BDL	497.30	0.30
3040-30.5	MDPO	0.17	5.60	99.68	1686.00	1.00	4.20	0.30	22.70	3.60	2.60	31.70	BDL	744.10	0.20
3040-322.6	Pontiac	0.13	1.90	99.68	1008.00	2.00	20.50	3.70	15.70	2.70	4.90	118.90	BDL	998.70	0.40
3040-340.2	MDPO	0.13	2.20	99.83	773.00	2.00	4.10	0.20	18.70	3.00	3.00	42.70	BDL	622.60	0.20
3040-362.5	Pontiac	0.16	5.70	99.76	604.00	3.00	21.30	1.80	25.30	3.10	5.50	72.70	BDL	701.50	0.30
3068-11	MDPO	0.13	2.30	99.61	1674.00	1.00	5.00	0.80	25.80	4.70	5.30	57.80	1.00	1174.00	0.30
3068-17	MDPO	0.14	3.70	98.74	6441.00	1.00	5.30	0.30	20.50	4.40	4.80	51.10	1.00	4126.00	0.20
3068-2	Piché	0.19	4.40	99.51	649.00	BDL	86.50	44.40	16.70	2.40	4.60	360.70	BDL	147.90	0.30
3068-27	MDPO	0.12	2.40	99.62	1621.00	2.00	6.30	1.00	26.40	4.80	6.10	44.40	1.00	1141.10	0.30
3068-29	Piché	0.20	4.80	99.67	729.00	3.00	36.10	9.60	15.70	3.30	4.80	132.90	1.00	412.30	0.30

Analyte	Litho.	Weight	LOI	Sum	Ba	Be	Co	Cs	Ga	Hf	Nb	Rb	Sn	Sr	Ta
Unit		kg	%	%	ppm										
MDL		0.01	-5.10	0.01	1.00	1.00	0.20	0.10	0.50	0.10	0.10	0.10	1.00	0.50	0.10
Sample (BA08)															
3119-10	Pontiac	0.15	4.60	99.57	322.00	1.00	94.00	28.30	10.50	0.80	1.00	288.20	BDL	59.20	BDL
3119-9	Piché	0.19	4.90	99.59	46.00	BDL	93.00	5.30	11.40	0.40	0.50	50.40	BDL	31.30	BDL
3121-1	MDPO	0.15	2.23	99.68	1147.00	3.00	10.30	1.60	23.40	5.10	6.40	30.00	2.00	811.30	0.30
3121-11	Pontiac	0.12	1.70	99.78	655.00	1.00	20.60	3.70	19.20	3.80	6.10	69.00	BDL	376.80	0.40
3121-5	MDPO	0.07	2.70	99.43	3066.00	2.00	9.20	0.30	27.40	5.20	4.90	38.70	1.00	1352.40	0.20
3121-8	MDPO	0.25	3.90	99.77	693.00	2.00	10.20	2.50	26.00	4.90	7.40	28.90	2.00	576.90	0.30
3594-11	Piché	0.16	5.40	99.22	400.00	2.00	37.30	1.10	9.20	1.10	3.00	11.20	BDL	4611.80	0.20
3594-13	Piché	0.21	3.20	99.79	22.00	1.00	41.70	0.40	17.10	2.50	4.40	3.50	BDL	214.20	0.30
3594-14	Piché	0.15	2.50	99.63	199.00	BDL	64.50	10.00	8.20	0.60	3.80	80.20	BDL	43.70	0.20
3594-15	Piché	0.14	2.80	99.30	1482.00	1.00	79.00	22.40	9.80	0.60	0.80	194.10	BDL	1344.50	BDL
3594-4	MDPO	0.19	5.20	99.79	147.00	14.00	36.70	1.30	5.10	0.30	0.30	40.70	BDL	335.50	BDL
3594-8	MDPO	0.13	7.60	99.72	332.00	2.00	36.30	1.30	13.40	2.30	4.80	61.60	1.00	765.40	0.30

Analyte	Litho.	Weight	Th	U	V	W	Zr	Y	La	Ce	Pr	Nd	Sm	Eu	Gd
Unit		kg	ppm	ppm	ppm	ppm	ppm	ppm	ppm	ppm	ppm	ppm	ppm	ppm	ppm
MDL		0.01	0.20	0.10	8.00	0.50	0.10	0.10	0.10	0.10	0.02	0.30	0.05	0.02	0.05
Sample (BA08)															
3008-116.9	Pontiac	0.17	6.30	2.00	116.00	18.50	110.50	13.50	23.70	51.20	5.91	22.80	3.87	1.00	3.09
3008-121.8	Pontiac	0.17	5.40	1.90	84.00	29.90	112.20	11.40	22.80	45.40	5.05	20.50	3.18	0.83	2.51
3008-126.9	Pontiac	0.14	5.60	1.70	31.00	26.00	105.80	10.90	22.60	48.10	5.39	21.90	3.42	0.90	2.65
3008-162.1	Piché	0.16	BDL	0.10	129.00	0.80	11.00	5.90	0.60	1.20	0.18	1.20	0.40	0.20	0.73
3008-169.7	Piché	0.18	BDL	BDL	111.00	0.70	12.90	6.80	0.60	1.60	0.25	1.80	0.59	0.24	0.90
3008-230.7	MDPO	0.12	7.60	2.00	73.00	33.30	212.10	7.10	57.40	130.00	15.38	62.70	9.59	2.28	5.60
3008-250.5	MDPO	0.24	5.40	2.20	21.00	7.50	146.20	2.80	26.90	58.60	6.83	28.70	4.21	1.04	2.27
3008-86.9	Pontiac	0.11	7.20	1.90	133.00	21.30	110.80	15.20	27.40	60.30	6.81	27.90	4.49	1.10	3.42
3040-131.7	Piché	0.13	BDL	0.10	134.00	BDL	14.10	7.20	0.60	1.10	0.21	1.20	0.45	0.17	0.83
3040-175.4	MDPO	0.20	4.10	1.10	13.00	22.30	108.30	3.70	29.70	66.30	7.85	31.80	4.97	1.17	3.01
3040-209.5	Piché	0.13	BDL	0.10	112.00	BDL	14.10	5.00	0.90	1.90	0.31	1.70	0.55	0.22	0.79
3040-241	MDPO	0.14	5.20	1.70	14.00	4.70	97.00	2.10	25.60	50.80	5.32	19.40	2.47	0.61	1.33
3040-271.2	Pontiac	0.24	4.70	1.40	62.00	16.80	107.30	9.40	19.40	41.20	4.61	17.70	2.90	0.79	2.20
3040-29.1	Piché	0.22	0.30	0.40	246.00	8.50	33.30	13.70	2.70	6.30	0.88	4.40	1.23	0.43	1.72
3040-299.6	Pontiac	0.11	5.50	1.60	100.00	13.20	92.00	9.50	17.00	37.70	4.39	16.70	2.82	0.83	2.29
3040-30.5	MDPO	0.17	3.80	1.70	18.00	14.30	135.60	2.30	23.90	52.60	6.03	23.60	3.73	0.84	2.05
3040-322.6	Pontiac	0.13	4.90	1.40	79.00	15.40	95.40	13.20	23.20	49.70	5.60	21.60	3.63	0.94	2.92
3040-340.2	MDPO	0.13	3.60	1.70	27.00	12.20	116.60	3.00	14.70	32.60	3.43	12.40	1.99	0.48	1.24
3040-362.5	Pontiac	0.16	6.20	2.30	47.00	29.70	111.40	12.90	22.60	49.10	5.62	22.00	3.79	0.99	2.88
3068-11	MDPO	0.13	6.00	1.60	42.00	4.90	165.90	4.70	39.80	88.90	10.49	42.40	6.61	1.60	3.91
3068-17	MDPO	0.14	5.50	1.20	35.00	13.30	160.20	5.40	46.60	100.40	11.68	45.00	7.15	1.79	4.47
3068-2	Piché	0.19	0.40	0.40	286.00	BDL	81.40	17.60	6.50	19.80	2.64	10.80	2.67	1.83	3.00
3068-27	MDPO	0.12	6.10	2.00	34.00	4.50	187.60	4.20	45.50	99.00	11.40	45.30	6.86	1.47	3.97
3068-29	Piché	0.20	3.90	1.40	210.00	0.60	113.70	22.50	22.20	52.10	6.68	29.00	6.22	1.67	5.52

Analyte	Litho.	Weight	Th	U	V	W	Zr	Y	La	Ce	Pr	Nd	Sm	Eu	Gd
Unit		kg	ppm	ppm	ppm	ppm	ppm	ppm	ppm	ppm	ppm	ppm	ppm	ppm	ppm
MDL		0.01	0.20	0.10	8.00	0.50	0.10	0.10	0.10	0.10	0.02	0.30	0.05	0.02	0.05
Sample (BA08)															
3119-10	Pontiac	0.15	BDL	BDL	226.00	BDL	27.70	12.30	1.50	4.20	0.64	3.20	1.02	0.23	1.47
3119-9	Piché	0.19	BDL	BDL	131.00	0.80	14.40	5.80	0.40	1.20	0.23	1.30	0.59	0.22	0.82
3121-1	MDPO	0.15	6.10	1.50	82.00	4.60	201.40	9.40	48.10	110.90	12.92	54.00	8.81	2.27	5.72
3121-11	Pontiac	0.12	6.80	2.10	104.00	4.20	151.40	13.60	30.60	66.50	7.46	29.10	4.85	1.23	3.46
3121-5	MDPO	0.07	5.70	1.50	43.00	33.80	193.40	4.40	42.90	96.00	11.00	44.80	6.69	1.53	3.68
3121-8	MDPO	0.25	6.10	1.90	67.00	17.60	185.70	8.10	65.30	143.40	15.69	61.00	9.62	2.33	5.95
3594-11	Piché	0.16	0.40	1.40	168.00	23.30	37.00	11.70	3.40	8.50	1.09	5.20	1.56	0.56	1.96
3594-13	Piché	0.21	0.50	0.10	392.00	1.00	87.60	31.30	4.90	13.90	1.99	10.80	3.35	1.08	4.22
3594-14	Piché	0.15	BDL	BDL	138.00	BDL	17.50	6.40	0.90	2.50	0.33	2.30	0.71	0.22	1.04
3594-15	Piché	0.14	BDL	0.10	179.00	BDL	17.60	7.10	1.30	3.40	0.47	2.30	0.77	0.21	1.07
3594-4	MDPO	0.19	BDL	BDL	144.00	0.90	6.10	2.70	0.20	0.60	0.11	0.60	0.21	0.08	0.34
3594-8	MDPO	0.13	0.50	1.00	158.00	42.00	72.50	22.10	5.30	14.30	2.02	9.70	2.62	0.78	3.37

Analyte	Litho.	Weight	Tb	Dy	Ho	Er	Tm	Yb	Lu	TOT/C	TOT/S	Mo	Cu	Pb	Zn
Unit		kg	ppm	%	%	ppm	ppm	ppm	ppm						
MDL		0.01	0.01	0.05	0.02	0.03	0.01	0.05	0.01	0.02	0.02	0.10	0.10	0.10	1.00
Sample (BA08)															
3008-116.9	Pontiac	0.17	0.44	2.39	0.46	1.27	0.20	1.26	0.19	0.46	1.24	7.90	54.10	2.60	66.00
3008-121.8	Pontiac	0.17	0.36	2.01	0.37	1.06	0.17	1.10	0.16	0.49	2.70	2.60	46.80	8.00	63.00
3008-126.9	Pontiac	0.14	0.36	1.95	0.36	1.01	0.15	1.13	0.16	0.97	2.71	4.60	4.90	10.90	36.00
3008-162.1	Piché	0.16	0.15	1.01	0.21	0.65	0.09	0.62	0.09	2.57	0.11	BDL	38.60	3.90	18.00
3008-169.7	Piché	0.18	0.17	1.15	0.24	0.70	0.09	0.64	0.09	2.92	0.11	4.00	46.50	3.30	17.00
3008-230.7	MDPO	0.12	0.54	1.82	0.19	0.41	0.06	0.36	0.05	0.47	1.59	0.20	26.50	14.60	54.00
3008-250.5	MDPO	0.24	0.21	0.70	0.07	0.17	0.03	0.17	0.02	0.32	0.52	4.20	18.80	16.80	32.00
3008-86.9	Pontiac	0.11	0.48	2.57	0.52	1.43	0.22	1.41	0.22	0.83	1.52	8.10	21.90	3.60	70.00
3040-131.7	Piché	0.13	0.18	1.16	0.27	0.74	0.12	0.68	0.12	1.88	0.43	0.10	77.40	4.30	28.00
3040-175.4	MDPO	0.20	0.31	0.96	0.13	0.17	0.04	0.17	0.04	0.59	0.71	21.80	12.20	9.30	33.00
3040-209.5	Piché	0.13	0.14	0.82	0.17	0.52	0.08	0.52	0.08	1.64	1.12	BDL	49.60	4.30	21.00
3040-241	MDPO	0.14	0.14	0.41	0.07	0.13	0.03	0.15	0.03	0.32	0.38	1.30	16.20	8.40	6.00
3040-271.2	Pontiac	0.24	0.32	1.59	0.31	0.93	0.15	0.89	0.15	0.28	1.69	8.20	42.60	7.50	57.00
3040-29.1	Piché	0.22	0.33	2.11	0.48	1.42	0.20	1.39	0.20	2.46	1.58	295.90	132.30	11.00	91.00
3040-299.6	Pontiac	0.11	0.32	1.73	0.31	1.01	0.16	1.01	0.15	0.11	1.93	4.90	13.80	5.40	45.00
3040-30.5	MDPO	0.17	0.18	0.58	0.05	0.15	0.02	0.11	0.01	0.30	0.28	4.10	16.50	4.00	25.00
3040-322.6	Pontiac	0.13	0.42	2.23	0.44	1.24	0.19	1.21	0.18	0.73	2.32	2.90	61.40	3.40	54.00
3040-340.2	MDPO	0.13	0.14	0.54	0.07	0.19	0.03	0.16	0.03	0.30	0.39	1.30	3.30	9.80	9.00
3040-362.5	Pontiac	0.16	0.42	2.22	0.43	1.26	0.19	1.29	0.20	0.86	3.43	3.10	16.10	4.90	83.00
3068-11	MDPO	0.13	0.40	1.34	0.12	0.24	0.03	0.20	0.02	0.42	0.15	0.10	32.20	4.80	105.00
3068-17	MDPO	0.14	0.46	1.43	0.14	0.27	0.03	0.19	0.02	0.85	0.37	0.20	4.30	12.50	44.00
3068-2	Piché	0.19	0.53	3.06	0.62	1.81	0.27	1.64	0.24	0.15	3.12	BDL	2.70	1.20	120.00
3068-27	MDPO	0.12	0.38	1.13	0.09	0.16	0.03	0.19	0.02	0.44	0.58	3.40	16.30	7.70	78.00
3068-29	Piché	0.20	0.81	3.93	0.76	2.09	0.31	1.90	0.29	0.94	0.40	1.20	86.40	8.30	95.00

Analyte	Litho.	Weight	Tb	Dy	Ho	Er	Tm	Yb	Lu	TOT/C	TOT/S	Mo	Cu	Pb	Zn
Unit		kg	ppm	%	%	ppm	ppm	ppm	ppm						
MDL		0.01	0.01	0.05	0.02	0.03	0.01	0.05	0.01	0.02	0.02	0.10	0.10	0.10	1.00
Sample (BA08)															
3119-10	Pontiac	0.15	0.29	1.84	0.41	1.31	0.18	1.12	0.17	0.65	BDL	BDL	68.00	1.40	33.00
3119-9	Piché	0.19	0.17	0.97	0.21	0.64	0.09	0.58	0.09	BDL	0.19	8.60	45.10	2.40	33.00
3121-1	MDPO	0.15	0.62	2.32	0.29	0.61	0.08	0.49	0.07	0.53	0.15	0.20	7.40	16.80	73.00
3121-11	Pontiac	0.12	0.48	2.47	0.43	1.25	0.18	1.21	0.18	BDL	0.41	1.50	87.20	3.10	68.00
3121-5	MDPO	0.07	0.33	1.00	0.12	0.22	0.03	0.22	0.03	0.33	1.17	8.60	8.90	25.10	52.00
3121-8	MDPO	0.25	0.61	2.12	0.23	0.46	0.07	0.40	0.06	0.82	1.60	1.00	7.20	13.10	53.00
3594-11	Piché	0.16	0.36	1.96	0.42	1.19	0.18	1.06	0.17	1.31	3.59	6.90	206.70	117.30	11.00
3594-13	Piché	0.21	0.82	5.06	1.14	3.38	0.50	3.22	0.50	0.72	0.24	3.20	76.30	11.80	35.00
3594-14	Piché	0.15	0.17	1.19	0.25	0.74	0.08	0.72	0.09	0.08	0.25	26.10	111.90	2.20	50.00
3594-15	Piché	0.14	0.21	1.23	0.26	0.77	0.12	0.69	0.10	0.23	0.32	0.10	9.00	0.50	57.00
3594-4	MDPO	0.19	0.08	0.40	0.10	0.29	0.05	0.27	0.04	1.12	1.06	1.10	4.20	24.80	70.00
3594-8	MDPO	0.13	0.63	4.01	0.86	2.44	0.36	2.29	0.36	0.84	6.03	0.60	357.50	26.80	34.00

Analyte	Litho.	Weight	As	Cd	Sb	Bi	Ag	Au	Hg	Tl	Se	Te
Unit		kg	ppm	ppm	ppm	ppm	ppm	ppb	ppm	ppm	ppm	ppm
MDL		0.01	0.50	0.10	0.10	0.10	0.10	0.50	0.01	0.10	0.50	1.00
Sample (BA08)												
3008-116.9	Pontiac	0.17	2.10	BDL	BDL	0.60	3.30	4867.90	BDL	0.40	BDL	1.00
3008-121.8	Pontiac	0.17	1.20	0.10	BDL	0.90	7.90	40751.90	BDL	0.40	0.90	3.00
3008-126.9	Pontiac	0.14	1.70	0.30	BDL	1.40	7.90	52771.40	BDL	0.20	0.80	4.00
3008-162.1	Piché	0.16	1.40	BDL	BDL	0.20	0.10	45.20	BDL	0.20	BDL	BDL
3008-169.7	Piché	0.18	1.30	BDL	BDL	BDL	BDL	110.70	BDL	0.10	BDL	BDL
3008-230.7	MDPO	0.12	1.50	BDL	BDL	0.70	2.40	4463.50	BDL	0.10	BDL	2.00
3008-250.5	MDPO	0.24	1.10	BDL	BDL	0.20	0.10	252.60	BDL	BDL	BDL	BDL
3008-86.9	Pontiac	0.11	1.20	BDL	BDL	0.70	2.80	7567.00	BDL	0.30	0.90	1.00
3040-131.7	Piché	0.13	1.70	BDL	BDL	0.50	BDL	50.40	BDL	1.00	0.60	BDL
3040-175.4	MDPO	0.20	0.70	0.10	BDL	1.30	0.70	2707.00	BDL	BDL	BDL	BDL
3040-209.5	Piché	0.13	1.30	BDL	BDL	0.20	0.10	183.80	BDL	0.80	BDL	BDL
3040-241	MDPO	0.14	0.50	BDL	BDL	0.20	BDL	76.10	BDL	BDL	BDL	BDL
3040-271.2	Pontiac	0.24	2.50	BDL	BDL	0.40	1.60	5480.80	BDL	0.30	0.50	1.00
3040-29.1	Piché	0.22	2.30	BDL	BDL	1.00	1.40	1060.20	BDL	0.80	0.80	BDL
3040-299.6	Pontiac	0.11	2.50	BDL	BDL	0.80	0.90	846.80	BDL	BDL	BDL	2.00
3040-30.5	MDPO	0.17	BDL	BDL	BDL	0.20	0.40	552.80	BDL	BDL	BDL	BDL
3040-322.6	Pontiac	0.13	2.70	0.20	BDL	0.40	1.80	1319.60	BDL	0.50	0.60	1.00
3040-340.2	MDPO	0.13	BDL	BDL	BDL	0.20	0.40	300.80	BDL	BDL	BDL	BDL
3040-362.5	Pontiac	0.16	1.60	0.40	0.20	0.60	3.60	2592.40	BDL	0.30	0.60	3.00
3068-11	MDPO	0.13	0.70	0.30	BDL	0.10	0.10	192.70	BDL	0.20	BDL	BDL
3068-17	MDPO	0.14	0.80	BDL	BDL	0.50	0.40	300.30	BDL	BDL	BDL	BDL
3068-2	Piché	0.19	2.50	BDL	BDL	0.40	BDL	2.80	BDL	2.40	1.40	BDL
3068-27	MDPO	0.12	0.90	0.10	BDL	0.30	0.90	1687.10	BDL	0.20	BDL	1.00
3068-29	Piché	0.20	1.90	0.10	BDL	0.30	0.20	46.20	BDL	0.80	BDL	BDL

Analyte	Litho.	Weight	As	Cd	Sb	Bi	Ag	Au	Hg	Tl	Se	Te
Unit		kg	ppm	ppm	ppm	ppm	ppm	ppb	ppm	ppm	ppm	ppm
MDL		0.01	0.50	0.10	0.10	0.10	0.10	0.50	0.01	0.10	0.50	1.00
Sample (BA08)												
3119-10	Pontiac	0.15	1.20	BDL	BDL	BDL	0.10	23.20	BDL	1.90	BDL	BDL
3119-9	Piché	0.19	1.40	BDL	BDL	0.60	BDL	BDL	BDL	0.40	BDL	BDL
3121-1	MDPO	0.15	1.30	BDL	BDL	0.20	0.10	104.20	BDL	0.20	BDL	BDL
3121-11	Pontiac	0.12	1.00	BDL	BDL	0.30	0.10	4.60	BDL	0.50	BDL	BDL
3121-5	MDPO	0.07	1.10	BDL	BDL	0.40	0.30	278.60	BDL	BDL	BDL	BDL
3121-8	MDPO	0.25	1.90	0.10	BDL	1.90	0.50	458.30	BDL	0.20	BDL	BDL
3594-11	Piché	0.16	2.70	0.20	0.10	3.60	6.30	53866.40	BDL	BDL	1.00	1.00
3594-13	Piché	0.21	3.00	BDL	0.20	0.40	0.20	9.80	BDL	BDL	BDL	BDL
3594-14	Piché	0.15	1.80	BDL	BDL	0.20	0.10	198.90	BDL	0.80	BDL	BDL
3594-15	Piché	0.14	0.80	BDL	BDL	BDL	BDL	9.90	BDL	1.20	BDL	BDL
3594-4	MDPO	0.19	1.60	BDL	BDL	0.30	2.00	8436.60	BDL	0.20	BDL	2.00
3594-8	MDPO	0.13	4.70	0.10	BDL	0.70	9.70	36917.20	BDL	0.30	1.30	4.00

APPENDIX C: ELECTRON MICROPROBE ANALYSES

DETAILS OF ELECTRON MICROPROBE ANALYSES

Standard	Element/Oxide	Detection Limit (ppm)	Count Time (ms)
ASTIMEX_Au	Au	1000	20
ASTIMEX_Ag	Ag	500	90
CANMET_AgBiSe2	Bi	1500	20
CANMET_CPY	Cu	500	30
CAMECA_Orth	K ₂ O	200	20
CAMECA_ablite	Na ₂ O	200	20
TAYLOR_Diopside	MgO	300	20
TAYLOR_Fe2O3-FeO	FeO	400	20
CAMECA_Orth	Al ₂ O ₃	200	20
TAYLOR_Diopside	SiO ₂	300	20
CAMECA_vana2	Cl	250	20
TAYLOR_spessartine	MnO	500	30
TAYLOR_tio2	TiO ₂	500	20
TAYLOR_chromite	Cr ₂ O ₃	525	30
MCGILL_BaOrth	BaO	950	60
CAMECA_vana2	V ₂ O ₃	400	40
TAYLOR_Diopside	CaO	300	20
MCGILL_CaF2	F	750	80

MICROPROBE ANALYSES OF NATIVE GOLD

	Analyte Unit	Au Wt %	Ag Wt %	Bi Wt %	Cu Wt %	Total Wt %
No.	Sample					
1	BA08_3002_182.6	92.85	7.68	BDL	BDL	100.88
2	BA08_3002_182.6	92.85	7.37	BDL	0.06	100.35
3	BA08_3002_182.6	92.33	7.44	BDL	0.07	99.84
4	BA08_3002_182.6	92.36	7.21	BDL	0.09	99.69
5	BA08_3002_182.6	92.13	7.49	BDL	0.05	99.67
6	BA08_3002_182.6	92.04	7.44	BDL	0.08	99.56
7	BA08_3002_182.6	91.43	7.46	BDL	BDL	98.93
8	BA08_3002_182.6	91.15	7.43	BDL	0.07	98.77
9	BA08_3002_182.6	91.07	7.58	BDL	0.09	98.74
10	BA08_3002_182.6	91.07	7.43	BDL	0.06	98.58
11	BA08_3002_182.6	90.92	7.41	BDL	0.10	98.48
12	BA08_3002_182.6	89.57	7.63	0.18	BDL	97.41
13	BA08_3002_182.6	87.76	7.55	0.20	0.05	95.56
14	BA08_3121_5	91.13	7.87	BDL	BDL	99.09
15	BA08_3121_5	90.65	8.01	BDL	BDL	98.66
16	BA08_3121_5	90.50	7.95	BDL	BDL	98.49
17	BA08_3121_5	90.02	8.18	BDL	0.06	98.26
18	BA08_3121_5	90.00	8.09	BDL	BDL	98.23
19	BA08_3121_5	90.17	7.95	BDL	BDL	98.23
20	BA08_3121_5	89.91	8.05	BDL	BDL	98.09
21	BA08_3121_5	90.05	7.96	BDL	BDL	98.05
22	BA08_3121_5	89.85	8.01	BDL	0.05	97.93
23	BA08_3121_5	88.75	8.20	BDL	BDL	96.96

	Analyte Unit	Au Wt %	Ag Wt %	Bi Wt %	Cu Wt %	Total Wt %
No.	Sample					
24	BA08_3040_338.5	83.13	16.25	BDL	BDL	99.53
25	BA08_3040_338.5	85.25	12.96	BDL	0.08	98.28
26	BA08_3040_338.5	83.92	13.92	BDL	0.05	97.89
27	BA08_3040_338.5	84.02	13.28	0.18	0.06	97.53
28	BA08_3040_338.5	81.96	14.77	BDL	BDL	96.85
29	BA08_3040_338.5	80.86	15.64	0.16	BDL	96.69
30	BA08_3040_338.5	83.36	13.12	BDL	BDL	96.49
31	BA08_3008_85.5	90.34	8.81	0.15	BDL	99.31
32	BA08_3008_85.5	89.67	8.96	BDL	BDL	98.66
33	BA08_3008_85.5	89.39	9.18	BDL	BDL	98.61
34	BA08_3008_85.5	88.06	10.33	BDL	0.05	98.51
35	BA08_3008_85.5	88.32	9.83	BDL	BDL	98.15
36	BA08_3008_85.5	88.31	8.73	BDL	0.06	97.10
37	BA08_3008_85.5	84.82	10.07	BDL	BDL	94.89
38	BA08_3040_211.2	78.92	17.25	BDL	BDL	96.19
39	BA08_3008_185.6	89.38	8.61	BDL	BDL	98.04
40	BA08_3040_51.3	92.74	5.40	BDL	BDL	98.17

MICROPROBE ANALYSES OF BIOTITE

	Analyte Unit	K₂O Wt %	Na₂O Wt %	MgO Wt %	FeO Wt %	Al₂O₃ Wt %	SiO₂ Wt %	F Wt %	Cl Wt %	Total Wt %
No.	Sample									
1	BA08_3008_123.9	10.44	BDL	14.12	15.08	16.25	37.43	0.17	BDL	96.10
2	BA08_3008_123.9	10.32	0.04	14.22	15.22	16.14	37.36	0.24	BDL	96.08
3	BA08_3008_123.9	10.43	0.04	14.15	14.92	16.18	37.57	0.17	BDL	95.84
4	BA08_3008_123.9	10.12	0.11	13.97	15.25	16.77	36.99	0.13	BDL	95.78
5	BA08_3008_123.9	10.69	0.04	13.81	14.72	16.47	37.34	0.26	BDL	95.68
6	BA08_3008_123.9	10.05	0.03	14.36	15.59	16.97	36.28	0.21	0.02	95.57
7	BA08_3008_123.9	9.91	0.04	14.22	14.74	17.07	36.77	0.28	0.02	95.47
8	BA08_3008_123.9	10.40	0.04	14.20	15.22	16.47	36.55	0.18	BDL	95.32
9	BA08_3008_123.9	9.19	0.03	14.96	15.40	16.75	36.42	0.23	0.02	95.28
10	BA08_3008_123.9	10.57	0.03	13.86	14.77	16.12	37.13	0.23	BDL	95.15
11	BA08_3008_123.9	9.90	0.04	14.97	14.90	16.57	36.22	0.21	0.03	95.06
12	BA08_3008_123.9	10.42	0.03	13.65	14.96	16.65	36.71	0.16	BDL	94.89
13	BA08_3008_123.9	10.37	0.03	14.06	15.30	16.62	35.86	0.15	BDL	94.88
14	BA08_3008_123.9	10.39	0.04	13.72	15.09	16.57	35.77	0.17	0.02	94.73
15	BA08_3008_123.9	10.07	0.05	13.79	15.12	16.41	36.18	0.23	BDL	94.59
16	BA08_3008_123.9	10.33	0.03	13.90	15.56	16.30	35.21	0.19	BDL	94.10
17	BA08_3008_123.9	10.45	0.03	13.40	14.82	15.86	36.88	0.20	BDL	94.06
18	BA08_3008_123.9	10.00	0.04	13.33	15.68	16.45	35.49	0.21	BDL	93.38
19	BA08_3008_85.5	10.58	0.05	15.01	13.47	16.46	37.75	0.58	BDL	95.90
20	BA08_3008_85.5	10.34	0.07	15.18	13.55	16.39	37.43	0.66	BDL	95.74
21	BA08_3008_85.5	10.72	0.05	14.96	12.90	16.47	37.68	0.65	0.02	95.65
22	BA08_3008_85.5	10.69	0.04	14.68	13.43	16.45	37.53	0.65	BDL	95.39

	Analyte	K₂O	Na₂O	MgO	FeO	Al₂O₃	SiO₂	F	Cl	Total
	Unit	Wt %	Wt %	Wt %	Wt %	Wt %	Wt %	Wt %	Wt %	Wt %
No.	Sample									
23	BA08_3008_85.5	9.97	0.04	15.33	14.11	16.40	36.81	0.63	BDL	95.17
24	BA08_3008_85.5	10.70	0.04	15.26	13.27	15.75	37.42	0.71	BDL	95.06
25	BA08_3008_85.5	10.52	0.05	14.36	14.03	16.24	36.99	0.66	BDL	95.03
26	BA08_3008_85.5	10.56	0.04	15.61	12.33	15.14	38.43	0.97	BDL	94.94
27	BA08_3008_85.5	10.54	0.02	14.55	14.29	15.68	36.67	0.59	BDL	94.47
28	BA08_3008_85.5	10.80	0.06	14.25	13.59	16.57	36.54	0.57	BDL	94.40
29	BA08_3008_85.5	10.30	0.07	13.90	13.09	15.95	36.08	0.67	BDL	94.28
30	BA08_3594_1	10.48	0.12	20.97	9.39	13.64	39.68	0.37	BDL	95.97
31	BA08_3594_1	10.90	0.07	20.83	9.18	13.61	39.26	0.47	BDL	95.65
32	BA08_3594_1	9.97	0.23	19.99	9.98	14.11	38.70	0.38	0.02	95.18
33	BA08_3594_1	10.51	0.38	21.83	8.33	13.49	39.43	0.22	BDL	95.16
34	BA08_3594_1	10.30	0.22	22.01	7.78	12.93	40.08	0.32	0.02	94.70
35	BA08_3594_1	9.89	0.09	22.35	8.40	11.91	40.55	0.14	BDL	94.57
36	BA08_3594_1	9.26	0.10	21.82	8.99	13.34	39.29	0.51	0.02	94.42
37	BA08_3594_1	10.20	0.22	22.37	7.84	12.69	39.58	0.34	0.02	94.20
38	BA08_3594_1	9.24	0.07	22.97	8.44	11.57	40.52	0.21	BDL	94.18
39	BA08_3594_1	10.50	0.15	22.29	7.76	12.85	38.95	0.34	BDL	94.07
40	BA08_3040_211.2	9.96	0.04	18.97	11.48	13.90	38.03	0.79	0.04	94.09
41	BA08_3040_211.2	10.44	0.05	18.48	11.59	14.49	38.93	0.88	BDL	95.67
42	BA08_3040_211.2	10.35	0.07	19.70	10.06	14.83	38.95	0.88	0.03	95.58
43	BA08_3040_211.2	10.24	0.06	18.97	10.63	13.65	39.12	0.86	0.02	95.24
44	BA08_3040_211.2	10.27	0.03	19.12	11.37	13.76	38.93	0.93	BDL	95.17
45	BA08_3040_211.2	10.35	0.05	18.38	11.66	14.12	38.18	0.85	0.03	95.09
46	BA08_3040_211.2	10.13	0.05	18.57	11.46	13.97	38.62	0.86	BDL	94.92

Analyte		K₂O	Na₂O	MgO	FeO	Al₂O₃	SiO₂	F	Cl	Total
Unit		Wt %	Wt %	Wt %	Wt %	Wt %	Wt %	Wt %	Wt %	Wt %
No.	Sample									
47	BA08_3040_211.2	10.41	0.03	18.50	11.43	13.94	37.99	0.81	BDL	94.75
48	BA08_3040_211.2	10.58	0.04	18.50	11.12	14.27	38.29	0.89	BDL	94.54
49	BA08_3040_249.6	10.59	0.05	14.43	14.65	16.05	37.12	0.58	BDL	95.51
50	BA08_3040_249.6	10.61	0.07	14.01	14.94	15.96	36.96	0.68	0.02	95.49
51	BA08_3040_249.6	10.55	0.07	14.01	14.64	16.10	36.90	0.58	BDL	95.10
52	BA08_3040_249.6	10.44	0.04	14.87	14.30	15.46	37.20	0.79	BDL	94.95
53	BA08_3040_249.6	10.56	0.10	14.55	14.23	15.67	36.69	0.62	BDL	94.64
54	BA08_3040_249.6	10.27	0.16	14.19	14.40	16.09	36.48	0.56	0.02	94.42
55	BA08_3040_249.6	10.54	0.10	14.11	14.58	16.28	35.96	0.50	0.02	94.29
56	BA08_3040_249.6	10.51	0.09	14.03	14.88	15.91	35.88	0.62	BDL	94.11
57	BA08_3040_249.6	10.18	0.10	14.28	14.54	15.70	36.41	0.64	BDL	94.00
58	BA08_3068_2	10.50	0.06	20.47	10.31	14.25	38.79	0.16	0.02	95.99
59	BA08_3068_2	10.68	0.05	19.98	10.47	14.17	38.95	0.19	BDL	95.93
60	BA08_3068_2	10.82	0.04	20.25	10.14	13.68	39.33	0.23	BDL	95.82
61	BA08_3068_2	10.56	0.06	20.24	9.87	13.90	39.06	0.31	BDL	95.35
62	BA08_3068_2	9.97	0.02	21.02	10.05	14.17	38.42	0.22	BDL	95.32
63	BA08_3068_2	10.61	0.05	20.69	9.13	13.60	39.41	0.28	BDL	95.14
64	BA08_3068_2	10.22	0.07	20.70	9.34	13.45	39.38	0.28	BDL	94.83
65	BA08_3068_2	10.13	0.07	21.01	9.01	13.30	39.62	0.37	BDL	94.76
66	BA08_3068_2	9.92	0.11	20.56	9.36	13.21	39.61	0.36	0.02	94.41
67	BA08_3040_37.8	9.94	0.06	14.24	15.48	15.11	35.44	0.79	0.05	94.79
68	BA08_3040_37.8	10.67	0.02	14.06	15.07	16.10	37.12	0.69	BDL	95.77
69	BA08_3040_37.8	10.66	0.03	14.21	15.23	15.96	36.92	0.71	BDL	95.66
70	BA08_3040_37.8	10.57	0.02	15.31	14.73	15.38	36.39	0.98	BDL	95.11

		Analyte	K₂O	Na₂O	MgO	FeO	Al₂O₃	SiO₂	F	Cl	Total
		Unit	Wt %	Wt %	Wt %	Wt %	Wt %	Wt %	Wt %	Wt %	Wt %
No.	Sample										
71	BA08_3040_37.8		10.44	0.05	13.96	15.45	16.10	36.31	0.62	BDL	95.07
72	BA08_3040_37.8		10.59	0.05	13.78	15.28	15.92	36.36	0.75	BDL	94.86
73	BA08_3040_37.8		10.31	0.10	14.03	15.29	15.93	35.91	0.70	0.03	94.26
74	BA08_3040_37.8		10.73	0.06	13.60	15.63	15.98	35.11	0.70	BDL	94.02
75	BA08_3068_29		10.17	0.16	15.35	13.59	15.80	37.85	0.42	BDL	95.91
76	BA08_3068_29		9.66	0.23	15.44	14.01	15.82	37.79	0.39	BDL	95.89
77	BA08_3068_29		10.07	0.14	15.50	13.98	15.86	37.45	0.33	BDL	95.86
78	BA08_3068_29		9.90	0.12	15.57	14.10	15.81	37.27	0.36	0.02	95.58
79	BA08_3068_29		10.17	0.15	15.36	13.47	15.89	37.73	0.39	0.02	95.42
80	BA08_3068_29		10.01	0.20	15.39	13.79	15.69	37.55	0.31	BDL	95.38
81	BA08_3068_29		9.69	0.18	15.76	13.80	15.37	36.99	0.51	BDL	94.61
82	BA08_3040_52.1		10.36	0.11	13.55	15.64	16.29	36.82	0.28	BDL	95.80
83	BA08_3040_52.1		10.50	0.11	13.51	15.54	16.42	36.64	0.25	BDL	95.76
84	BA08_3040_52.1		10.73	0.03	13.61	15.27	16.07	36.94	0.41	BDL	95.73
85	BA08_3040_52.1		10.10	0.04	14.44	15.59	16.22	36.10	0.36	BDL	95.46
86	BA08_3040_52.1		10.18	0.09	13.66	15.35	15.68	36.55	0.22	BDL	94.84
87	BA08_3040_52.1		10.17	0.14	13.64	15.01	15.99	36.40	0.29	BDL	94.14
88	BA08_3068_15		10.61	0.05	13.60	15.37	16.62	37.11	0.42	BDL	95.93
89	BA08_3068_15		10.65	0.08	13.64	15.17	16.68	37.47	0.45	BDL	95.37
90	BA08_3068_15		10.30	0.09	12.79	16.00	16.85	36.40	0.33	BDL	95.05
91	BA08_3068_15		10.17	0.06	13.62	16.26	16.57	35.68	0.45	0.02	94.80
92	BA08_3068_15		10.42	0.05	13.51	16.07	16.15	35.73	0.42	BDL	94.24
93	BA08_3121_1		10.84	0.02	13.72	16.27	15.59	36.97	0.97	BDL	95.94
94	BA08_3121_1		10.59	0.04	15.15	15.21	15.27	36.74	1.14	BDL	95.64

		Analyte	K₂O	Na₂O	MgO	FeO	Al₂O₃	SiO₂	F	Cl	Total
		Unit	Wt %	Wt %	Wt %	Wt %	Wt %	Wt %	Wt %	Wt %	Wt %
No.	Sample										
95	BA08_3121_1		9.43	0.02	16.59	14.58	15.35	36.59	0.93	BDL	94.89
96	BA08_3121_1		10.16	0.02	15.27	15.21	15.07	36.11	1.16	BDL	94.54
97	BA08_3119_16		10.62	0.13	12.28	16.73	16.06	36.82	0.64	BDL	95.82
98	BA08_3119_16		10.45	0.08	12.09	16.89	16.10	36.83	0.50	BDL	95.59
99	BA08_3119_16		10.35	0.18	12.89	16.74	15.62	36.08	0.56	BDL	94.89
100	BA08_3119_16		11.44	0.24	1.78	4.58	29.04	45.37	0.06	BDL	94.29
101	BA08_3068_1		10.07	0.10	21.73	8.59	13.76	39.57	0.34	BDL	95.27
102	BA08_3068_1		10.53	0.05	21.16	8.92	13.58	39.71	0.26	0.02	95.20
103	BA08_3068_1		10.33	0.07	21.77	8.50	12.93	39.86	0.27	BDL	95.12
104	BA08_3068_1		10.05	0.07	21.46	8.72	13.85	38.45	0.26	BDL	94.12
105	BA08_3008_185.6		10.78	0.04	14.13	14.93	15.87	37.50	0.50	BDL	95.89
106	BA08_3008_185.6		10.64	0.04	14.22	14.71	15.70	37.08	0.45	BDL	95.02
107	BA08_3008_185.6		9.99	0.10	14.49	15.04	15.25	35.81	0.55	0.02	93.25
108	BA08_3068_7		10.88	BDL	15.79	14.30	15.81	37.09	0.13	BDL	95.75
109	BA08_3068_7		10.95	0.03	16.26	13.64	15.01	38.10	0.17	BDL	95.71
110	BA08_3068_7		10.43	0.08	16.27	13.53	15.28	37.51	0.26	BDL	94.78
111	BA08_3068_28		10.48	BDL	18.20	12.05	14.30	38.89	0.29	BDL	95.68
112	BA08_3068_28		10.62	0.02	17.48	12.36	14.30	37.33	0.26	BDL	94.15
113	BA08_3002_182.6		9.83	0.03	12.51	19.30	15.78	34.92	0.22	BDL	94.41

		Analyte	MnO	TiO₂	Cr₂O₃	BaO	V₂O₃	CaO	Total
		Unit	Wt(%)	Wt(%)	Wt(%)	Wt(%)	Wt(%)	Wt(%)	Wt(%)
No.	Sample								
1	BA08_3008_123.9		0.13	1.89	0.39	0.25	BDL	BDL	96.10
2	BA08_3008_123.9		0.11	1.92	0.35	0.25	BDL	BDL	96.08
3	BA08_3008_123.9		0.10	1.92	0.24	0.19	BDL	BDL	95.84
4	BA08_3008_123.9		0.15	1.70	0.37	0.19	BDL	0.07	95.78
5	BA08_3008_123.9		0.08	1.95	0.24	0.20	BDL	BDL	95.68
6	BA08_3008_123.9		0.09	1.73	0.13	0.21	BDL	BDL	95.57
7	BA08_3008_123.9		0.10	1.84	0.30	0.25	BDL	0.06	95.47
8	BA08_3008_123.9		0.10	1.91	0.12	0.20	BDL	BDL	95.32
9	BA08_3008_123.9		0.13	1.80	0.22	0.20	BDL	BDL	95.28
10	BA08_3008_123.9		0.09	1.83	0.50	0.13	BDL	BDL	95.15
11	BA08_3008_123.9		0.11	1.75	0.16	0.27	BDL	BDL	95.06
12	BA08_3008_123.9		0.12	1.92	0.15	0.19	BDL	BDL	94.89
13	BA08_3008_123.9		0.14	1.85	0.24	0.33	BDL	BDL	94.88
14	BA08_3008_123.9		0.16	1.90	0.59	0.37	BDL	BDL	94.73
15	BA08_3008_123.9		0.14	1.87	0.49	0.23	BDL	0.08	94.59
16	BA08_3008_123.9		0.12	1.84	0.40	0.30	BDL	BDL	94.10
17	BA08_3008_123.9		0.14	1.93	0.25	0.20	BDL	BDL	94.06
18	BA08_3008_123.9		0.09	1.86	0.14	0.17	BDL	BDL	93.38
19	BA08_3008_85.5		0.07	2.09	0.09	BDL	BDL	BDL	95.90
20	BA08_3008_85.5		0.12	2.07	0.13	BDL	BDL	BDL	95.74
21	BA08_3008_85.5		0.07	2.12	0.26	BDL	BDL	BDL	95.65
22	BA08_3008_85.5		0.07	1.96	0.09	BDL	BDL	BDL	95.39

	Analyte Unit	MnO Wt(%)	TiO₂ Wt(%)	Cr₂O₃ Wt(%)	BaO Wt(%)	V₂O₃ Wt(%)	CaO Wt(%)	Total Wt(%)
No.	Sample							
23	BA08_3008_85.5	0.10	1.72	0.11	BDL	BDL	0.16	95.17
24	BA08_3008_85.5	0.05	1.94	0.18	BDL	BDL	BDL	95.06
25	BA08_3008_85.5	BDL	2.08	0.11	BDL	BDL	0.13	95.03
26	BA08_3008_85.5	0.08	2.08	0.09	BDL	BDL	BDL	94.94
27	BA08_3008_85.5	0.07	2.07	0.16	BDL	BDL	BDL	94.47
28	BA08_3008_85.5	0.07	2.07	0.06	BDL	BDL	0.03	94.40
29	BA08_3008_85.5	0.06	4.20	0.10	0.09	BDL	0.05	94.28
30	BA08_3594_1	0.13	1.11	0.07	0.13	BDL	BDL	95.97
31	BA08_3594_1	0.13	1.16	0.12	0.13	BDL	BDL	95.65
32	BA08_3594_1	0.16	1.27	0.15	0.16	BDL	0.25	95.18
33	BA08_3594_1	0.12	0.85	BDL	BDL	BDL	BDL	95.16
34	BA08_3594_1	0.12	0.77	0.09	BDL	BDL	0.12	94.70
35	BA08_3594_1	0.08	0.93	0.09	BDL	BDL	0.17	94.57
36	BA08_3594_1	0.10	0.95	BDL	BDL	BDL	0.14	94.42
37	BA08_3594_1	0.13	0.72	0.07	0.11	BDL	0.08	94.20
38	BA08_3594_1	0.06	0.85	0.20	0.11	BDL	0.04	94.18
39	BA08_3594_1	0.14	0.84	0.27	BDL	BDL	0.07	94.07
40	BA08_3040_211.2	0.09	0.72	0.31	BDL	BDL	BDL	95.67
41	BA08_3040_211.2	0.07	0.86	0.07	BDL	BDL	0.06	95.58
42	BA08_3040_211.2	0.09	0.76	0.08	BDL	BDL	1.11	95.24
43	BA08_3040_211.2	0.06	0.71	0.30	BDL	BDL	0.03	95.17
44	BA08_3040_211.2	0.08	1.31	0.42	BDL	BDL	BDL	95.09
45	BA08_3040_211.2	0.08	1.13	0.31	BDL	BDL	0.08	94.92
46	BA08_3040_211.2	0.07	1.29	0.49	BDL	BDL	0.04	94.75

	Analyte	MnO	TiO₂	Cr₂O₃	BaO	V₂O₃	CaO	Total
	Unit	Wt(%)	Wt(%)	Wt(%)	Wt(%)	Wt(%)	Wt(%)	Wt(%)
No.	Sample							
47	BA08_3040_211.2	0.08	0.64	0.44	BDL	0.04	BDL	94.54
48	BA08_3040_211.2	0.07	0.66	0.40	BDL	0.04	0.05	94.09
49	BA08_3040_249.6	BDL	2.12	BDL	0.11	BDL	BDL	95.51
50	BA08_3040_249.6	0.06	2.37	BDL	0.09	BDL	BDL	95.49
51	BA08_3040_249.6	BDL	2.27	BDL	0.18	BDL	BDL	95.10
52	BA08_3040_249.6	BDL	2.05	BDL	BDL	BDL	0.04	94.95
53	BA08_3040_249.6	BDL	2.32	BDL	0.13	BDL	BDL	94.64
54	BA08_3040_249.6	BDL	2.33	BDL	0.11	BDL	0.04	94.42
55	BA08_3040_249.6	0.06	2.15	0.05	0.15	BDL	BDL	94.29
56	BA08_3040_249.6	BDL	2.31	BDL	0.11	BDL	BDL	94.11
57	BA08_3040_249.6	BDL	2.20	BDL	0.09	BDL	0.08	94.00
58	BA08_3068_2	0.09	1.34	BDL	0.09	BDL	BDL	95.99
59	BA08_3068_2	0.11	1.35	BDL	BDL	BDL	BDL	95.93
60	BA08_3068_2	0.10	1.27	BDL	BDL	BDL	BDL	95.82
61	BA08_3068_2	0.06	1.27	BDL	0.12	BDL	0.03	95.35
62	BA08_3068_2	0.11	1.37	BDL	BDL	BDL	BDL	95.32
63	BA08_3068_2	0.14	1.27	BDL	BDL	BDL	0.04	95.14
64	BA08_3068_2	0.14	1.25	BDL	BDL	BDL	0.07	94.83
65	BA08_3068_2	0.08	1.21	BDL	BDL	BDL	0.04	94.76
66	BA08_3068_2	0.07	1.24	BDL	BDL	BDL	0.06	94.41
67	BA08_3040_37.8	0.05	2.15	BDL	0.11	BDL	BDL	95.77
68	BA08_3040_37.8	BDL	2.11	BDL	0.09	BDL	BDL	95.66
69	BA08_3040_37.8	0.08	1.92	BDL	0.14	BDL	BDL	95.11
70	BA08_3040_37.8	0.12	2.10	BDL	0.09	BDL	0.05	95.07

Analyte		MnO	TiO₂	Cr₂O₃	BaO	V₂O₃	CaO	Total
Unit		Wt(%)	Wt(%)	Wt(%)	Wt(%)	Wt(%)	Wt(%)	Wt(%)
No.	Sample							
71	BA08_3040_37.8	0.08	2.26	BDL	0.09	BDL	BDL	94.86
72	BA08_3040_37.8	0.05	3.82	BDL	0.12	BDL	BDL	94.79
73	BA08_3040_37.8	0.06	2.03	BDL	0.11	BDL	0.04	94.26
74	BA08_3040_37.8	0.08	2.26	BDL	0.17	BDL	BDL	94.02
75	BA08_3068_29	0.13	1.94	0.47	0.18	BDL	BDL	95.91
76	BA08_3068_29	0.13	1.88	0.39	0.24	BDL	0.07	95.89
77	BA08_3068_29	0.11	1.77	0.47	0.30	BDL	BDL	95.86
78	BA08_3068_29	0.11	1.86	0.38	0.20	BDL	BDL	95.58
79	BA08_3068_29	0.09	1.90	0.23	0.20	BDL	BDL	95.42
80	BA08_3068_29	0.16	1.91	0.32	0.15	BDL	0.03	95.38
81	BA08_3068_29	0.14	1.80	0.43	0.15	BDL	BDL	94.61
82	BA08_3040_52.1	0.06	2.45	BDL	0.35	BDL	BDL	95.80
83	BA08_3040_52.1	0.07	2.43	BDL	0.35	BDL	BDL	95.76
84	BA08_3040_52.1	0.09	2.53	BDL	0.22	BDL	BDL	95.73
85	BA08_3040_52.1	0.10	2.07	BDL	0.54	BDL	BDL	95.46
86	BA08_3040_52.1	0.09	2.49	BDL	0.61	BDL	BDL	94.84
87	BA08_3040_52.1	0.06	2.33	BDL	0.20	BDL	BDL	94.14
88	BA08_3068_15	0.10	1.66	BDL	0.55	BDL	BDL	95.93
89	BA08_3068_15	0.14	1.10	BDL	0.19	BDL	BDL	95.37
90	BA08_3068_15	0.12	2.00	BDL	0.30	BDL	BDL	95.05
91	BA08_3068_15	0.18	1.49	0.09	0.40	BDL	BDL	94.80
92	BA08_3068_15	0.10	1.65	BDL	0.30	BDL	BDL	94.24
93	BA08_3121_1	BDL	1.85	BDL	BDL	BDL	BDL	95.94
94	BA08_3121_1	BDL	1.84	BDL	BDL	BDL	BDL	95.64

Analyte		MnO	TiO₂	Cr₂O₃	BaO	V₂O₃	CaO	Total
Unit		Wt(%)	Wt(%)	Wt(%)	Wt(%)	Wt(%)	Wt(%)	Wt(%)
No.	Sample							
95	BA08_3121_1	BDL	1.59	BDL	0.14	BDL	BDL	94.89
96	BA08_3121_1	0.05	1.82	BDL	0.17	BDL	BDL	94.54
97	BA08_3119_16	0.08	2.56	BDL	0.16	BDL	BDL	95.82
98	BA08_3119_16	0.11	2.55	BDL	0.18	BDL	BDL	95.59
99	BA08_3119_16	0.10	2.46	BDL	0.08	BDL	0.04	94.89
100	BA08_3119_16	BDL	1.59	BDL	0.20	BDL	BDL	94.29
101	BA08_3068_1	0.14	0.81	0.19	BDL	BDL	0.07	95.27
102	BA08_3068_1	0.10	0.81	0.08	BDL	BDL	BDL	95.20
103	BA08_3068_1	0.10	0.75	0.17	BDL	BDL	0.44	95.12
104	BA08_3068_1	0.12	0.77	0.30	BDL	BDL	0.11	94.12
105	BA08_3008_185.6	0.14	2.06	BDL	0.15	BDL	BDL	95.89
106	BA08_3008_185.6	0.08	2.02	BDL	0.20	BDL	BDL	95.02
107	BA08_3008_185.6	0.11	1.89	BDL	0.17	BDL	0.08	93.25
108	BA08_3068_7	0.13	1.57	BDL	BDL	0.04	BDL	95.75
109	BA08_3068_7	0.13	1.43	BDL	BDL	BDL	BDL	95.71
110	BA08_3068_7	0.14	1.28	BDL	BDL	0.05	BDL	94.78
111	BA08_3068_28	0.05	1.15	0.30	BDL	BDL	BDL	95.68
112	BA08_3068_28	0.08	1.27	0.44	0.09	BDL	BDL	94.15
113	BA08_3002_182.6	0.13	1.52	0.07	0.09	BDL	0.07	94.41

APPENDIX D: MASS BALANCE ASSOCIATED WITH
HYDROTHERMAL ALTERATION

FORMULAS FOR CALCULATION OF MASS BALANCE

Mass changes in elements accompanying hydrothermal alteration and gold mineralization were estimated using the methods of Gresens (1967), Grant (1986) and MacLean and Kranidiotis (1987). Least altered compositions (C_i^0) were compared to altered compositions (C_i^A) and elements that were immobile during alteration were defined graphically by isocons (Grant, 1986). Immobile components generate, through the origin, a straight line of slope (M^0/M^A) for which ($\Delta C_i = 0$). In this study, the tightest fit to a line was obtained for aluminum and titanium and as aluminum is distributed among the principal rock-forming minerals, mass changes were estimated by normalizing compositions of altered rocks to a constant aluminum concentration corresponding to that of the least-altered rock. The equation of the isocon is defined as

$$C^A = (C_{Al_2O_3}^A / C_{Al_2O_3}^0) C^0$$

and absolute mass changes are calculated by

$$(\Delta C_i / C_i) = (M^0 / M^A) (C_i^A / C_i^0) - 1$$

Relative mass change (%) is calculated by multiplying the above formula by 100.

MEAN COMPOSITIONS OF LEAST ALTERED AND ALTERED SAMPLES FOR THE
CANADIAN MALARTIC OREBODY

Alteration		C_i^O	$C_A^O 1$	$C_A^O 2$	$C_A^O 3$	$C_A^O 4$
M^O/M^A			0.94	1.02	1.10	1.72
SiO₂	wt.%	64.94	63.49	61.57	61.49	75.26
TiO₂	wt.%	0.56	0.60	0.59	0.53	0.33
Al₂O₃	wt.%	15.32	16.37	15.02	13.96	8.89
Fe₂O₃	wt.%	5.75	5.96	5.80	5.20	3.44
MnO	wt.%	0.07	0.07	0.07	0.07	0.04
MgO	wt.%	3.14	2.99	2.93	2.55	1.21
CaO	wt.%	2.63	2.68	2.68	3.66	2.49
Na₂O	wt.%	3.79	4.12	3.92	4.23	2.61
K₂O	wt.%	2.45	2.95	3.26	4.15	2.43
P₂O₅	wt.%	0.16	0.15	0.14	0.11	0.09
BaO	ppm	640.00	778.50	786.00	803.50	574.00
Ce	ppm	54.50	40.00	15.00	16.50	7.50
Co	ppm	23.45	21.00	20.50	20.00	9.00
Cr₂O₃	ppm	324.00	338.50	310.00	288.50	175.00
Ni	ppm	86.00	96.00	102.00	86.00	48.00
Sc	ppm	12.50	9.00	5.00	5.00	5.00
V	ppm	97.50	106.50	119.50	79.00	26.00
LOI	wt.%	1.01	1.61	3.52	4.85	3.37
Total	wt.%	100.36	100.24	100.19	99.89	100.10
Ga	ppm	19.35	18.86	20.89	20.43	12.79
Nb	ppm	4.80	5.59	5.43	4.73	2.80
Rb	ppm	81.85	91.11	86.07	63.39	27.42
Sr	ppm	440.19	405.81	457.47	581.50	317.78
Th	ppm	5.56	5.88	6.13	5.29	4.00
U	ppm	1.60	2.61	2.93	3.18	1.80
Y	ppm	12.53	13.01	13.00	12.05	7.10
Zr	ppm	136.69	136.72	134.07	124.77	86.30
Ta	ppm	-	1.60	0.80	1.05	0.65
W	ppm	5.70	8.50	19.20	26.25	23.60
Mo	ppm	1.62	2.25	3.40	3.17	43.67
Cu	ppm	51.96	49.56	51.29	42.40	10.96
Pb	ppm	4.00	4.00	6.70	6.13	32.75
Zn	ppm	72.75	74.80	66.65	63.50	41.30
Au	ppb	2.55	11.95	693.85	1162.00	1136.90

Alteration		C_i^0	$C_A^0 1$	$C_A^0 2$	$C_A^0 3$	$C_A^0 4$
M^O/M^A			0.94	1.02	1.10	1.72
Ag	ppb	89.00	96.50	652.50	1786.00	1632.00
Co	ppm	21.40	23.40	23.35	19.65	11.70
Mn	ppm	429.00	444.50	427.00	444.00	285.00
Fe	%	3.52	3.56	3.35	3.17	2.22
As	ppm	0.40	0.50	1.20	1.40	1.00
Cd	ppm	0.06	0.06	0.07	0.10	0.09
Sb	ppm	0.02	0.03	0.04	0.05	0.05
Bi	ppm	0.22	0.33	0.49	0.75	2.78
Tl	ppm	0.43	0.43	0.33	0.23	0.04
S	%	0.24	0.27	0.99	2.07	1.63
Hg	ppb	3.00	2.50	2.50	2.50	2.50
Se	ppm	0.30	0.30	0.35	0.50	0.40
Te	ppm	0.05	0.08	1.04	2.64	3.17
C/TOT	%	-	0.08	0.47	0.83	0.40
S/TOT	%	-	0.24	1.39	1.65	2.09

Notes: Altered compositions 1 through 4 correspond to different alteration facies/degrees of alteration. 1) weakly altered; 2) weakly to moderately altered (early alteration); 3) moderately to strongly altered (dominantly potassic), and; 4) strongly altered (dominantly silicic).

RELATIVE MASS CHANGES FOR THE CANADIAN MALARTIC OREBODY

Alteration	$C_A^0 1$	$C_A^0 2$	$C_A^0 3$	$C_A^0 4$
SiO₂	-8.48	-3.26	3.92	99.73
TiO₂	0.16	7.88	4.04	3.15
Al₂O₃	0.00	0.00	0.00	0.00
Fe₂O₃	-2.96	2.92	-0.67	3.19
MnO	-7.67	-8.45	2.98	-3.21
MgO	-10.72	-4.64	-10.87	-33.49
CaO	-4.42	4.17	53.01	63.47
Na₂O	1.64	5.53	22.48	18.67
K₂O	12.76	35.83	86.05	71.27
P₂O₅	-9.09	-6.17	-19.55	-4.69
BaO	13.87	25.31	37.78	54.56
Ce	-31.29	-71.92	-66.78	-76.29
Co	-16.16	-10.80	-6.40	-33.86
Cr₂O₃	-2.20	-2.38	-2.28	-6.92
Ni	4.50	21.01	9.74	-3.82
Sc	-32.60	-59.19	-56.10	-31.07
V	2.26	25.05	-11.08	-54.05
LOI	49.97	256.86	429.06	477.86
Total	-6.49	1.86	9.23	71.89
Ga	-8.76	10.15	15.84	13.91
Nb	11.09	15.44	8.25	0.63
Rb	5.10	8.21	-14.28	-41.77
Sr	-13.70	6.04	44.97	24.41
Th	-2.57	10.61	2.65	22.00
U	52.42	86.53	117.77	93.87
Y	-2.83	5.82	5.49	-2.39
Zr	-6.36	0.08	0.18	8.80
Ta	-	-	-	-
W	39.60	243.68	405.39	613.50
Mo	30.13	114.80	115.41	4559.80
Cu	-10.71	0.72	-10.46	-63.65
Pb	-6.27	70.99	68.39	1312.71
Zn	-3.75	-6.52	-4.21	-2.17
Au	338.70	27662.52	49907.98	76731.46

Alteration	$C_A^0 1$	$C_A^0 2$	$C_A^0 3$	$C_A^0 4$
Ag	1.50	648.04	2101.24	3060.00
Co	2.36	11.33	0.77	-5.78
Mn	-3.00	1.56	13.58	14.48
Fe	-5.19	-2.76	-1.03	8.84
As	17.02	206.09	284.10	330.82
Cd	-6.39	10.53	82.90	158.49
Sb	17.02	104.06	146.92	330.82
Bi	43.69	132.54	280.27	2128.25
Tl	-6.39	-20.78	-41.90	-83.78
S	3.37	318.75	844.24	1070.40
Hg	-21.99	-14.97	-8.55	43.61
Se	-6.39	19.04	82.90	129.77
Te	66.43	2246.72	6338.20	12039.58
C/TOT	-	-	-	-
S/TOT	-	-	-	-

Notes: Altered compositions 1 through 4 correspond to different alteration facies/degrees of alteration. 1) weakly altered; 2) weakly to moderately altered (early alteration); 3) moderately to strongly altered (dominantly potassic), and; 4) strongly altered (dominantly silicic).

APPENDIX E: SULFUR ISOTOPE ANALYSES

SULPHUR EXTRACTION: SAMPLE, REAGENT AND SILVER SULPHIDE
 QUANTITIES

Sample ID	Material	Sample (mg)	Reagent (mL)	Ag ₂ S (mg)
BA08_3121_5	Pyrite	1.1	CRS_15	3.5
BA08_3121_8	Pyrite	1.5	CRS_15	3.3
BA08_3594_8	Pyrite	3.5	CRS_15	6.6
BA08_3594_15	Pyrite	19	CRS_15	148.1
BA08_3594_11	Pyrite	10.84	CRS_15	54.8
BA08_3594_14	Pyrite	4.8	CRS_15	13.2
BA08_3594_13	Pyrite	0.5	CRS_15	1.2
BA08_3068_29	Pyrite	1.5	CRS_15	4.5
BA08_3121_10	Pyrite	<1	CRS_15	1.1
BA08_3121_11	Pyrite	0.3	CRS_15	1.4
BA08_3040_209.5	Pyrite	4.1	CRS_15	13.6
BA08_3008_230.7	Pyrite	2.4	CRS_15	9
BA08_3040_340.2	Pyrite	0.4	CRS_15	1
BA08_3068_11	Pyrite	1.4	CRS_15	5.2
BA08_3594_4	Pyrite	2.3	CRS_15	6.8
BA08_3119_9	Pyrite	4.5	CRS_15	10.6
BA08_3068_2	Pyrite	6.7	CRS_15	9.9
BA08_3040_30.5	Pyrite	8.1	CRS_15	19.8
BA08_3040_271.2	Pyrite	2.9	CRS_15	5.9
BA08_3040_362.5	Pyrite	3.6	CRS_15	8.4
BA08_3008_116.9	Pyrite	4.1	CRS_15	10.4
BA08_3068_27	Pyrite	2.7	CRS_15	7.9
BA08_3008_121.8	Pyrite	6.2	CRS_15	10.2
BA08_3040_299.6	Pyrite	1.7	CRS_15	3.6
BA08_3068_17	Pyrite	166	CRS_15	4.9

Sample ID	Material	Sample (mg)	Reagent_(mL)	Ag ₂ S (mg)
BA08_3121_1	Pyrite	1.1	CRS_15	7.9
BA08_3040_241	Pyrite	2.2	CRS_15	4.1
BA08_3008_169.7	Pyrite	6.5	CRS_15	18.6
BA08_3040_131.7	Pyrite	7.2	CRS_15	41.4
BA08_3040_29.1	Pyrite	8	CRS_15	40.1
BA08_3008_250.5	Pyrite	2.4	CRS_15	8.2
BA08_3040_322.6	Pyrite	1.5	CRS_15	5.4
BA08_3008_126.9	Pyrite	166	CRS_15	109.1
BA08_3008_86.9	Pyrite	1.9	CRS_15	5.8
BA08_3040_175.4	Pyrite	3.2	CRS_15	9.1
BA08_3008_162.1	Pyrite	3	CRS_15	18
BA08_3008_202.2	Whole Rock	~3	CRS_15	~10
BA08_3008_186.6	Whole Rock	~3	CRS_15	~10
BA08_3040_52.1	Whole Rock	~3	CRS_15	~10
BA08_3040_180	Whole Rock	~3	CRS_15	~10
BA08_3040_340.2	Whole Rock	~3	CRS_15	~10
CM06_719_200	Whole Rock	~3	CRS_15	~10
BA08_3040_297.9	Whole Rock	~3	CRS_15	~10
CM06_701_298.5	Whole Rock	~3	CRS_15	~10
CM05_667_256.3	Whole Rock	~3	CRS_15	~10
CM07_1499_201.0	Whole Rock	~3	CRS_15	~10
BA08_3008_189.6	Whole Rock	25	CRS_626	1600
BA08_3008_189.6*	Whole Rock	25	THODE_15	1.2
BA08_3008_186.6	Whole Rock	35.4	CRS_886	1708
BA08_3008_186.6*	Whole Rock	35.4	THODE_15	0.5
BA08_3040_52.1	Whole Rock	32.5	CRS_813	1255
BA08_3040_52.1*	Whole Rock	32.5	THODE_15	tr

Notes: '*' indicates data from sulphate

- an average of 3.5 mg Ag₂S was used for mass spectrometry

SULFUR ISOTOPIC COMPOSITIONS

Sample ID	$\delta^{33}\text{S}$	\pm	$\delta^{34}\text{S}$	\pm	$\delta^{36}\text{S}$	\pm	$\Delta^{33}\text{S}$	\pm	$\Delta^{36}\text{S}$	\pm
BA08_3121_5	-0.4869	0.0096	-0.9399	0.0035	-1.2420	0.0150	-0.0028	0.0086	0.5431	0.0213
BA08_3121_8	1.4354	0.0159	2.7527	0.0075	6.7988	0.1161	0.0187	0.0125	1.5621	0.1131
BA08_3594_8	0.3663	0.0129	0.5559	0.0068	1.4027	0.2007	0.0800	0.0138	0.3463	0.2135
BA08_3594_15	1.5829	0.0173	3.0089	0.0055	6.2056	0.0643	0.0345	0.0148	0.4810	0.0707
BA08_3594_11	1.8550	0.0674	3.6720	0.1225	4.9456	3.7808	-0.0344	0.1251	-2.0428	4.0080
BA08_3594_14	1.3102	0.0182	2.5125	0.0040	5.0241	0.1183	0.0170	0.0161	0.2449	0.1124
BA08_3594_13	2.2537	0.0163	4.2959	0.0070	8.8037	0.0906	0.0436	0.0198	0.6256	0.1036
BA08_3068_29	1.2709	0.0176	2.3430	0.0032	4.8094	0.0137	0.0649	0.0161	0.3529	0.0184
BA08_3121_10	-0.2897	0.0413	-0.6442	0.0205	-0.3620	0.2145	0.0421	0.0507	0.8616	0.2058
BA08_3121_11	-1.7345	0.0229	-3.4508	0.0072	-6.2199	0.1549	0.0442	0.0256	0.3264	0.1467
BA08_3040_209.5	0.5470	0.0249	1.0110	0.0070	2.0412	0.6222	0.0265	0.0250	0.1195	0.6285
BA08_3008_230.7	-0.3539	0.0208	-0.7870	0.0129	-1.1078	0.1057	0.0515	0.0171	0.3869	0.0975
BA08_3040_340.2	-0.6908	0.0127	-1.5202	0.0189	-2.0952	0.2482	0.0924	0.0188	0.7912	0.2699
BA08_3068_11	-0.6257	0.0168	-1.2661	0.0038	-2.3045	0.1323	0.0266	0.0158	0.0997	0.1350
BA08_3594_4	1.1422	0.0025	2.0470	0.0117	3.8786	0.3056	0.0885	0.0075	-0.0142	0.2998
BA08_3119_9	0.7872	0.0100	1.4579	0.0150	2.6570	0.0369	0.0366	0.0041	-0.1149	0.0360
BA08_3068_2	-1.5759	0.0257	-3.1090	0.0239	-5.8463	0.0173	0.0264	0.0151	0.0526	0.0284
BA08_3040_30.5	-1.6703	0.0242	-3.3547	0.0293	-6.4017	0.1887	0.0588	0.0122	-0.0375	0.1364
BA08_3040_271.2	0.6840	0.0182	1.2400	0.0395	2.2237	0.1143	0.0456	0.0091	-0.1337	0.0415
BA08_3040_362.5	1.3243	0.0084	2.4093	0.0127	4.3984	0.0364	0.0842	0.0146	-0.1843	0.0154
BA08_3008_116.9	0.0764	0.0204	-0.0305	0.0288	-0.2179	0.1071	0.0921	0.0061	-0.1601	0.0713
BA08_3068_27	0.4758	0.0083	0.8665	0.0123	1.6538	0.0348	0.0296	0.0020	0.0069	0.0220
BA08_3008_121.8	0.1120	0.0055	0.0653	0.0090	0.2061	0.0861	0.0784	0.0089	0.0820	0.0787
BA08_3040_299.6	1.1540	0.0155	2.0970	0.0225	4.0375	0.0432	0.0745	0.0072	0.0493	0.0018
BA08_3068_17	-0.3982	0.0090	-0.8848	0.0093	-1.7936	0.0516	0.0575	0.0058	-0.1132	0.0679

Sample ID	$\delta^{33}\text{S}$	\pm	$\delta^{34}\text{S}$	\pm	$\delta^{36}\text{S}$	\pm	$\Delta^{33}\text{S}$	\pm	$\Delta^{36}\text{S}$	\pm
BA08_3121_1	-0.4983	0.0133	-1.0651	0.0059	-2.2201	0.1356	0.0503	0.0124	-0.1973	0.1349
BA08_3040_241	-0.1443	0.0104	-0.3867	0.0101	-0.5977	0.0615	0.0549	0.0113	0.1370	0.0429
BA08_3008_169.7	0.5372	0.0214	0.9660	0.0188	2.2652	0.1326	0.0399	0.0125	0.4291	0.1121
BA08_3040_131.7	0.0616	0.0076	0.0348	0.0075	0.1519	0.0866	0.0437	0.0095	0.0857	0.1006
BA08_3040_29.1	-0.7701	0.0202	-1.5949	0.0076	-3.0047	0.0584	0.0516	0.0163	0.0236	0.0441
BA08_3008_250.5	0.2171	0.0081	0.3438	0.0116	0.5533	0.1232	0.0401	0.0029	-0.0999	0.1024
BA08_3040_322.6	0.8500	0.0146	1.4884	0.0107	2.5925	0.1554	0.0837	0.0104	-0.2373	0.1404
BA08_3008_126.9	-0.4933	0.0042	-1.1250	0.0055	-2.2602	0.0348	0.0862	0.0046	-0.1238	0.0332
BA08_3008_86.9	-0.3223	0.0085	-0.7843	0.0021	-1.5168	0.1554	0.0816	0.0085	-0.0272	0.1578
BA08_3040_175.4	-1.3482	0.0031	-2.7490	0.0076	-5.2847	0.0249	0.0685	0.0067	-0.0680	0.0108
BA08_3008_162.1	-0.0382	0.0119	-0.1512	0.0010	-0.2900	0.0722	0.0397	0.0123	-0.0026	0.0738
BA08_3008_202.2	-0.1470	0.0214	-0.4706	0.0081	-1.9648	0.0280	0.0954	0.0247	-1.0708	0.0425
BA08_3008_186.6	-0.6112	0.0140	-1.3266	0.0291	-3.2753	0.1320	0.0722	0.0232	-0.7562	0.1360
BA08_3040_52.1	-0.4056	0.0261	-0.9345	0.0093	-2.5899	0.0795	0.0757	0.0229	-0.8151	0.0690
BA08_3040_180	0.9947	0.0074	1.7841	0.0129	2.8402	0.0781	0.0763	0.0097	-0.5523	0.0705
BA08_3040_340.2	0.3105	0.0108	0.4398	0.0224	0.1749	0.0777	0.0840	0.0182	-0.6610	0.0751
CM06_719_200	-0.4298	0.0205	-1.0712	0.0112	-2.7899	0.0125	0.1220	0.0260	-0.7556	0.0137
BA08_3040_297.9	1.1610	0.0186	2.1244	0.0125	3.5880	0.0437	0.0675	0.0121	-0.4523	0.0216
CM06_701_298.5	-0.1591	0.0172	-0.5102	0.0215	-1.6650	0.0766	0.1037	0.0143	-0.6958	0.0865
CM05_667_256.3	0.4727	0.0006	0.7914	0.0138	0.8909	0.0667	0.0653	0.0070	-0.6133	0.0854
CM07_1499_201.0	1.1476	0.0118	2.0334	0.0015	3.1417	0.1055	0.1009	0.0122	-0.7253	0.1074
BA08_3008_189.6	-1.5870	0.0081	-3.1862	0.0075	-6.3911	0.1789	0.0551	0.0107	-0.3460	0.1841
BA08_3008_189.6*	4.1747	0.0141	8.0630	0.0199	16.2606	0.1917	0.0304	0.0196	0.8852	0.1701
BA08_3008_186.6	N/A	N/A								
BA08_3008_186.6*	N/A	N/A								
BA08_3040_52.1	N/A	N/A								
BA08_3040_52.1*	N/A	N/A								

Notes: - all data given in permil (‰). ‘*’ indicates data from sulphate

APPENDIX F: OXYGEN AND HYDROGEN ISOTOPE DATA

OXYGEN AND HYDROGEN SAMPLE QUANTITIES AND ISOTOPIC COMPOSITIONS

Sample	Material	Sample (mg)	Yield
BA08_3040_249.6	Quartz	62.0	16.9
BA08_3040_249.6	Biotite	43.2	12.7
BA08_3040_52.1	Quartz	139.1	16.1
BA08_3040_52.1	Biotite	33.0	14.7
BA08_3121_2	Quartz	20.7	14.7
BA08_3121_2	Biotite	16.2	12.8
BA08_3119_16	Quartz	53.8	11.3
BA08_3119_16	Biotite	62.2	12.6
BA08_3121_5	Quartz	70.7	17.7
BA08_3121_5	Hematite	10.5	10.2
BA08_3040_189.8	Quartz	113.4	16.5
BA08_3040_189.8	Hematite	25.3	13.6

OXYGEN AND HYDROGEN ISOTOPIC COMPOSITIONS

Sample	Material	$\delta^{18}\text{O}$	\pm	H_2O (Wt %)	δD	\pm
BA08_3040_249.6	Quartz	11.9	0.3			
BA08_3040_249.6	Biotite	6.8	0.3	4.1	-47.0	0.3
BA08_3040_52.1	Quartz	8.9*	0.3			
BA08_3040_52.1	Biotite	8.9*	0.3	3.9	-49.0	0.3
BA08_3121_2	Quartz	12.0	0.3			
BA08_3121_2	Biotite	6.9	0.3	3.7	-52.0	0.3
BA08_3119_16	Quartz	8.8*	0.3			
BA08_3119_16	Biotite	5.9*	0.3	4.1	-45.0	0.3
BA08_3121_5	Quartz	11.8	0.3			
BA08_3121_5	Hematite	6.3	0.3			
BA08_3040_189.8	Quartz	13.4	0.3			
BA08_3040_189.8	Hematite	6.9	0.3			

Notes: - all data given in permil (‰)
 ‘*’ indicates disequilibrium

APPENDIX G: ISOTOPIC GEOTHERMOMETRY

FRACTIONATION EQUATIONS

Isotopic geothermometry makes use of the temperature-dependency of equilibrium fractionation of isotopes between mineral pairs. As this fractionation is independent of other physicochemical parameters, it can be used to calculate the temperatures at which the phases of interest equilibrated. To employ an isotopic geothermometer, one must assume or have textural evidence that the two species formed contemporaneously.

The partitioning of stable isotopes between two substances, A and B, is described quantitatively by a fractionation factor, α , which is also equal to the equilibrium constant, K_{eq} , for the isotopic exchange reaction between A and B:

$$K_{eq} = \alpha_{(A-B)} = \frac{R_A}{R_B} = \frac{\left[\left(\frac{y_X}{z_X} \right)_A \right]}{\left[\left(\frac{y_X}{z_X} \right)_B \right]}$$

where X is the element of interest and y and z relate to stable isotopes of that element; for example X = S and y and z relate to ^{34}S and ^{32}S respectively

This equation can be recast in terms of δ :

$$\alpha_{(A-B)} = \frac{1 + \frac{\delta_A}{1000}}{1 + \frac{\delta_B}{1000}} = \frac{1000 + \delta_A}{1000 + \delta_B}$$

Most mineral systems can be approximated by:

$$1000 \ln \alpha_{(A-B)} = \frac{A \times 10^6}{T^2} + \frac{B \times 10^3}{T} + C; \quad (T \text{ in K})$$

where $\alpha_{(A-B)}$ is measured and subsequently calculated from $^{34}\delta_A$ and $^{34}\delta_B$ and A, B, and C are variables of the fractionation equation calibrated for the mineral pair or the difference between separate fractionation equations for each mineral with respect to the same isotopic exchange medium

The above equation can be rearranged to solve for T:

$$T \text{ (}^\circ\text{C)} = \frac{\sqrt{\alpha_{A-B} \times 10^6}}{1000 \ln \alpha_{(A-B)}} - 273.15$$

As $1000 \ln(1.00X)$ is approximately equal to X

$$1000 \ln \alpha_{(A-B)} \approx \Delta_{A-B}$$

Where Δ_{A-B} is defined as:

$$\Delta_{A-B} = \delta_A - \delta_B$$

Uncertainties associated with the above temperature calculation were assessed with the following equation derived using standard error propagation techniques (Farquhar et al., 1993):

$$\sigma_T^2 = \left[\frac{(1000A_{ij})}{4 \left(\frac{\ln 1000 + \delta_i}{1000 + \delta_j} \right)^3} \right] \left[\frac{\sigma_{\delta_i}^2}{(1000 + \delta_i)^2} + \frac{\sigma_{\delta_j}^2}{(1000 + \delta_j)^2} + \frac{\sigma_{A_{ij}}^2 \left(\ln \frac{(1000 + \delta_i)}{(1000 + \delta_j)} \right)^2}{A_{ij}^2} \right],$$

where

A_{ij} is the temperature coefficient of the fractionation factor

δ_i and δ_j are the measured isotopic compositions of phases i and j

$\sigma_{\delta_i}^2$ and $\sigma_{\delta_j}^2$ are the analytical errors on the measured isotopic compositions of phases i and j

$\sigma_{A_{ij}}^2$ is the error associated with the fractionation factor

FRACTIONATION FACTORS

Phase-Exchange Medium	Fractionation Parameters				Temperature Range T°C	Reference
	A	B	C	±		
Barite-H ₂ S	6.463		0.56	0.5	200-400	Ohmoto and Lasaga, 1982
Pyrite-H ₂ S	0.4			0.08	200-700	Ohmoto and Rye, 1979
Quartz-H ₂ O	4.1		-3.7	0.04	500-800	Bottinga and Javoy, 1995
Hematite-H ₂ O	0.413		-2.56	0.0027	25-120	Clayton and Epstein, 1961
Biotite-Quartz	-3.69		0.6	0.04	-	Bottinga and Javoy, 1973
Biotite-H ₂ O	-38.0				650	Suzuoki and Epstein, 1976

CALCULATED TEMPERATURES FROM SULPHUR AND OXYGEN ISOTOPE FRACTIONATION

Sample ID	Mineral Pair	Calculated T (°C)	±
BA08_3008_189.6	Barite-Pyrite	480.94	25.47
BA08_3040_249.6	Quartz-Biotite	640.93	23.24
BA08_3040_52.1	Quartz-Biotite	2246.63*	410.28
BA08_3121_2	Quartz-Biotite	631.11	23.02
BA08_3119_16	Quartz-Biotite	1003.81*	30.77
BA08_3121_5	Quartz-Hematite	475.71	44.38
BA08_3040_189.8	Quartz-Hematite	419.77	40.66

Notes: ‘*’ indicates disequilibrium

APPENDIX H: BULK-INCLUDED FLUID DATA

SAMPLE AMOUNTS

Sample ID	Quartz Grains (mg)	Crushed Quartz (mg)	Qtz for Anion Leach (mg)	Qtz for Cation Leach (mg)
BA08_3121_5	548.05	500	249.64	248.45
BA08_3040_52.1	973.3	839.2	251.03	250.76
BA08_3068_15	843.64	948.95	250.89	250.96
BA08_3040_189.8	827.245	936	250.4	250.07
CM07_1540_20.15A	1414.4	1324.65	250.6	250.4
CM07_1540_20.15B	691.4	600.01	250.62	250.64
CM08_1969_165.4	1565.3	1465.18	250.33	250.44
BA08_3040_249.6	1244.43	1165.27	250.89	250.43
CM06_799_40.9	931.5	944.01	250.43	250.56
BA08_3121_4	1585.81	1376.59	251.23	250.01
99.99% Silica Powder	2200?	1832.89	250.18	250.07
CM07-1540-20.1bt_pre-crush	1414.4	N/A	681.63	712.69
BA08_3040-52.1_pre-crush	973.3	N/A	486.07	479.8
1M HNO ₃ Stock A	N/A	N/A	N/A	N/A
1M HNO ₃ Stock B	N/A	N/A	N/A	N/A
Filtered Leachate	N/A	N/A	N/A	N/A

BULK INCLUDED FLUID RESULTS

Analyte	Ca	Na	Mg	Al	K	S	Si	Fe	Cl	SO ₄	NO ₃	Ti	Cu	
Method	AES	OES	MS	MS	MS	AES	AES	MS	IC	IC	IC	MS	MS	
DL (ppb)	30	100	10	50	50	135	15	30	30	30	10	1	2	
Sample ID	G.V.													
BA08_3121-5	1	57.0000	5.2632	1.4561	1.5789	1.5789	15.8070	-	0.9298	7.5439	25.6140	-	0.0316	0.7193
BA08_3121-4	1	82.0000	0.0000	1.4268	1.1585	0.8537	11.1585	5.9878	1.0854	3.2927	4.7561	-	0.0780	0.3159
BA08_3040-189.8	1	193.0000	-	0.3938	0.3057	0.3109	-	3.1192	0.4197	2.1244	3.5751	-	0.0098	0.0264
CM07-1540-20.1	2	42.0000	7.1429	1.7143	-	-	5.2381	7.2143	-	29.2857	9.0476	0.4762	0.0238	0.0762
CM07-1540-20.1	2	140.0000	-	0.2071	0.4643	-	4.4500	-	0.2143	1.8571	1.2143	0.5714	0.0114	0.1071
CM08-1969-165.4	2	182.0000	2.1978	0.3462	0.3462	0.6044	-	2.1978	-	4.3407	5.7692	75.5495	0.0060	0.0670
BA08_3040-249.6	2	214.0000	0.0000	0.7196	0.5981	0.5140	5.5093	2.1355	0.7477	1.9626	4.6729	0.3271	0.0621	0.0393
CM06-799-40.9	2	63.0000	4.7619	0.7937	0.0000	0.9524	-	12.6190	-	5.3968	5.5556	-	0.0190	0.0873
BA08_3068-15	2	501.0000	0.1996	0.5948	1.1257	0.5389	1.3253	1.9102	0.7625	0.9581	1.2974	0.0399	0.0647	0.0431
Analyte	W	Pb	Sn	Ba	Rb	Sr	Co	Cs	Tl	Cd	Li	V	Cr	
Method	MS	MS	MS	MS	MS	MS	MS	MS	MS	MS	MS	MS	MS	
DL (ppb)	0.1	0.02	0.1	0.2	0.05	1	0.05	0.005	0.01	0.1	0.1	0.03	0.2	
Sample ID	G.V.													
BA08_3121-5	1	0.0047	0.0167	-	40.4009	0.0028	2.1596	0.0026	0.0003	0.0005	-	-	0.0023	0.0039
BA08_3121-4	1	0.0015	0.0231	-	0.9107	0.0026	0.0780	-	0.0003	0.0002	0.0121	0.0018	0.0046	-
BA08_3040-189.8	1	0.0007	0.0019	-	0.4981	0.0009	1.2725	-	0.0001	0.0001	-	-	0.0007	0.0012
CM07-1540-20.1	2	0.0062	0.0367	-	0.8274	0.0019	0.1786	-	0.0004	-	-	-	0.0021	-
CM07-1540-20.1	2	0.0009	0.0067	0.0009	0.6993	0.0008	0.0686	0.0004	0.0001	0.0001	-	-	0.0008	0.0034
CM08-1969-165.4	2	0.0005	0.0085	0.0007	0.0177	0.0009	0.0148	-	0.0001	0.0002	0.0451	0.0009	0.0003	0.0015
BA08_3040-249.6	2	0.0007	0.0026	0.0007	1.8498	0.0020	1.2888	0.0003	0.0002	0.0001	-	0.0011	0.0035	0.0018
CM06-799-40.9	2	0.0084	0.0089	-	0.0440	0.0019	-	-	0.0004	0.0005	-	-	0.0016	-
BA08_3068-15	2	0.0021	0.0035	0.0003	0.4179	0.0019	0.0259	0.0005	0.0001	0.0001	-	0.0007	0.0017	0.0010

Notes: - elements below detection include F, NO₂, Br, PO₄, Be, B, Sc, Mn, As, Se, Zr, Nb, Mo, Ni, Zn, Ag, Sb, Te, Au, Bi, Ta, U, Th, Hf and Ga
 - La and all other REEs disregarded due to preparation of leaching solution for cations

BULK INCLUDED FLUID DATASETS FOR COMPARISON

BRINES/FORMATION WATERS									
Sample	Na	K	Li	Mg	Ca	Sr	Ba	Fe	Cl
Connolly et al., 1990									
Belly River	5690.00	72.00	1.00	47.00	163.00	17.00	43.00	0.01	8890.00
Belly River	6050.00	33.00	1.00	50.00	179.00	21.00	47.00	0.02	9590.00
Belly River	5990.00	47.00	1.00	52.00	186.00	21.00	41.00	0.21	9500.00
Belly River	4210.00	34.00	1.00	30.00	125.00	15.00	27.00	2.46	6250.00
Cardium	2450.00	28.00	1.00	11.00	32.00	7.00	5.00	0.03	2140.00
Cardium	2040.00	9.00	1.00	3.00	8.00	1.00	4.00	0.11	1860.00
Cardium	2150.00	22.00	1.00	3.00	9.00	1.00	4.00	0.02	1930.00
Viking	20800.00	107.00	5.00	233.00	431.00	104.00	175.00	30.11	33300.00
Viking	22000.00	102.00	5.00	416.00	1070.00	182.00	365.00	7.13	36100.00
Viking	25100.00	209.00	8.00	884.00	2020.00	230.00	203.00	8.20	44700.00
Viking	25200.00	275.00	9.00	942.00	2040.00	217.00	189.00	0.21	44500.00
Glauconitic	24700.00	348.00	11.00	280.00	1030.00	234.00	350.00	59.94	39700.00
Glauconitic	24800.00	489.00	12.00	207.00	510.00	88.00	7.00	20.19	38900.00
Glauconitic	31900.00	576.00	19.00	867.00	4040.00	360.00	176.00	0.50	58300.00
Ostracod	25900.00	330.00	12.00	390.00	1350.00	264.00	395.00	36.74	42700.00
Ostracod	22600.00	354.00	11.00	236.00	888.00	151.00	72.00	0.21	37200.00
Basal Quartz	25100.00	478.00		795.00	2100.00	180.00	83.00	85.94	44100.00
Basal Quartz	30600.00	740.00	19.00	1178.00	2870.00	199.00	14.00	18.39	54400.00
Basal Quartz	35000.00	944.00	27.00	1307.00	5780.00	375.00	3.00	0.26	67400.00
Basal Quartz	35900.00	1050.00	30.00	1344.00	4030.00	376.00	2.00	0.18	69500.00
Basal Quartz	24900.00	818.00	24.00	1154.00	4570.00	289.00	2.00	0.20	61700.00

Basal Quartz	22900.00	390.00	11.00	150.00	626.00	64.00	27.00	93.05	35900.00
Rock Creek	8470.00	119.00	4.00	46.00	123.00	26.00	14.00	0.15	12700.00
Rock Creek	8440.00	134.00	4.00	49.00	240.00	38.00	36.00	52.20	12300.00
Middle Jurassic	22300.00	395.00	11.00	155.00	698.00	60.00	2.00	129.17	34800.00
Middle Jurassic	23600.00	555.00	16.00	179.00	793.00	54.00	2.00	0.25	36800.00
Nordeg	35300.00	1050.00	33.00	1039.00	4240.00	239.00	2.00	0.24	64100.00
Nordeg	33800.00	573.00	17.00	1038.00	3180.00	463.00	105.00	63.59	60700.00
Banff	36900.00	924.00	25.00	800.00	2180.00	323.00	2.00	0.16	61700.00
Banff	31100.00	659.00	19.00	568.00	1250.00	208.00	2.00	1.76	52500.00
Wabamun	30700.00	714.00	18.00	1051.00	3550.00	325.00	4.00	2.18	55900.00
Wabamun	33200.00	714.00	22.00	1292.00	3890.00	359.00	5.00	11.87	62600.00
Wabamun	41200.00	1480.00	36.00	2071.00	7380.00	446.00	4.00	9.34	84100.00
Wabamun	33600.00	992.00	26.00	1498.00	4810.00	393.00	2.00	0.27	66100.00
Nisku	50600.00	3200.00	55.00	2545.00	12200.00	365.00	2.00	0.26	108000.00
Nisku	33300.00	1930.00	37.00	1841.00	6720.00	187.00	1.00	0.27	67600.00
Nisku	32700.00	1840.00	36.00	1768.00	6400.00	184.00	1.00	0.34	67000.00
Leduc	34200.00	896.00	20.00	1870.00	4380.00	219.00	1.00	0.31	63100.00
Leduc	31100.00	842.00	19.00	1582.00	4260.00	168.00	1.00	0.28	60000.00
Leduc	33000.00	1000.00	22.00	1862.00	4850.00	187.00	1.00	0.28	65100.00
Leduc	34900.00	1080.00	23.00	1987.00	5220.00	198.00	1.00	0.27	66100.00
Leduc	50000.00	3640.00	50.00	5035.00	30000.00	1190.00	7.00	17.48	144000.00
Leduc	34500.00	1560.00	28.00	2109.00	11100.00	397.00	3.00	0.62	78300.00

Carpenter et al., 1974

1	79000.00	7080.00	49.00	3920.00	34000.00	1520.00	25.00	79.00	198700.00
2	31000.00	5770.00		1860.00	25300.00	2310.00	10.00	2.00	104000.00
3	63000.00	6150.00	52.00	2770.00	44600.00	1770.00	89.00	320.00	200400.00
4	65000.00	6080.00	52.00	2790.00	47300.00	1780.00	100.00	318.00	197700.00
5	63200.00	6100.00	51.00	2960.00	45900.00	1740.00	110.00	315.00	196100.00

6	52400.00	551.00		1360.00	16800.00	666.00	29.00	104.00	115300.00
7	52100.00	636.00		1460.00	17700.00	672.00	19.00	105.00	116400.00
8	53000.00	243.00		1530.00	20000.00	702.00	23.00	120.00	126300.00
9	53800.00	4430.00		3610.00	39200.00	3340.00	18.00	3.00	166200.00
10	52100.00	519.00		1660.00	22200.00	700.00	21.00	114.00	124600.00
11	53300.00			1780.00	25800.00	899.00	13.00	166.00	140800.00
12	54200.00	485.00		1770.00	27600.00	962.00	24.00	181.00	143600.00
13	59500.00	538.00		1730.00	36400.00	1110.00	61.00	298.00	158200.00
14	78400.00	856.00		1210.00	30000.00	1620.00	103.00	309.00	176700.00
15	54200.00	863.00	12.00	2550.00	41200.00	1360.00	20.00	335.00	169000.00
16	58300.00	2030.00	31.00	3740.00	55600.00	1620.00	75.00	74.00	203300.00
17	69500.00	9520.00	85.00	2720.00	32600.00	1730.00	25.00		184200.00
18	69000.00	10100.00	83.00	2620.00	32800.00	1740.00	20.00		184400.00
19	47300.00	595.00	9.00	1150.00	13200.00	422.00	20.00	278.00	103200.00
20	49900.00	461.00	2.00	2290.00	29500.00	859.00	30.00	68.00	138400.00
21	50100.00	474.00	2.00	2510.00	30700.00	902.00	20.00	63.00	140100.00
22	48800.00	625.00	2.00	2550.00	37200.00	1060.00	40.00	121.00	150500.00
23	59700.00	1340.00	18.00	3230.00	45000.00	1390.00	50.00	433.00	182100.00
24	40100.00	343.00		574.00	5060.00	412.00	BDL	3.00	71520.00
25	40100.00	333.00		582.00	4140.00	419.00	5.00	4.00	71900.00
26	53700.00	750.00		1640.00	16800.0	718.00	18.00	76.00	118500.00
27	54200.00	727.00		1650.00	16700.00	770.00	17.00	68.00	122000.00
28	54400.00	708.00		2250.00	25800.00	1130.00	32.00	145.00	138900.00
29	53900.00	888.00		2150.00	28900.00	1800.00	55.00	121.00	141600.00
30	53600.00	649.00		2200.00	19300.00	1100.00	34.00	129.00	123100.00
31	46500.00	6800.00		2970.00	30600.00	1300.00	66.00	98.00	141700.00
32	52400.00	5980.00		3010.00	37400.00	1770.00	85.00	5.00	159700.00
33	29200.00	3830.00		2480.00	25700.00	1040.00	88.00	5.00	103300.00
34	52000.00	6080.00		3410.00	37700.00	1610.00	144.00	3.00	156900.00

35	82800.00	8000.00		611.00	6520.00	2640.00	38.00	2.00	148900.00
36	57200.00	545.00		1840.00	26800.00	1390.00	17.00	490.00	140800.00
37	58200.00	916.00		2220.00	29900.00	1750.00	56.00	123.00	150300.00
38	54000.00	979.00		1630.00	26500.00	1750.00	48.00	210.00	139300.00
39	61100.00	854.00		1830.00	28800.00	1820.00	56.00	338.00	150700.00
40	57100.00	851.00		1570.00	19900.00	789.00	24.00	95.00	125600.00
41	59900.00	704.00		2230.00	32100.00	2020.00	51.00	241.00	154700.00
42	29000.00	3030.00	28.00	1470.00	25000.00	477.00	110.00	151.00	99100.00
43	53200.00	635.00	23.00	1880.00	27300.00	1070.00	14.00	255.00	144900.00
45	45000.00	435.00	21.00	1380.00	23200.00	1150.00	17.00	310.00	122500.00
46	55700.00	735.00	14.00	1660.00	19600.00	825.00	23.00	160.00	126200.00
47	57400.00	776.00	11.00	1630.00	19500.00	810.00	29.00	143.00	128400.00
48	62500.00	749.00	33.00	2240.00	30000.00	1940.00	29.00	365.00	160500.00
49	60400.00	1140.00	18.00	3300.00	29100.00	1230.00	BDL	23.00	156700.00
50	60900.00	1610.00	36.00	3510.00	31800.00	1300.00	20.00	125.00	161600.00
51	62300.00	2080.00	31.00	3560.00	31800.00	1410.00	BDL	163.00	167700.00
52	64000.00	2850.00	36.00	3700.00	31800.00	1430.00	BDL	123.00	173800.00
53	65400.00	3000.00	39.00	3700.00	32600.00	1500.00	BDL	113.00	175400.00
54	65300.00	2720.00	38.00	3780.00	33000.00	1580.00	20.00	95.00	177000.00
55	60600.00	2610.00	33.00	3520.00	31800.00	1360.00	BDL	60.00	167300.00
56	64300.00	5600.00	57.00	3650.00	32600.00	1490.00	20.00	379.00	174200.00
57	65000.00	970.00	26.00	2180.00	30500.00	2320.00	98.00	345.00	163900.00
58	63500.00	815.00	28.00	2310.00	34800.00	2300.00	125.00	385.00	166400.00
59	60300.00	950.00	24.00	2150.00	30800.00	2400.00	BDL	285.00	156900.00
60	70500.00	960.00	30.00	2200.00	34300.00	2450.00	143.00	468.00	181900.00
61	67700.00	1090.00	27.00	2140.00	32800.00	2410.00	135.00	434.00	164200.00
62	63000.00	1410.00	19.00	3220.00	41200.00	2620.00	90.00	338.00	181100.00
63	68500.00	940.00	19.00	2650.00	33900.00	2250.00	66.00	318.00	167900.00
64	64500.00	1020.00	20.00	2430.00	33700.00	1900.00	59.00	325.00	171400.00

65	77800.00		18.00	2760.00	30800.00	2310.00	59.00	440.00	193800.00
66	76200.00	979.00		2400.00	36500.00	2260.00	109.00	294.00	193400.00
67	79100.00	860.00	18.00	2680.00	37700.00	2260.00	59.00	420.00	194600.00
68	76200.00	905.00		2410.00	37700.00	2290.00	109.00	298.00	190100.00
69	58300.00	1040.00		3510.00	51100.00	2340.00	79.00	363.00	185900.00
70	58600.00	900.00		3240.00	74800.00	2260.00	86.00	341.00	186500.00
71	55800.00	830.00		2180.00	26000.00	1370.00	43.00	85.00	139700.00
72	57700.00	1000.00		2570.00	34700.00	2060.00	43.00	180.00	156400.00
73	56900.00	913.00		2380.00	34700.00	1910.00	38.00	190.00	158100.00
74	56400.00	882.00		2460.00	36100.00	2090.00	72.00	224.00	161300.00
75	55200.00	960.00		2490.00	35600.00	2000.00	70.00	204.00	161800.00
76	55600.00	1030.00		2330.00	33000.00	2150.00	87.00	192.00	156100.00
77	56900.00	1170.00		2370.00	34700.00	2340.00	107.00	214.00	156100.00
78	56100.00	1320.00		2380.00	35200.00	2360.00	105.00	281.00	159100.00
79	57100.00	917.00		2410.00	36100.00	1880.00	42.00	211.00	156100.00
80	65100.00	7640.00	64.00	2650.00	45600.00	1670.00	80.00	245.00	195700.00
81	66700.00	7860.00	63.00	2840.00	47200.00	2190.00	80.00	414.00	207400.00
82	55400.00	9000.00	55.00	3070.00	46100.00	1330.00	80.00	20.00	188300.00

METAMORPHIC WATERS									
Sample	Na	K	Li	Mg	Ca	Sr	Ba	Fe	Cl
Banks et al., 1999									
50176	57484.00	5219.00	633.00	1305.00	16687.00	1132.00	638.00	2771.00	130639.00
50173	57832.00	6001.00	680.00	1460.00	17905.00	1018.00	709.00	2802.00	127397.00
49453	57940.00	2799.00	487.00	869.00	26670.00	2606.00	1072.00	759.00	146009.00
50182	41772.00	1630.00	456.00	919.00	28187.00	1228.00	1028.00	1516.00	129282.00
50181	40486.00	2203.00	352.00	210.00	29664.00	1271.00	271.00	839.00	125620.00
50180	42638.00	2294.00	316.00	519.00	30534.00	1334.00	354.00	2053.00	130560.00
49454	34945.00	2432.00	130.00	349.00	38933.00	1024.00	231.00	245.00	119446.00
50177	29135.00	1218.00	215.00	1133.00	39004.00	1145.00	370.00	2372.00	124875.00
McCaig et al., 2000									
Gistain									
P94-5Q	41871.00	2851.00	207.00	4086.00	45037.00	2856.00		3716.00	136284.00
P94-5Ba	45891.00	268.00	429.00	3410.00	45650.00	17622.00		4643.00	139215.00
P-94-3	22790.00	1587.00	20.00	317.00	4925.00	595.00		640.00	48219.00
P94-3b	15228.00	1189.00	39.00	504.00	4639.00	613.00		775.00	30298.00
P94-3X	21070.00	2107.00	118.00	3427.00	13375.00	624.00		2998.00	47716.00
P. De Larri									
PL90-9d2	13552.00	1717.00	72.00	57.00	8584.00	817.00		197.00	42211.00
P94-11	48873.00	1291.00	241.00	504.00	17582.00	2183.00		364.00	103131.00
P94-10	30609.00	8587.00	0.00	92842.00	220402.00	838.00		3351.00	60667.00
P94-9	24908.00	2257.00	0.00	24043.00	194085.00	778.00		1678.00	54459.00
P94-8	18107.00	1341.00	57.00	209.00	5691.00	810.00		607.00	42132.00

Liena P94-19	56694.00	3660.00	647.00	647.00	7935.00	1019.00	1073.00	96265.00
Pic Long (Neouvielle)								
*55141-1	62213.00	14564.00	1879.00	1207.00	47637.00	3421.00	2868.00	187405.00
*55141-2	63959.00	13687.00	1996.00	876.00	35785.00	3939.00	2814.00	200231.00
*55141-3	70090.00	12462.00	1591.00	1107.00	31197.00	4500.00	3960.00	197381.00
*54185	51533.00	7271.00	170.00	216.00	53094.00	1850.00	1597.00	185627.00
*55138	57725.00	8404.00	300.00	727.00	47260.00	1986.00	266.00	177787.00
*54192	66914.00	8618.00	448.00	790.00	32279.00	1204.00	2382.00	180775.00
LaGlere (Neouvielle)								
*55137	56303.00	7747.00	810.00	692.000	49946.00	1964.00	1334.00	179561.00
*N90-6	57234.00	5626.00	132.00	80.000	33236.00	1797.00	441.00	175023.00
*N90-10	58705.00	8806.00	0.00	1174.00	49547.00	2290.00	1585.00	189912.00
*N90-4	53366.00	7829.00	0.00	155.00	31790.00	1894.00	486.00	155332.00
*N90-13	58111.00	9803.00	267.00	744.00	36279.00	2406.00	645.00	166552.00
*N90-5	45823.00	5531.00	0.00	729.00	46487.00	2497.00	916.00	163198.00
P de PV								
#IH31C	39545.00	2879.00	289.00	210.00	35088.00	1578.00	289.00	119213.00
#54319-t	59165.00	2006.00	497.00	840.00	27334.00	1160.00	1444.00	133700.00
#54319-m	55187.00	1600.00	530.00	1065.00	30320.00	2809.00	2539.00	131421.00
#54319-b	50639.00	1453.00	0.00	815.00	23679.00	2157.00	1139.00	145587.00
#52763-t	45402.00	1884.00	354.00	268.00	20553.00	1739.00	268.00	126803.00
#52763-m	45083.00	1758.00	345.00	307.00	23033.00	1754.00	365.00	124731.00
#52763-b	44711.00	2361.00	335.00	380.00	25883.00	1736.00	478.00	121252.00
\$50,176	57484.00	5219.00	633.00	1305.00	16687.00	1132.00	2771.00	130639.00
\$50,173	57832.00	6001.00	680.00	1460.00	17905.00	1018.00	2802.00	127397.00
\$49,453	57940.00	2799.00	487.00	869.00	26670.00	2606.00	759.00	146009.00

\$50,182	41772.00	1630.00	456.00	919.00	28187.00	1228.00		1516.00	129282.00
\$50,181	40486.00	2203.00	352.00	210.00	29664.00	1271.00		839.00	125620.00
\$50,180	42638.00	2294.00	316.00	519.00	30534.00	1334.00		2053.00	130560.00
\$49,454	34945.00	2432.00	130.00	349.00	38933.00	1024.00		245.00	119466.00
\$50,177	29135.00	1218.00	215.00	1133.00	39004.00	1145.00		2372.00	124875.00

Munz et al., 1995

D0V-1	17118.00	1032.00	13.00	27.00	5457.00	83.00	31.00	53.00	35661.00
D0V-1H	16820.00	906.00	12.00	61.00	5966.00	97.00	34.00	81.00	35134.00
IA-527	18153.00	1361.00	40.00	45.00	4900.00	78.00	35.00	51.00	34748.00
IA-463	22615.00	2072.00	64.00	206.00	4454.00	81.00	37.00	93.00	29633.00
IA-432	20516.00	2263.00	30.00	78.00	4239.00	107.00	75.00	164.00	30885.00
IA-432H	19902.00	2574.00	32.00	86.00	4448.00	112.00	80.00	239.00	31218.00
IA-5IIG	45707.00	7110.00	208.00	128.00	24581.00	1307.00	2163.00	2370.00	74456.00
IA-511GH	45951.00	3414.00	207.00	1379.00	26197.00	862.00	1413.00	4240.00	72465.00

Banks et al., 2000

Quartz GG-5	54590.00	11622.00	2031.00	639.00	44027.00	1605.00	1064.00	23791.00	211091.00
Emerald GG-6	130946.00	5795.00	944.00	1062.00	6746.00	144.00	118.00	4300.00	230082.00
Quartz GG-16	92542.00	10467.00	2212.00	250.00	59847.00	250.00	250.00	3822.00	254132.00
Emerald GG-7	94823.00	18813.00	1261.00	5424.00	16821.00	228.00	303.00	10772.00	224306.00
Quartz GG-18	63557.00	11567.00	4322.00	3082.00	43302.00	1347.00	966.00	21749.00	230481.00
Quartz GG-19	110776.00	5449.00	432.00	111.00	18931.00	399.00	432.00	13071.00	227371.00
Emerald GG-10	122677.00	8829.00	1165.00	3606.00	15972.00	356.00	196.00	6747.00	242430.00
Emerald GG-11	116142.00	5888.00	430.00	1568.00	19515.00	407.00	198.00	5086.00	230202.00
Emerald GG-12	98923.00	10248.00	1959.00	6440.00	32556.00	1048.00	604.00	9388.00	240698.00
Quartz GG-20	68344.00	8796.00	2549.00	1435.00	31855.00	1524.00	1503.00	4579.00	183208.00
Quartz GG-15	78554.00	17415.00	2090.00	385.00	32356.00	825.00	652.00	23252.00	242078.00

MAGMATIC WATERS									
Sample	Na	K	Li	Mg	Ca	Sr	Ba	Fe	Cl
Klemm et al., 2007									
ID ₂₋₀									
1786-237.5	37800.00	18100.00	20.00	320.00	13300.00	70.00	120.00	14900.00	117178.15
LK04-ET16-I	34700.00	16000.00	35.00	750.00	2000.00	40.00	55.00	4000.00	76657.52
B ₂₋₁									
1786-237.5	96900.00	47700.00	7.00	420.00	16600.00	240.00	280.00	67100.00	307309.54
1786-259-I	112400.00	42100.00	150.00	510.00	15900.00	220.00	670.00	63600.00	320459.48
LK04-ET9	104600.00	52100.00	60.00	130.00	32200.00	630.00	540.00	73700.00	359160.90
LK04-ET16-II	139500.00	54200.00	380.00	810.00	35000.00	200.00	150.00	45700.00	384306.441
2212-335-2a.IV	92400.00	56900.00	50.00	480.00	3000.00	140.00	90.00	76200.00	296201.32
2212-335-2a.VI	86600.00	52300.00	340.00	830.00	51000.00	70.00	80.00	70300.00	360522.46
V ₂₋₁									
2212-355-3	8800.00	4500.00	570.00	890.00	11000.00	16.00	20.00	4700.00	43087.28
2212-335-6	900.00	780.00	45.00	60.00	310.00	5.00	2.00	1500.00	4548.81
2212-335-2a.I	2900.00	1500.00	70.00	5.00	3000.00	5.00	5.00	1200.00	12665.85
2212-355-2a.VIa	2200.00	1100.00	15.00	80.00	13000.00	2.00	10.00	BDL	BDL
2212-355-2a.VIb	7500.00	5000.00	200.00	100.00	3000.00	3.00	4.00	2100.00	24078.83
2212-335-8.XI	1200.00	720.00	20.00	100.00	8000.00	1.00	8.00	700.00	17548.15
2212-355-2a.IV	1900.00	1000.00	150.00	40.00	1200.00	4.00	1.00	2800.00	9516.35
B ₂₋₂									
LK04-ET16-I	114200.00	91500.00	60.00	160.00	5500.00	300.00	360.00	87600.00	380107.17
LK04-ET16-0	152000.00	70900.00	10.00	140.00	13900.00	200.00	190.00	28300.00	359307.26
2212-355-6	159800.00	118800.00	30.00	310.00	10900.00	360.00	310.00	51100.00	438420.45

2212-355-2a.III	166200.00	89900.00	140.00	50.00	16700.00	350.00	280.00	25400.00	399715.78
2212-355-2a.VI	176400.00	8900.00	160.00	55.00	8300.00	270.00	150.00	44800.00	351762.53
S ₂									
2212-355-6	350000.00	10900.00	30.00	50.00	1200.00	8.00	8.00	690.00	552810.41
2212-355-SI	308500.00	16700.00	120.00	100.00	2200.00	40.00	20.00	5300.00	501673.24
B ₂₋₃									
LK04-ET16.V	97800.00	30800.00	120.00	140.00	16400.00	290.00	190.00	19200.00	232199.15
2212-355-ID	81000.00	30200.00	110.00	70.00	27800.00	480.00	260.00	16000.00	221846.74
2212-355-2a.VI	75300.00	37400.00	160.00	640.00	10000.00	550.00	25.00	55800.00	238621.85
2212-355-8.VII	98400.00	46800.00	410.00	810.00	24000.00	90.00	45.00	7800.00	246607.74
V ₂₋₂									
2212-355-2a.V	2800.00	3400.00	320.00	100.00	6100.00	11.00	BDL	280.00	18551.68
2212-355-5	3000.00	1900.00	40.00	140.00	4100.00	2.00	4.00	1700.00	15764.06
2212-355-1	6800.00	3200.00	130.00	130.00	15000.00	8.00	25.00	3100.00	43869.13
2212-355-8.X	14200.00	6700.00	110.00	130.00	15500.00	8.00	10.00	3700.00	60105.32
2212-355-8.XI	6400.00	3100.00	35.00	170.00	2300.00	4.00	25.00	2700.00	20182.08
ID ₂₋₁									
1784-337-2.II	5400.00	3100.00	30.00	11.00	8400.00	5.00	4.00	3500.00	30448.56
1784-337-2.I	8600.00	6200.00	170.00	680.00	13800.00	40.00	40.00	5200.00	49909.62
LK04-ET9	10200.00	4500.00	280.00	430.00	14000.00	4.00	15.00	5100.00	51063.07
LK04-ET16-I	5100.00	4200.00	60.00	190.00	11000.00	6.00	7.00	1700.00	33298.32
2212-355-ID	15400.00	5600.00	120.00	190.00	65000.00	14.00	6.00	3100.00	147782.58
ID ₃									
LK04-ET19-II	14400.00	5600.00	610.00	55.00	13000.00	35.00	50.00	3000.00	54103.98
1784-337-III	11800.00	3800.00	5.00	470.00	5900.00	2.00	5.00	3800.00	36913.71
LK04ET3	17300.00	7100.00	10.00	830.00	7300.00	30.00	30.00	5300.00	52772.68
LK04-ET19-III	8100.00	7800.00	270.00	380.00	6500.00	30.00	25.00	2600.00	34371.45

LK04-ET27	20800.00	6200.00	920.00	290.00	4800.00	16.00	BDL	BDL	
B ₃									
1784-337-III	96100.00	41500.00	12.00	510.00	6600.00	85.00	85.00	80600.00	299899.66
L ₄									
2212-335-8.II	19800.00	3500.00	670.00	150.00	14600.00	90.00	35.00	120.00	59704.13
Smith et al., 1996									
54150	16310.00	4186.00	58.00	598.00	4411.00		29.00	9130.00	28119.00
54157	20130.00	7555.00	324.00	690.00	5992.00		188.00	3048.00	32218.00
54158	17275.00	6699.00	303.00	503.00	6553.00		146.00	1939.00	27967.00
54435	24559.00	5795.00	336.00	664.00	4347.00		164.00	3848.00	39321.00
54154vc	24065.00	3834.00	352.00	564.00	6534.00		61.00	3190.00	43116.00
55239	16390.00	3802.00	338.00	652.00	4828.00		148.00	4992.00	27955.00
CH-88-1	24944.00	5004.00	241.00	223.00	2608.00		91.00	1056.00	37396.00
Campbell et al., 1995									
MTE	178632.00	74868.00	54.00	268.00	42336.00	1822.00	982.00	13915.00	429504.00
W3-3	199935.00	71017.00	60.00	500.00	34349.00	1220.00	540.00	7538.00	433416.00
BS	188582.00	56971.00		114.00	37905.00	605.00	1131.00	7751.00	405167.00
CPU-2	182438.00	61409.00	128.00	383.00	30723.00	784.00	345.00	16310.00	398937.00
CM 242	187110.00	75873.00		188.00	41351.00	413.00	695.00	7578.00	401931.00
CMX	195717.00	65409.00		450.00	38412.00	1096.00	509.00	5754.00	428248.00
FN	173686.00	68902.00		297.00	37342.00	1361.00	767.00	14347.00	402066.00

APPENDIX I: TITANIUM CONCENTRATIONS IN VEIN QUARTZ AND
TITANIQ GEOTHERMOMETRY

TITANIUM CONCENTRATIONS IN VEIN QUARTZ

Sample ID	Sample Name	Concentration (ppm)		Error (1 σ)		MDL (99% confidence)	
		Si	Ti	Si	Ti	Si	Ti
NIST6101	Standard	328329.19	431.69	10382.89	13.23	38.25	0.388
NIST6102	Standard	328329.16	436.17	10382.88	13.37	36.75	0.365
NIST6103	Standard	328329.16	434.72	10382.89	13.65	38.46	0.573
NIST6104	Standard	328329.16	433.17	10382.89	13.63	37.5	0.536
NIST6101	Standard	328329.16	434.68	10382.88	13.15	40.27	0.517
NIST6102	Standard	328329.16	433.18	10382.88	13.11	36.12	0.465
NIST6103	Standard	328329.13	435.1	10382.88	13.27	35.74	0.515
NIST6104	Standard	328329.13	433.07	10382.88	13.23	35.51	0.501
Helt-Qtz-1a	BA08_3040_249.6	467439.47	4.34	14782.43	0.27	42.68	0.435
Helt-Qtz-1b	BA08_3040_249.6	467439.44	3.51	14783.24	0.32	38.37	0.413
Helt-Qtz-2a	CM07_1540_20.15	467439.44	4.66	14782.1	0.24	34.09	0.384
Helt-Qtz-2b	CM07_1540_20.15	467439.44	4.71	14782.22	0.27	40.82	0.472
Helt-Qtz-3a	CM06_698_218.2*	467439.44	7.57	14794.74	0.96	87.07	1.01
Helt-Qtz-3b	CM06_698_218.2*	467439.41	6.44	14786.9	0.66	86.32	1.09
Helt-Qtz-3c	CM06_698_218.2	467439.41	7.17	14787.95	0.79	98.56	1.30
Helt-Qtz-4a	BA08_3040_37.8	467439.41	2.53	14782.35	0.23	33.22	0.419
Helt-Qtz-4b	BA08_3040_37.8	467439.34	1.80	14782.35	0.24	34.38	0.455
Helt-Qtz-5a	BA08_3068_24	467439.41	5.99	14782.16	0.28	34.37	0.411
Helt-Qtz-5b	BA08_3068_24	467439.41	6.62	14782.03	0.27	29.21	0.363
Helt-Qtz-6a	SLADEN 2	467439.44	4.21	14782.2	0.26	36.74	0.474
Helt-Qtz-6b	SLADEN 2	467439.41	4.72	14782.24	0.28	36.96	0.487
Helt-Qtz-7a	CM05_665_31.5	467439.41	5.24	14782.34	0.29	33.18	0.438

		Concentration (ppm)		Error (1 σ)		MDL (99% confidence)	
		Si	Ti	Si	Ti	Si	Ti
Sample ID	Sample Name						
Helt-Qtz-7b	CM05_665_31.5	467439.41	4.89	14781.96	0.24	33.00	0.452
Helt-Qtz-8a	CM06_794_40.9	467439.41	5.64	14782.03	0.27	34.28	0.468
Helt-Qtz-8b	CM06_794_40.9	467439.38	5.65	14782.05	0.27	31.18	0.45
Helt-Qtz-8c	CM06_794_40.9	467439.38	5.96	14784.09	0.48	37.38	0.499
Helt-Qtz-9a	CM08_1969_165.4	467439.38	4.41	14782.01	0.25	36.24	0.516
Helt-Qtz-9b	CM08_1969_165.4	467439.41	4.30	14782.1	0.27	34.89	0.511
Helt-Qtz-10a	BA08_3040_52.1	467439.38	4.10	14782.23	0.28	36.45	0.526
Helt-Qtz-10b	BA08_3040_52.1	467439.38	5.88	14782.37	0.34	36.06	0.534
Helt-Qtz-11a	CM07_1402_227	467439.38	2.10	14782.22	0.22	32.58	0.442
Helt-Qtz-11b	CM07_1402_227	467439.38	2.62	14782.18	0.27	49.20	0.678
Helt-Qtz-12a	CM07_840_41.7*	467439.41	31.68	14784.02	1.17	37.12	0.531
Helt-Qtz-12b	CM07_840_41.7*	467439.38	14.98	14787.74	0.97	33.06	0.482

Notes: "*" indicates unreliable results due to instrument error

EQUATIONS FOR TITANIQ GEOTHERMOMETRY

A titanium in quartz geothermometer, TitaniQ, has been calibrated from synthesizing quartz in the presence of rutile at temperatures ranging from 600-1000°C at 1.0 GPa (Wark & Watson, 2006). The temperature of crystallization is given by the equation:

$$T(^{\circ}C) = \frac{-3765 \pm 24}{\log \left(X_{Ti \pm \sigma_{X_j}}^{qtz} | a_{TiO_2} \right) - 5.69 \pm 0.02} - 273$$

where X is the concentration of titanium in quartz in ppm and a_{TiO_2} is the activity of titania. If the system is saturated in respect to rutile, the activity of titania should be equal to 1 and if undersaturated should be less than unity. In the absence of an independent determination of a_{TiO_2} , the TitaniQ geothermometer gives a minimum estimate of the temperature of crystallization.

The error on the TitaniQ geothermometer (σ_T^2) is derived using standard error propagation:

$$\sigma_T^2 = \left[\frac{B^2}{\left(\log \left(X_j^i / a_j \right) + C \right)^2} \right] \left[\frac{\sigma_B^2}{B^2} + \frac{\frac{(X_j^i)^2 \left[\frac{\sigma_{X_j^i}^2}{(X_j^i)^2} + \frac{\sigma_{a_j}^2}{a_j^2} \right]}{\left(\log \left(X_j^i / a_j \right) \ln 10 \right)^2 + \sigma_C^2}}{\left(\log \left(X_j^i / a_j \right) + C \right)^2} \right]$$

Where

$B = -3765$,

$\sigma_B = 24$,

$C = -5.69$,

$\sigma_C = 0.02$,

$\sigma_{a_j} = 0$,

X_j^i = measured Ti in quartz in ppm,

a_j = activity of TiO_2 ,

$\sigma_{X_j^i}$ = error on measured Ti in quartz (1 σ error)

CALCULATED TEMPERATURES USING TITANIQ

Titania Activity	aTiO₂=1 T (°C)	aTiO₂=0.5 T (°C)	aTiO₂=0.1 T (°C)
Sample Name			
BA08_3040_249.6	472.17	519.38	656.05
BA08_3040_249.6	458.82	504.30	635.39
CM07_1540_20.15	476.76	524.57	663.19
CM07_1540_20.15	477.45	525.35	664.27
CM05_698_218.2	509.60*	561.83*	714.95*
CM05_698_218.2	498.34	549.04	697.08
CM05_698_218.3	505.78	557.49	708.88
BA08_3040_37.8	439.14	482.14	605.26
BA08_3040_37.8	419.77	460.39	575.98
BA08_3068_24	493.40	543.43	689.28
BA08_3068_24	500.24	551.19	700.08
SLADEN 2	470.23	517.19	653.04
SLADEN 2	477.59	525.51	664.49
CM05_665_31.5	484.44	533.27	675.20
CM05_665_31.5	479.90	528.12	668.09
CM06_794_40.9	489.34	538.83	682.89
CM06_794_40.9	489.46	538.96	683.08
CM06_794_40.9	493.06	543.04	688.76
CM08_1969_165.4	473.20	520.55	657.65
CM08_1969_165.4	471.58	518.71	655.13
BA08_3040_52.1	468.55	515.29	650.42

Titania Activity	aTiO₂=1		aTiO₂=0.5		aTiO₂=0.1	
	T (°C)		T (°C)		T (°C)	
Sample Name						
BA08_3040_52.1	492.15		542.01		687.31	
CM07_1402_227	428.41		470.08		588.99	
CM07_1402_227	441.19		484.44		608.38	
CM07_840_41.7	625.74*		695.32*		907.54*	
CM07_840_41.7	560.98		620.57		798.28	
	AVERAGE T (°C)	471.28	AVERAGE T (°C)	518.42	AVERAGE T (°C)	654.90
	MAX T (°C)	500.24	MAX T (°C)	551.19	MAX T (°C)	700.08
	MIN T (°C)	419.77	MIN T (°C)	460.39	MIN T (°C)	575.98

Notes: "*" indicates unreliable results due to instrument error

APPENDIX J: PHASE EQUILIBRIUM MODELING

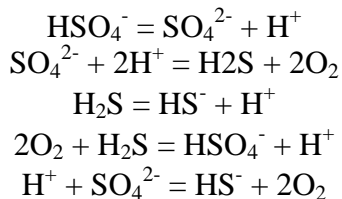
ΔG_f DATA

Temperature (°C)		475				
Pressure (bar)		1000	2000	3000	4000	5000
ΔG_f (kJ)		ΔG_f				
Species	Ref.					
HSO ₄ ⁻	5	-802.227	-810.809	-811.094	-810.024	-808.332
SO ₄ ²⁻	2	-689.375	-706.598	-713.063	-716.150	-717.495
H ₂ S	2	-117.753	-113.223	-109.549	-106.126	-102.834
HS ⁻	2	8.997	1.44	-0.648	-1.165	-0.909
O ₂	1	-99.584	-99.584	-99.584	-99.584	-99.584
H ⁺		0	0	0	0	0
FeS ₂	4	-197.945	-195.551	-193.157	-190.763	-188.369
Fe _(0.875) S	4	-138.29	-136.541	-134.792	-133.043	-131.294
Fe ₂ O ₃	1	-809.118	-806.091	-803.064	-800.037	-797.010
Fe ₃ O ₄	1	-1116.283	-1111.831	-1107.380	-1102.930	-1098.480
H ₂ O		-284.338	-281.628	-279.249	-277.056	-274.986
KAl ₃ Si ₃ O ₁₀ (OH) ₂	1	-5813.757	-5799.674	-5785.59	-5771.510	-5757.430
SiO ₂	1	-885.894	-883.265	-881.357	-879.088	-876.818
K ⁺	2	-330.425	-329.915	-329.062	-328.032	-326.892
KAlSiO ₈	1	-3894.097	-3883.206	-3872.31	-3861.420	-3850.53
AuOH	6	-153.965	-156.873	-155.450	-152.925	-149.920
AuHS	8	-44.063	-47.779	-46.580	-43.971	-40.676
Au(HS) ₂ ⁻		-78.751	-81.669	-78.830	-74.283	-68.882
AuCl ₂ ⁻	7	-190.055	-197.607	-197.331	-194.754	-191.036
Au(OH) ₂ ⁻	6	-299.432	-315.173	-318.326	-318.191	-316.566
Cl ⁻	2	-121.858	-129.841	-132.366	-133.313	-133.480
Au _{0.9} /Ag _{0.1}	3	-27.475	-26.453	-25.431	-24.409	-23.387
NaCl	9	-499.726	-446.754	-444.141	-441.644	-439.213
KCl	9	-474.039	-469.778	-465.971	-462.345	-458.830
NaAlSi ₃ O ₈	1	-3855.503	-3845.497	-3835.49	-3825.490	-3815.480

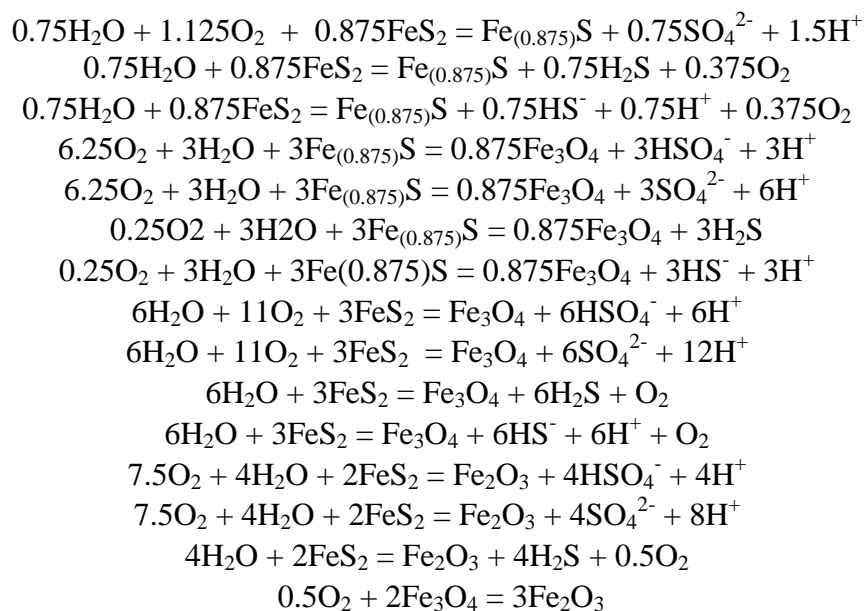
1. Holland and Powell, 1998
2. Johnson et al., 1992
3. Pal'yanova and Drebuschak, 2002
4. Robie and Hemingway, 1995
5. Shock et al., 1997
6. Stefansson and Seward, 2003a
7. Stefansson and Seward, 2003b
8. Stefansson and Seward, 2004
9. Sverjensky et al., 1997

REACTIONS

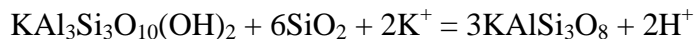
Aqueous Sulphur Speciation Reactions



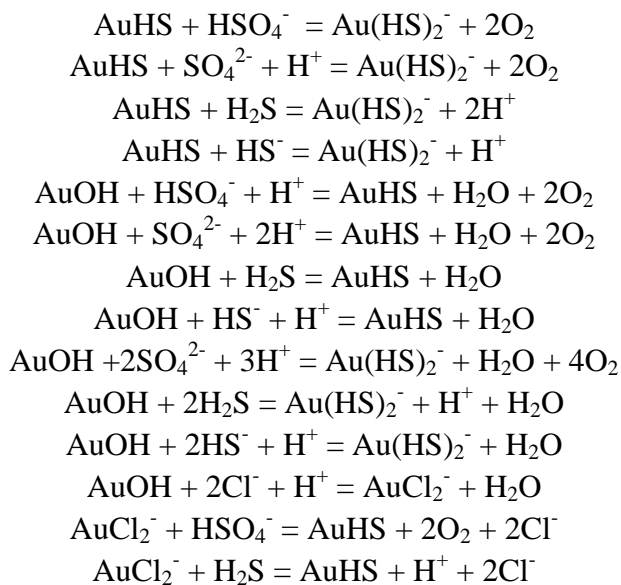
Fe-S-O Mineral-Aqueous Species Reactions



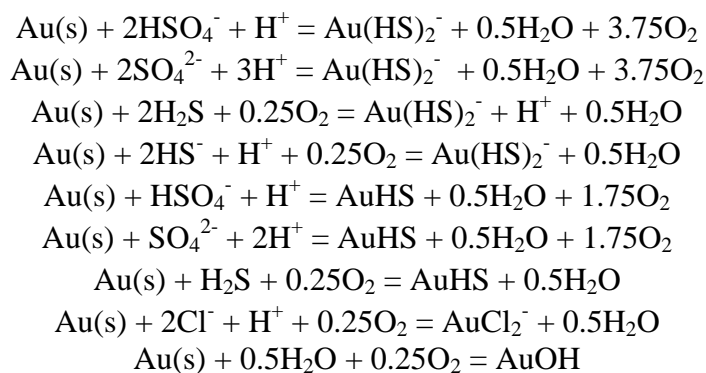
Buffer



Gold Speciation Reactions



Gold Saturation Reactions



EQUATIONS FOR CALCULATION OF SULFUR ISOTOPE CONTOURS

The following equations of Ohmoto (1972) were used to calculate sulfur isotope contours in $\log f_{O_2}$ -pH space:

The mean isotopic composition of sulfur in the solutions, $\delta^{34}S_{\Sigma S}$, can be closely approximated by

$$\begin{aligned} \delta^{34}S_{\Sigma S} = & (\delta^{34}S_{H_2S} \cdot X_{H_2S}) + (\delta^{34}S_{HS^-} \cdot X_{HS^-}) + (\delta^{34}S_{S^{2-}} \cdot X_{S^{2-}}) \\ & + (\delta^{34}S_{SO_4^{2-}} \cdot X_{SO_4^{2-}}) + (\delta^{34}S_{HSO_4^-} \cdot X_{HSO_4^-}) + (\delta^{34}S_{KSO_4^-} \cdot X_{KSO_4^-}) \\ & + (\delta^{34}S_{NaSO_4^-} \cdot X_{NaSO_4^-}) \end{aligned}$$

Where $\delta^{34}S_i$ is the isotopic composition of sulfur species i, and X_i is the mole fraction of the sulfur species i relative to total sulfur content:

$$X_i = \frac{m_i}{m_{\Sigma S}} = \frac{m_i}{m_{H_2S} + m_{HS^-} + m_{S^{2-}} + m_{SO_4^{2-}} + m_{HSO_4^-} + m_{KSO_4^-} + m_{NaSO_4^-}}$$

Where m_i is the molality of the species i.

When the $\delta^{34}S_{H_2S}$ value is taken as a reference, $\delta^{34}S$ values of other sulfur species in solution and of minerals which precipitate from the same solution at the same temperature can be expressed as

$$\delta^{34}S_i = \delta^{34}S_{H_2S} + \Delta_i$$

In which Δ_i is the relative isotopic enrichment factor between a sulfur species i and H_2S .

Therefore,

$$\begin{aligned} \delta^{34}S_i = & \delta^{34}S_{\Sigma S} + \Delta_i \\ & - [(\Delta_{HS^-} \cdot X_{HS^-}) + (\Delta_{S^{2-}} \cdot X_{S^{2-}}) + (\Delta_{SO_4^{2-}} \cdot X_{SO_4^{2-}}) \\ & + (\Delta_{HSO_4^-} \cdot X_{HSO_4^-}) + (\Delta_{KSO_4^-} \cdot X_{KSO_4^-}) + (\Delta_{NaSO_4^-} \cdot X_{NaSO_4^-})] \end{aligned}$$

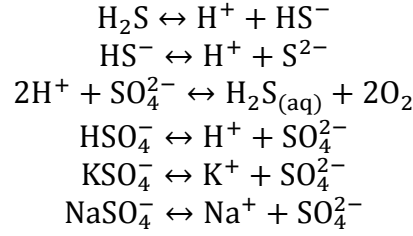
If isotopic equilibrium is established among sulfur species in a system, the relative isotopic enrichment factor (Δ) can be shown to be related to the isotopic fractionation factor (α) by

$$\Delta_i \cong 1000\alpha_{H_2S}^i$$

It is assumed that all the ionic sulfate species have similar Δ values

$$\Delta_{SO_4^{2-}} \cong \Delta_{HSO_4^-} \cong \Delta_{KSO_4^-} \cong \Delta_{NaSO_4^-}$$

If chemical equilibrium is established in a hydrothermal system, the mole fractions of aqueous sulfur species relative to total sulfur content, X_i , can be evaluated from the following reactions:



Expressing the equilibrium constants for the above reactions in terms of K_{HS^-} , $K_{\text{H}_2\text{S}}$, $K_{\text{SO}_4^{2-}}$, $K_{\text{HSO}_4^-}$, $K_{\text{KSO}_4^-}$ and $K_{\text{NaSO}_4^-}$, respectively, the mole fractions of sulfur species can be expressed as

$$\begin{aligned} X_{\text{H}_2\text{S}} &= \frac{1}{C} \\ X_{\text{HS}^-} &= \frac{K_{\text{H}_2\text{S}} \cdot \gamma_{\text{H}_2\text{S}}}{C \cdot a_{\text{H}^+} \cdot \gamma_{\text{HS}^-}} \\ X_{\text{S}^{2-}} &= \frac{K_{\text{H}_2\text{S}} \cdot K_{\text{HS}^-} \cdot \gamma_{\text{H}_2\text{S}}}{C \cdot (a_{\text{H}^+})^2 \cdot \gamma_{\text{S}^{2-}}} \\ X_{\text{SO}_4^{2-}} &= \frac{(f_{\text{O}_2})^2 \cdot \gamma_{\text{H}_2\text{S}}}{C \cdot K_{\text{SO}_4^{2-}} \cdot (a_{\text{H}^+})^2 \cdot \gamma_{\text{SO}_4^{2-}}} \\ X_{\text{HSO}_4^-} &= \frac{(f_{\text{O}_2})^2 \cdot \gamma_{\text{H}_2\text{S}}}{C \cdot K_{\text{SO}_4^{2-}} \cdot K_{\text{HSO}_4^-} \cdot a_{\text{H}^+} \cdot \gamma_{\text{HSO}_4^-}} \\ X_{\text{KSO}_4^-} &= \frac{(f_{\text{O}_2})^2 \cdot m_{\text{K}^+} \cdot \gamma_{\text{K}^+} \cdot \gamma_{\text{H}_2\text{S}}}{C \cdot K_{\text{SO}_4^{2-}} \cdot K_{\text{HSO}_4^-} \cdot (a_{\text{H}^+})^2 \cdot \gamma_{\text{KSO}_4^-}} \\ X_{\text{NaSO}_4^-} &= \frac{(f_{\text{O}_2})^2 \cdot m_{\text{Na}^+} \cdot \gamma_{\text{Na}^+} \cdot \gamma_{\text{H}_2\text{S}}}{C \cdot K_{\text{SO}_4^{2-}} \cdot K_{\text{NaSO}_4^-} \cdot (a_{\text{H}^+})^2 \cdot \gamma_{\text{NaSO}_4^-}} \end{aligned}$$

In which

$$\begin{aligned} C &= 1 + \left(\frac{K_{\text{H}_2\text{S}} \cdot \gamma_{\text{H}_2\text{S}}}{a_{\text{H}^+} \cdot \gamma_{\text{HS}^-}} \right) \cdot \left(1 + \frac{K_{\text{HS}^-} \cdot \gamma_{\text{HS}^-}}{a_{\text{H}^+} \cdot \gamma_{\text{S}^{2-}}} \right) + \left(\frac{(f_{\text{O}_2})^2 \cdot \gamma_{\text{H}_2\text{S}}}{K_{\text{SO}_4^{2-}} \cdot (a_{\text{H}^+})^2} \right) \\ &\quad \cdot \left(\frac{1}{\gamma_{\text{SO}_4^{2-}}} + \frac{a_{\text{H}^+}}{K_{\text{HSO}_4^-} \cdot \gamma_{\text{HSO}_4^-}} + \frac{m_{\text{K}^+} \cdot \gamma_{\text{K}^+}}{K_{\text{KSO}_4^-} \cdot \gamma_{\text{KSO}_4^-}} + \frac{m_{\text{Na}^+} \cdot \gamma_{\text{Na}^+}}{K_{\text{NaSO}_4^-} \cdot \gamma_{\text{NaSO}_4^-}} \right) \end{aligned}$$

and m_i and γ_i are, respectively, the molality and activity coefficient of species i .

The mean activity coefficient, γ_{\pm} , of a completely dissociated binary electrolyte can be calculated using the Debye-Hückel equation with the extended term parameter:

$$\log \gamma_i = -\frac{A|Z_{M^+}Z_{X^-}|^{1/2}}{(1 + aBI^{1/2})} + \Gamma + bI$$

Where Z_{M^+} and Z_{X^-} are the respective charges of the cation and anion of the electrolyte, a is the ion size parameter, I is the ionic strength ($I \cong (m_{K^+}) + (m_{Na^+})$), A and B are defined by

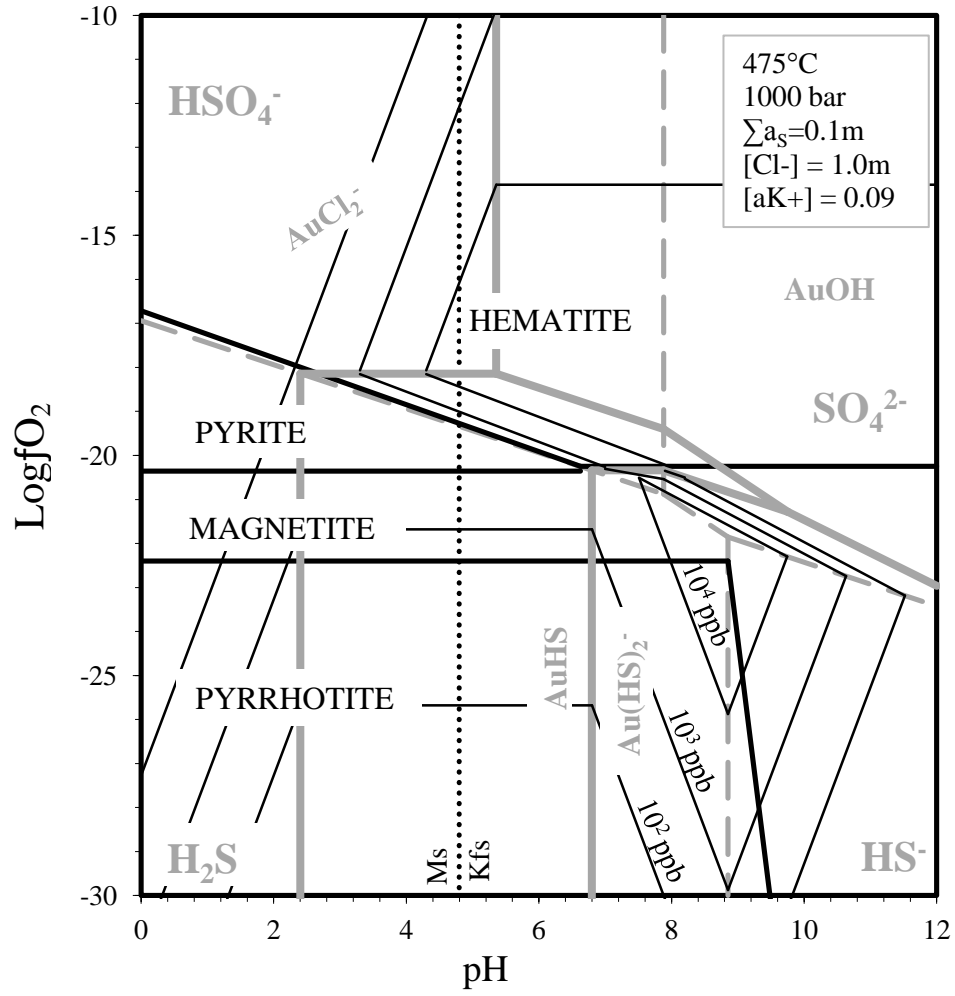
$$A \equiv \frac{(2\pi)^{1/2} e^3 \rho e^{1/2}}{2.302585(1000)^{1/2} (\epsilon kT)^{3/2}} = \frac{1.824829238 \times 10^6 \rho^{1/2}}{(\epsilon T)^{3/2}}$$

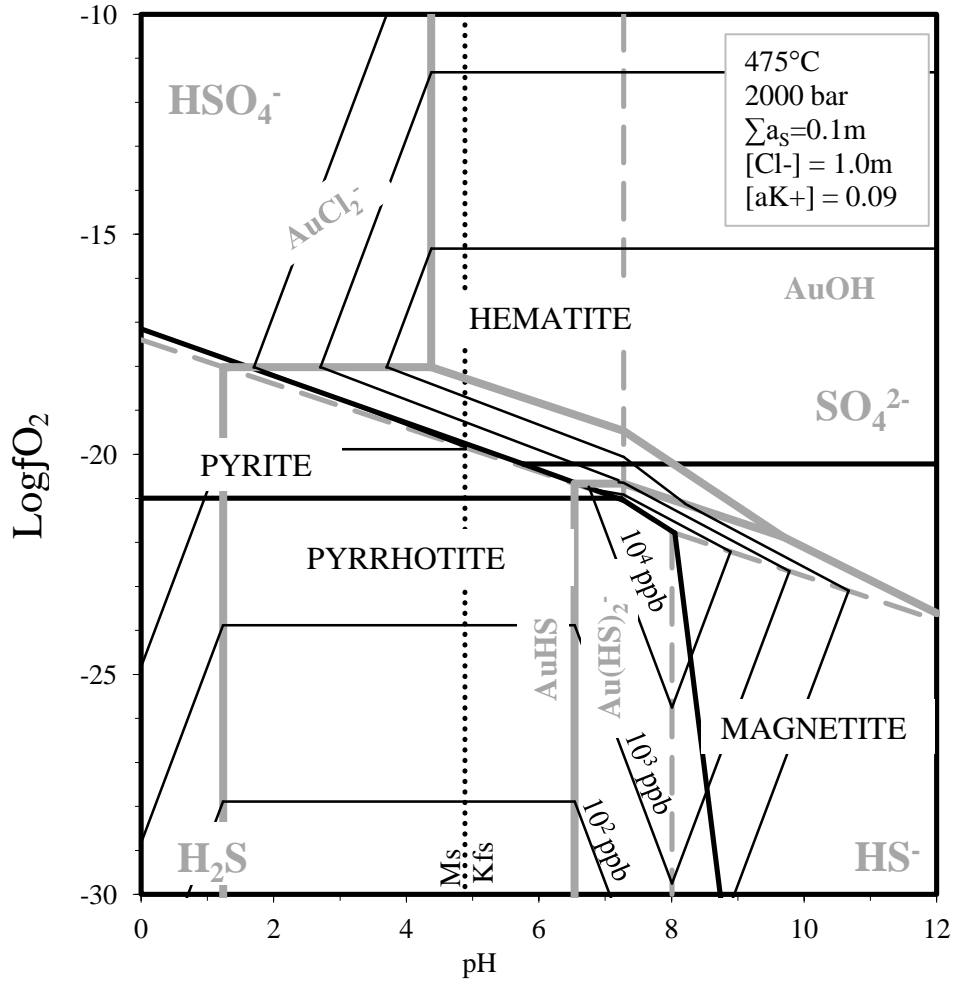
And for the Debye-Hückel equation with a expressed in centimetres

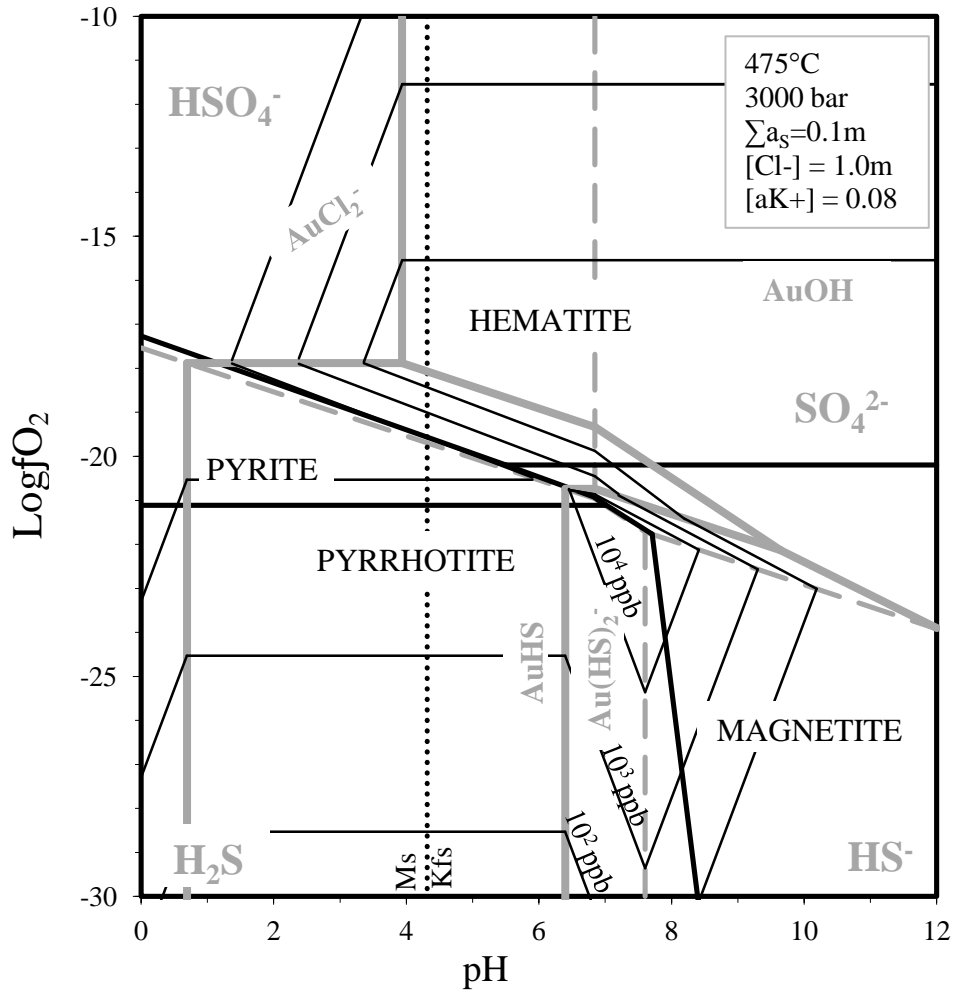
$$B \equiv \left(\frac{8\pi N_{\rho} e^2}{1000 \epsilon kT} \right)^{1/2} = \frac{50.29158649 \times 10^8 \rho^{1/2}}{(\epsilon T)^{1/2}}$$

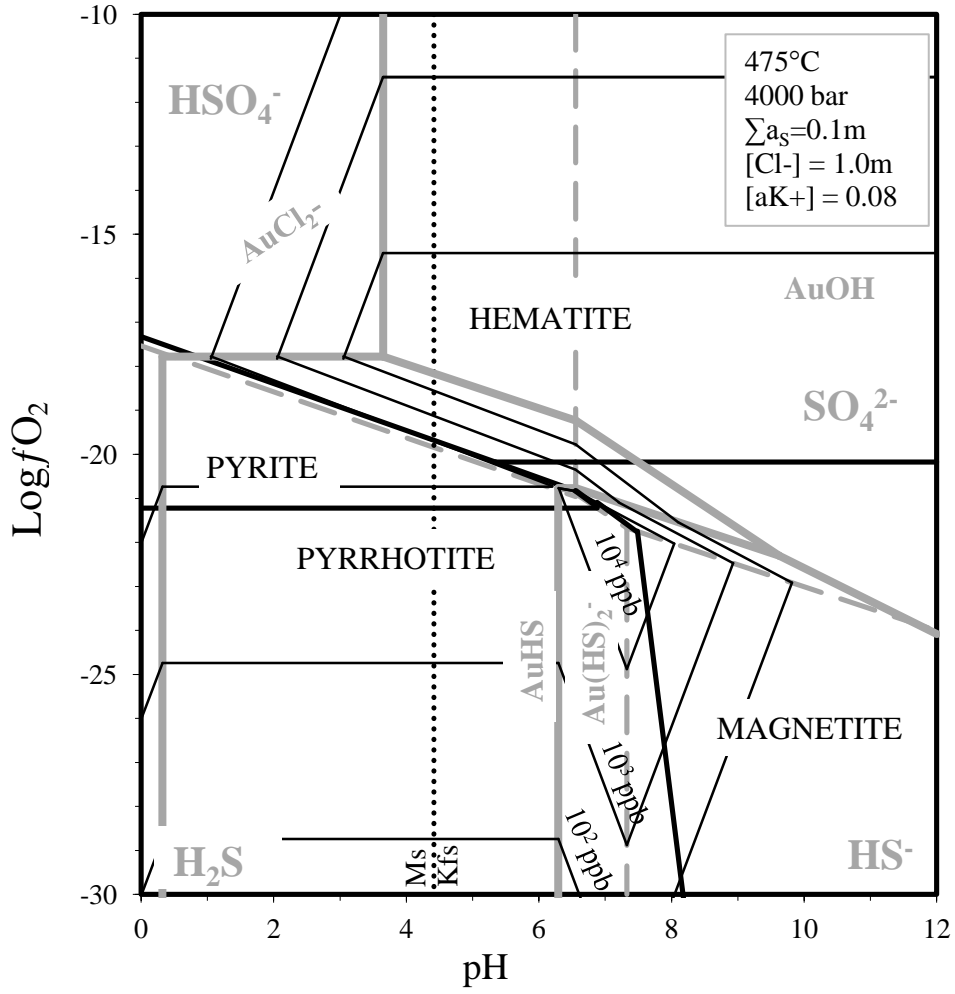
Where $\pi = 3.14159265$, N refers to Avogadro's number ($6.02252 \times 10^{23} \text{ mole}^{-1}$), e stands for the absolute electronic charge ($4.80289 \times 10^{-10} \text{ esu}$), ρ is the density in g cm^{-3} and ϵ the dielectric constant of H_2O , T (K) designates the temperature and k is the Boltzmann's constant ($1.38054 \times 10^{-16} \text{ erg } (^\circ\text{K})^{-1}$). The extended parameter, $\Gamma + bI$, is given by the mole fraction to molality conversion ($\Gamma = -\log(1 + 0.01810153)$) added to the extended term for NaCl-dominated solutions, b , multiplied by the ionic strength, I .

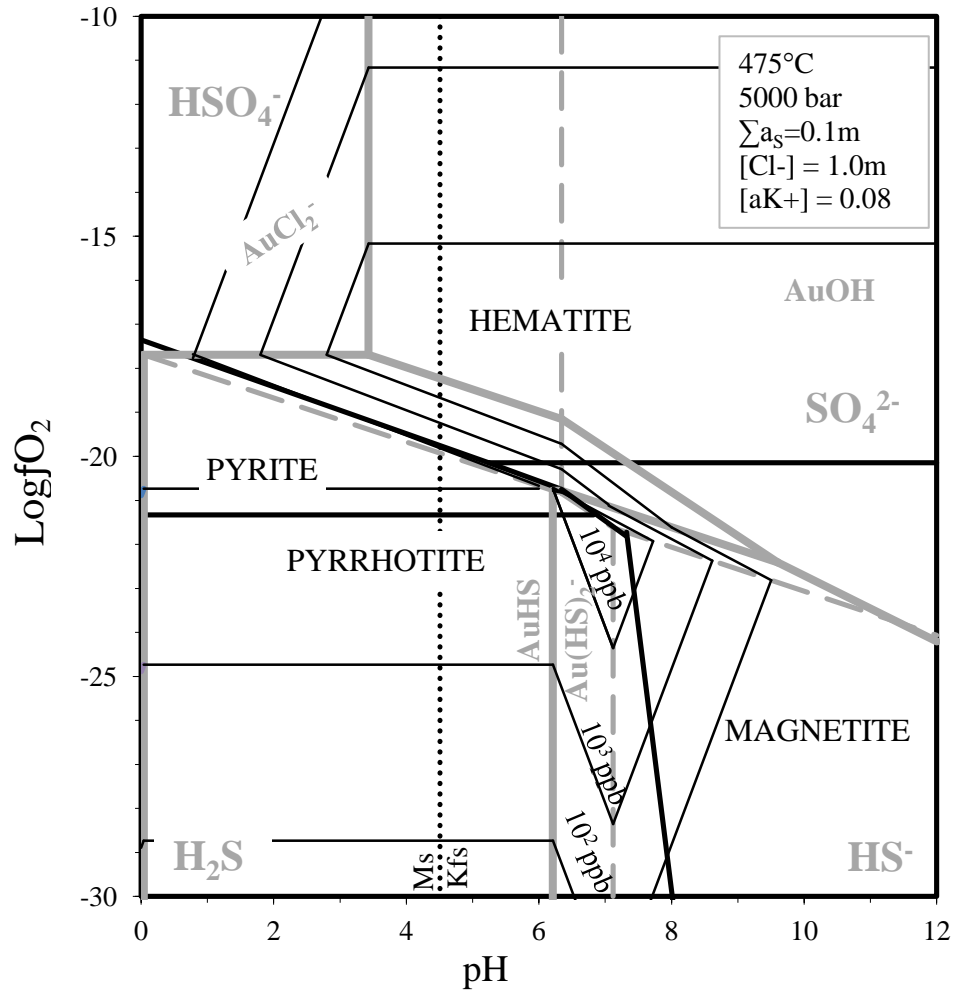
PHASE DIAGRAMS IN LOG fO_2 - PH SPACE











PHASE DIAGRAMS IN $\text{LOG}\Sigma\text{aS} - \text{LOG}f\text{O}_2$ SPACE

